NASA Contractor Report 2988

Design and Analytical Study of a Rotor Airfoil

L. U. Dadone

CONTRACT NAS1-14659
MAY 1978

NASA

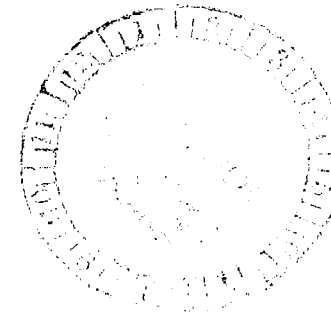

NASA Contractor Report 2988

Design and Analytical Study of a Rotor Airfoil

L. U. Dadone
Boeing Vertol Company
Philadelphia, Pennsylvania

Prepared for
Langley Research Center
under Contract NAS1-14659

NASA
National Aeronautics
and Space Administration

Scientific and Technical Information Office

1978

TABLE OF CONTENTS

SUMMARY

An airfoil section for use on helicopter rotor blades has been defined and analyzed by means of potential-flow/boundary-layer interaction and viscous transonic flow methods. Such a section was designed to meet as closely as possible twelve objectives expressed in terms of lift, drag and pitching-moment requirements at conditions representative of the helicopter rotor environment. The levels of performance required to meet the design objectives are to test the feasibility of extending the operational boundaries of state-of-the-art helicopter airfoils.

The design efforts showed that the first priority objectives can be met, though marginally. However, the lift requirements at M=0.5 and most of the profile drag requirements cannot be met without some compromise of at least one of the first three priorities, and namely:

1) the zero-lift pitching moment at low speeds, or
2) the maximum lift coefficient at M=0.4, or
3) the drag-divergence Mach number at zero lift.

As a result of the contour compromises necessary to meet the highest priority objectives, the low-drag capability of the new airfoil is limited by premature trailing edge separation, while the performance at negative lift levels is adversely influenced by an excessively tight lower-surface leading-edge radius. Several contour changes have been defined to overcome the most obvious weaknesses of the basic airfoil design, but all such changes require some compromise among the first-order priorities.

INTRODUCTION

Helicopter Rotor Environment

Basically, the performance of a helicopter is evaluated over the three distinct flight regimes of hover, transition and forward flight. In actual operation, a large number of flight conditions can be defined, but such conditions are included by the few parameters which influence the flight envelope and performance limits.

The characteristics of the airfoils employed on a rotor cannot be used in any simple manner to evaluate a helicopter performance. References (1) through (4) discuss in detail the empirical relationship between sectional characteristics and rotor requirements. Figure 1 illustrates the most significant lift and Mach number combinations encountered along a rotor in flight. The critical conditions are:

1. Supercritical flow at low lift, typical of the advancing blade tip in forward flight (Region I).

2. Lift levels of $C_\ell \approx 0.6$ at Mach numbers about M=0.6, representative of hover requirements (Region II).

3. High lift (quasi-steady $C_{\ell_{max}}$ and higher) for $0.3 \leqslant M \leqslant 0.5$, associated with retreating blade stall (Region III).

The objectives for the design efforts described in the present report specify lift, drag and pitching moment characteristics within one of the three regions of figure 1. The design objectives are listed in table I. The objectives will be discussed within the report, and an evaluation will be presented of the theoretical and empirical means to assess airfoil performance for each of the proposed design goals.

Helicopter Airfoil Development

The design of airfoils for helicopter rotor applications is not a new field of research. References (5) and (6), dating to the early 1940's, report on wind tunnel tests of cambered NACA H-series airfoils designed for low profile drag, but which also had reflexed trailing edges to reduce the pitching moment associated with camber. The H-series sections did not work as well as expected because the low drag requirements implied the presence of extensive laminar flow, and because the low-drag thickness shapes in conjunction with the trailing-edge reflex penalized too much the maximum lift capability. Although not generally used on helicopters, some of the NACA H-series sections have been used on autogyros.

Until the mid-1960's, helicopter rotors mostly employed symmetrical sections of the NACA four-digit series, with maximum thicknesses ranging from 10% to 15%. Such airfoils had been developed during the early 1930's by empirical means and, although designed for fixed wing applications, they were used on helicopters until the advances in technology made it possible to utilize cambered sections. Most of the new cambered sections introduced during the 1960's were related to the NACA 230-series, also developed and tested during the 1930's.

Reference (1) outlines the early steps in rotor airfoil design and it offers guidelines to quantify the sectional requirements which have the greatest impact on rotor performance. Specifically, these are

- Near zero pitching-moments about the aerodynamic center.
- High maximum-lift capability at M=0.4.
- Low drag at the high subsonic Mach number levels typical of the advancing blade tip.
- Low profile drag at the lift and Mach number levels typical of the hover flow environment.

Such guidelines are still valid. Since 1966, however, computational methods have progressed to the point that today it is possible to narrow down analytically most of the characteristics of an airfoil prior to wind tunnel testing, instead of carrying out most of the airfoil development experimentally.

During the late 1960's and the early 1970's, new helicopter sections were defined utilizing theoretical knowledge and test experience from advanced fixed-wing technology. The new design methods lead to airfoils which can be roughly separated into two groups. The first group includes sections with good high-Mach number characteristics but poor maximum lift capability at $0.3 \leq M \leq 0.5$, while the sections in the second group have good lifting capability, at a cost in supercritical performance. Within this subdivision, additional distinctions could be made with respect to drag and pitching moment characteristics. A comparison of several of the new sections is shown in reference (2), while detailed data are presented in reference (4).

Unsteady Aerodynamics Considerations

During the late 1960's as new airfoil sections were being developed, significant progress was also made in the field of unsteady aerodynamics. One of the main contributions to

helicopter technology was the definition of dynamic-stall delay in a form applicable to helicopter rotor blades (reference 7). The tests described in references (8) through (10) were part of the experimental evidence used to define the method of reference (7). The method was later updated to include a more accurate description of stall inception and recovery. Other empirical stall delay representation methods have been defined since then. The remarkable improvements in performance and load prediction methodology, gained from the understanding of unsteady aerodynamic effects, naturally lead to the search for an advanced airfoil which would take advantage of whatever unsteady effects are present in the rotor environment. That proved to be much harder to achieve than expected.

Several attempts have been made to improve the unsteady characteristics of a section through contour changes, or by boundary layer control. A number of active and passive boundary layer control methods was tried to alter the dynamic stall characteristics of the V23010-1.58 airfoil. Such data have not been formally documented or otherwise released, but the main conclusion from those tests was that most passive boundary layer control devices and local contour changes have little effect when they do not actually cause some performance degradation. The benefits to be gained from active boundary layer control were generally too small to justify the added complexity, although such a position should be reassessed periodically to keep up with new helicopter performance and mission requirements.

Several observations can be made as a result of correlation between static and dynamic data carried out to identify key flow phenomena. First, a qualitative assessment of the dynamic stall characteristics in forced pitch oscillation at the 1/rev to 2/rev drive frequencies can be derived from quasi-steady stall information. Second, the stall delay from the unsteady aerodynamic effects associated with 1/rev angle-of-attack variations is independent of airfoil to a first order of approximation. In conclusion, the static design objectives which reflect favorable unsteady aerodynamic effects are high maximum lift capability and a gradual stall, or better, as little static-stall hysteresis as possible.

Test data is generally lacking on the effect of specific design parameters on unsteady aerodynamics. Firm guidelines about the effect of contour variations on the onset and development of dynamic stall are not available. Another area which has not been systematically explored is the effect of airfoil thickness, camber, and L.E./T.E. contours on the dynamic-stall recovery characteristics. However, such tasks should prove to be quite complex because, during cyclic airfoil motions involving stall, the attached-flow portion of each cycle is quite

repetitive while the separated flow portion is totally dominated by the unsteady nature of the wake and is highly non-repetitive.

Airfoil Design Methods

Airfoil analysis methods, essential for design, have seen significant improvements in recent years. Methods combining potential-flow solutions and boundary-layer theory have been defined and tried quite successfully for the first time during the 1930's. The only limitation which prevented a wider use of such techniques was the length and complexity of the computations required. Later, additional and even more serious obstacles were encountered when airfoil solutions were required at supercritical flow conditions. The advent of high-speed computers and the adaptation of new numerical solutions to such computers have virtually eliminated the need for lengthy hand-calculations. As a consequence, it has become practically possible to understand in detail the flow phenomena observed in wind tunnel tests, and to develop airfoil sections which meet complex design requirements.

A discussion of the development of subcritical and supercritical flow analysis methods is beyond the scope of this report. However, such techniques have been developed by different individuals and organizations, each involving increasing complexity and sophistication, and each relying on correlation with test data from a variety of sources. The most efficient of these airfoil solutions have been acquired by the U.S. Government through NASA. References (11) and (12) describe the computer codes used for this study. At NASA, these programs are continuously improved and updated, and, as a result, the private development of airfoil analysis methods has been de-emphasized while more attention is being paid to airfoil design techniques and correlation with test data. Typically, advanced helicopter airfoils have been the last to benefit of new design methods. For this reason, the flow solutions described in references (11) and (12) have not been thoroughly calibrated over the range of conditions necessary to expand helicopter rotor performance boundaries.

SYMBOLS

a	quantity used to define mean lines of NACA 6-series airfoils, where a is the distance in chords from the leading edge over which the loading is uniform at the design lift coefficient.
a	speed of sound, m/s
c	airfoil chord, m

C_d	drag coefficient
C_f	skin friction coefficient
C_ℓ	lift coefficient
C_m	pitching moment coefficient, resolved about the quarter chord unless otherwise noted
C_n	normal force coefficient
C_p	pressure coefficient, $(P-P_\infty)/\frac{1}{2}\rho V_\infty^2$
f_D	drive frequency in oscillating airfoil test
k	reduced frequency, $c\Omega/2V$
M	Mach number
p	pressure, static pressure when no subscripts are used
q	dynamic pressure, $\frac{1}{2}\rho V_\infty^2$
R	leading edge radius of an airfoil section, m
Rn	Reynolds number, $\rho VL/\mu$
t	maximum thickness of an airfoil, m
T	absolute temperature, °K
V	velocity, m/s
x	abscissa of an airfoil contour, m
y	ordinate of an airfoil contour, m
α	angle of attack, degrees
δ_{tab}	trailing edge tab angle measured from the chordline of an airfoil, defined as positive in the direction for which positive camber is increased.
Δ	increment
μ	absolute viscosity, N s/m^2
ρ	density, kg/m^3
Ω	rotational velocity, rad/s

Subscripts

ac	aerodynamic center
c/4	for quantities referenced to the quarter chord
c, comp	compressible
c	camber or mean-line
i	"ideal" or design value
inc	incompressible
ℓ	lower surface, in identification of airfoil coordinates
ℓ	local, in reference to flow conditions
L.E.	leading edge
max	maximum value
min	minimum value
o	zero lift condition
sep	separation (flow separation)
t	total
t	thickness distribution
tab	trailing edge tab
T.E.	trailing edge
u	upper surface, in identification of airfoil coordinates
∞	freestream condition

Abbreviations

BSWT	Boeing Supersonic Wind Tunnel
BTWT	Boeing Transonic Wind Tunnel
c.g.	center of gravity

TECHNICAL DISCUSSION

REVIEW OF DESIGN CRITERIA

The design criteria are summarized and divided into three groups in table I. The three groups have a priority each assigned to it. Although there could be some disagreement about the placement of sectional characteristics under one priority or the other, the assignment of priorities is not the main concern of this study, but rather the determination of some of the physical boundaries within which helicopter airfoils can be optimized. In the following sections, the design priorities will be briefly described and discussed.

FIRST PRIORITY

Design Objective (1): $|C_{m_o}| \leq 0.01$ at M=0.3

It has been pointed out in a number of instances, e.g., reference (13), that small and in some cases nose-up pitching moments are necessary to minimize rotor loads in forward flight. Although the theoretical zero-lift pitching moment is generally quoted from incompressible and inviscid flow solutions, a low Mach number value is more meaningful when viscous and compressible flow solutions are available. As shown in the sketch below, low or nose-up pitching moments require:

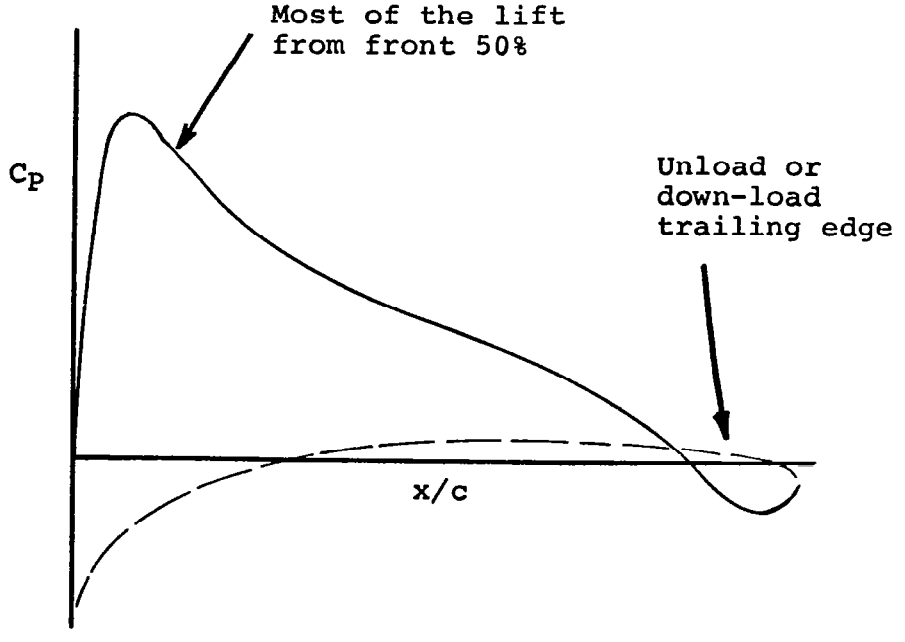

Since present analysis methods do not account for the effect of thick boundary layers or separated flow, theory generally overpredicts the effectiveness of the contour changes used to compensate pitching moments in the nose-up direction.

Design Objective (2): $C_{\ell_{max}} \geq 1.50$ at M=0.4

The maximum lift between M=0.3 and M=0.5 has been shown to be critical in delaying retreating blade stall. The flow phenomena which cause separation at high lift levels are a function of both free stream Mach number and airfoil shape. For the airfoils typically employed on helicopter rotors, the maximum lift at M=0.3 and M=0.4 is associated with only a small supersonic region at the leading edge, so that the use of potential flow/boundary layer interaction methods, such as reference (11), is generally acceptable. At M=0.5, the local flow can include larger supersonic regions and the analysis must be carried out with different techniques (see Design Objective 6).

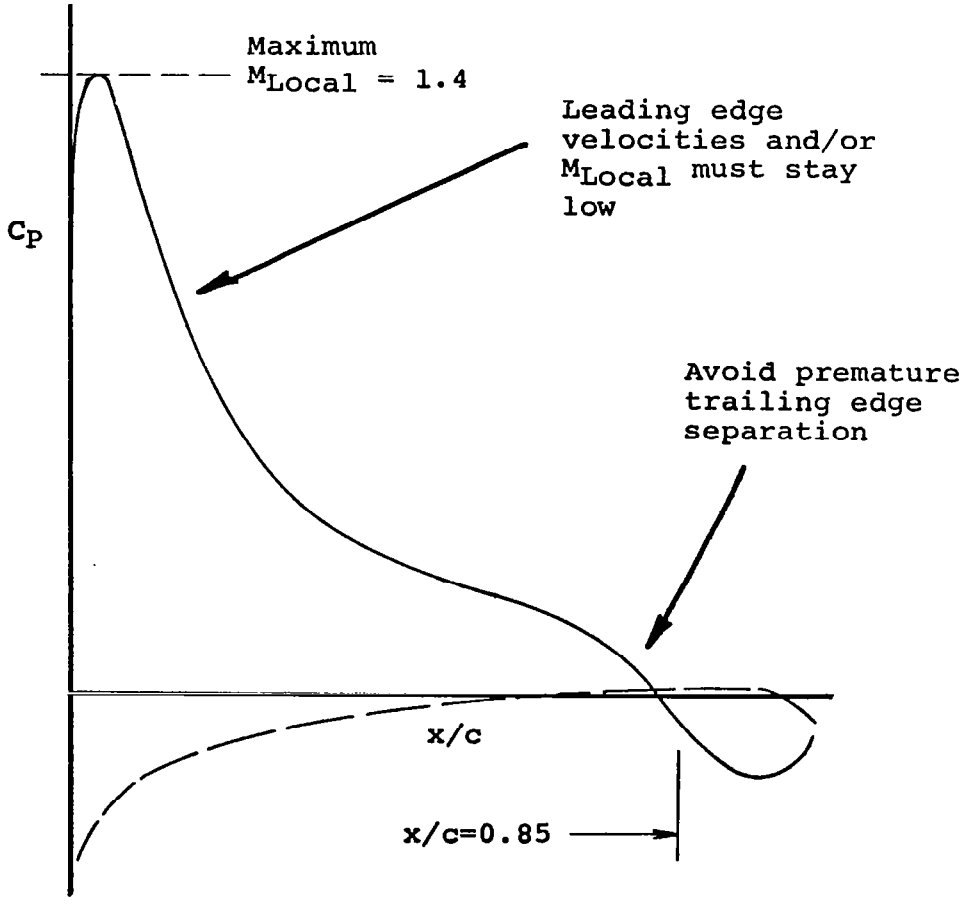

In order to fulfill this objective, as well as the requirement for a gradual stall (Objective 11), it is necessary to achieve the proper balance between the buildup in leading-edge velocities and the onset of trailing-edge separation. While this can be accomplished fairly easily with more conventional airfoil sections, the pitching-moment restrictions of Design Objective (1) require trailing-edge configurations which slow down the flow so abruptly that significant trailing-edge separation is almost inevitable at high lift levels. The main difficulty, then, is in minimizing the extent of T.E. separation without losing the pitching-moment compensation. By theoretical means, this compromise can be exercised only to a limited extent.

The use of potential-flow/boundary-layer interaction methods, e.g., reference (11), used in this study, requires careful correlation with test data. Most of the correlation necessary for the present work was carried out using data from reference (4) for airfoils acquired in one wind tunnel facility. The best correlation for the maximum lift at M=0.4 was obtained by assuming that the flow over an airfoil cannot sustain additional lift when the local Mach number exceeds M_{ℓ}=1.4 near the leading edge, or when the turbulent separation reaches the x/c=0.85 chord location.

Design Objective (3): $M_{DD_O} \geq 0.81$

The drag-divergence Mach number at zero lift is a measure of the usefulness of a section near the tip of a helicopter rotor blade in forward flight. While the drag-divergence Mach number is not the best parameter to quantify the drag penalty associated with strong compressibility effects, the method available to evaluate it (crest-line theory, reference 14) is simple and reliable. Therefore, crest-line theory is the most efficient way of approaching airfoil design at the onset of supercritical flow conditions. The sketch below summarizes some of the geometric characteristics which have a dominant role in increasing M_{DD}.

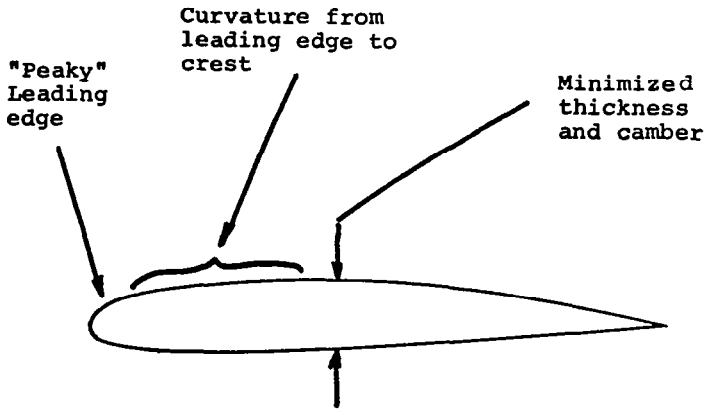

The theoretical drag-divergence boundary as estimated from crest-line theory is always conservative with respect to wind tunnel test data. Although it is possible that in some cases the test data show some relief due to wall effects, the discrepancy between theory and test appears to be quite consistently $\Delta M_{DD} \approx 0.02$. The viscous transonic flow method of reference (12) does not improve this correlation, and a $\Delta M_{DD}=0.02$ discrepancy between theory and test is reported in the text.

Crest-line theory alone does not give any indication of the presence of drag creep at Mach numbers below M_{DD}, nor does it quantify the rate of growth in drag beyond M_{DD}. Other empirical methods are available to provide guidelines (reference 14). In the case of drag creep, the information obtained from crest-line theory at least establishes the optimum potential of an airfoil. More sophisticated methods of analysis and, ultimately, test verification are necessary to rigorously establish the drag divergence Mach number and the level of drag <u>at</u> drag divergence.

Design Objective (4): $|C_{m_o}| \leq 0.015$ for $M < 0.7$.

This restriction on compressibility effects for the zero-lift pitching moment coefficient will ensure that the pitching moment does not grow to unacceptable levels before pitching moment divergence. In this case, no separation needs to be involved because the growth in pitching moments can arise from compressibility effects alone. An airfoil satisfying the low speed pitching moment objective (1), and the drag divergence objective (3), will probably satisfy this pitching moment restriction as well. If not, only a small adjustment over the low speed C_{mo} level should be required. Such adjustment can be accomplished in the wind tunnel by means of the trailing edge adjustments shown below. Because of separation effects, theory does not correctly predict the magnitude of such adjustments.

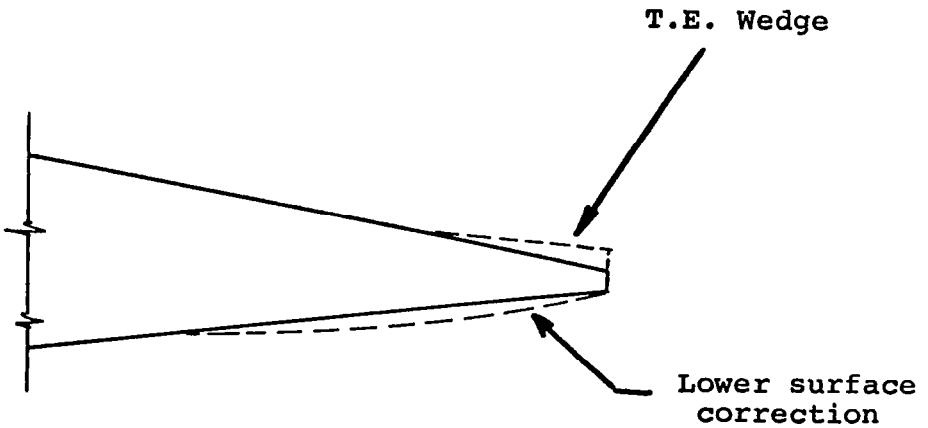

SECOND PRIORITY

Design Objective (5): $C_d \leq 0.008$ at $C_\ell = 0.6$ and $M = 0.6$

The above lift and Mach number combination is commonly used as a reference level in assessing the usefulness of an airfoil section on a rotor in hover. To the extent that most of the profile drag of an airfoil is due to skin friction, this design objective is best met by airfoils which can maintain a laminar boundary layer over large portions of the surface. The proper combination of thickness and camber alone would satisfy this drag objective for almost any thickness, at least for $0.06 \leq t/c \leq 0.15$, but this would lead to airfoils with poor performance as far as most of the other design objectives are concerned.

The best airfoils for low drag at Mach numbers above M=0.4 are rooftop sections, such as the NACA 6X-series, or the VR-7 and VR-8 airfoils. However, such sections have either too large pitching moments, or too low drag divergence Mach number characteristics. When non-rooftop sections are used, a considerably reduced extent of laminar boundary layer can be maintained on the upper surface because of the velocity gradients at the leading edge. In any case the extent of laminar flow possible over a helicopter rotor blade is still an unresolved question.

Two general guidelines can be suggested. The first is to delay as much as possible the transition from laminar to turbulent boundary layer. The second, and more significant, is to avoid trailing edge contours causing premature T.E. separation.

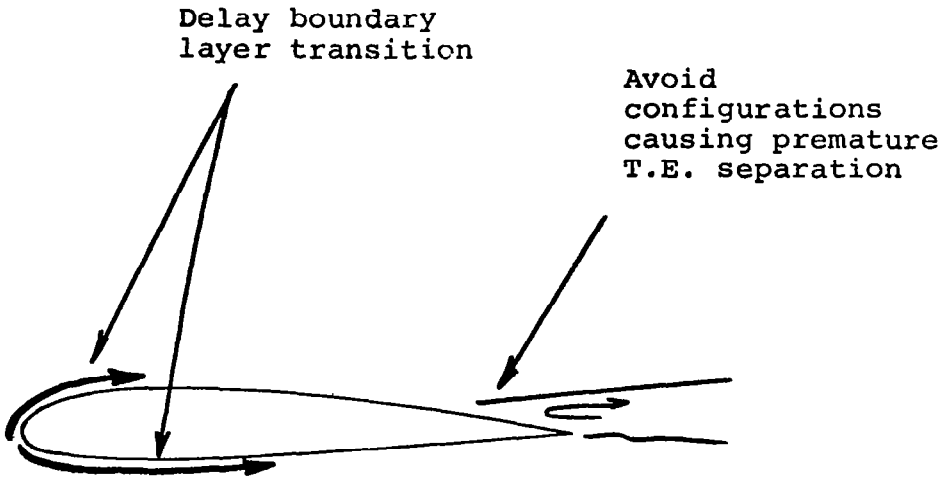

Any theoretical results obtained with presently available methods will have to be corrected to account for trailing-edge separation effects. The method of reference (11) accounts only for a momentum loss proportional to the thickness of the boundary layer at separation; it does not include the additional "base drag" due to the separated region at the trailing edge. Such additional drag is significant in airfoils employing trailing edge devices for pitching moment compensation.

Design Objective (6): $C_{\ell_{max}} \geq 1.5$ at $M=0.5$

High maximum lift capability at $M=0.5$ is desirable for operating conditions which result in retreating blade stall at $M>0.4$. Dr. Wortmann, reference (15), pointed out that the chances for a high maximum lift capability at $M=0.5$ can be improved by properly tailoring the upper surface between the leading edge and the 10% chord location. However, the supersonic region near the leading edge levels can be of a significant size. When this is the case, conventional subcritical flow analysis methods cannot be meaningfully extended to the flow conditions near maximum lift. Transonic flow methods are then necessary.

A transonic analysis allows the evaluation of the supersonic region near the leading edge. The resulting local velocities display a significant redistribution compared to the subcritical potential flow solution. When transonic flow effects are included, the maximum lift levels based on a "maximum" allowable local Mach number (e.g., $M_\ell=1.4$) can be higher than those possible with subcritical flow solutions. A more meaningful correlation could be obtained by interpreting shock/boundary-layer interaction effects, but such correlation was not attempted within the scope of this report.

The viscous, transonic flow analysis, reference (12), predicts quite successfully the maximum lift trend of airfoils benefiting of favorable transonic effects. The only question which remains unanswered is the magnitude of the maximum lift possible above the potential flow level. Such additional lift could not be determined with any degree of confidence because it is not clear at this time to what extent wall effects influenced the high lift levels measured on airfoils such as the VR-7, reference (4).

Design Objective (7): $|C_m| \leq 0.02$ at $M=0.3$ for $0.0 < C_\ell \leq 1.0$

This restriction primarily sets a limit to the growth of the nose-down pitching moment on airfoils with the aerodynamic center located behind the quarter chord. Airfoils with a forward aerodynamic center will not be affected by this guideline as long as the maximum lift at $M=0.3$ is well above $C_\ell=1.0$ and no separation is present. When the low-speed C_{m_o} objective (1) is met, little or no additional corrections should be necessary. Final adjustments can be made during wind tunnel test verification by means of the trailing edge devices described for Design Objective (4).

Design Objective (8): $C_{d_o} \leq 0.01$ at $M = M_{DD_o} + 0.02$

Low drag rise beyond drag divergence is desirable because a portion of the advancing blade generally operates beyond M_{DD}. The drag rise at supercritical conditions is due to the growth of wave drag. The theoretical prediction method available for this study was the viscous transonic-flow analysis of reference (12). However, transonic flow analysis results can be used only on a comparative basis; as pointed out under Design Objective (3), significant difficulties remain unresolved when the available computer programs are applied in this region. Independently of drag creep and other effects attributable to camber and thickness, rooftop sections have a comparatively steeper drag rise beyond drag divergence than other sections.

THIRD PRIORITY

Design Objective (9): $M_T > M_{DD}$

where M_T is the Mach number

for $\frac{dC_{mo}}{dM} = -0.25$

By delaying the onset of pitching-moment break until after drag divergence, it is possible to improve the chances that a rotor will be power-limited rather than structurally (or "load") limited. At present, an accurate and quantitative assessment of the tradeoff between Mach "tuck" and drag divergence is not possible. However, rotor test experience reported in reference (2) shows that such a margin is beneficial. This requirement will become more clear as additional experience is gained with torsionally "soft" rotors manufactured with new composite materials. Reference (2) also points out that the relationship between drag-divergence and pitching-moment break can be adjusted by nose-up compensation with trailing-edge devices. Such devices (tabs, wedges, or

other means of reflexing the mean-line) cause a slight degradation in drag divergence when applied in the nose-up direction, while delaying the Mach number for pitching moment break. It is again noted that results from viscous, transonic flow analyses should be treated as comparative, not absolute.

Design Objective (10): $0.01 \geq M^2 C_{m_o} \geq -0.04$

This criterion attempts to incorporate some realistic considerations for loads as dimensional quantities. Airfoil force and moment data are always nondimensionalized by a reference area and by the dynamic pressure. While this is a convenient way of reducing and correlating sectional data, the lift, drag and pitching-moment coefficients conceal the magnitude of the airloads because of the V_∞^2 term in the dynamic pressure. The effect of dynamic pressure can be partially restored to the sectional coefficients by means of an M^2 factor. The use of this factor offers an insight into the relative importance of the loads, particularly when it is applied to the drag and to the pitching moment. Therefore, a pitching-moment limit has been defined by specifying a $M^2 \times C_{m_o}$ boundary. The boundary of Design Objective (10) is compared to the pitching moment of several airfoil sections in figure (2). Such data shows that airfoils with moderate low speed pitching moments can usually meet Design Objective (10) without additional T.E. adjustments, particularly if Design Objective (9) has been also met.

Design Objective (11): Gradual Stall at $0.3 \leq M \leq 0.4$

This design guideline is aimed at the reduction in load excursions associated with stall. A further consideration is that gradual stall in the quasi-steady regime has been correlated with positive aerodynamic damping for pitch oscillations through stall at the 1/rev and 2/rev frequencies, figures 1A and 2A in the Appendix. While the stall character cannot be predicted rigourously, potential-flow/boundary-layer interaction methods give a good indication of which type of stall is most likely to take place. Trailing-edge stall, characterized by the movement upstream of the turbulent separation point, is qualitatively predictable. Leading-edge stall is very likely when the local Mach number at the leading edge reaches M=1.4. However, the prediction of the actual shape of the $C_{\ell,\alpha}$ and $C_{m,\alpha}$ curves at and beyond stall can be approximated only by comparison with known test data. A correctly optimized airfoil will display a combination of leading-edge and trailing-edge stall characteristics, with trailing-edge separation becoming dominant somewhat ahead of leading-edge separation.

Design Objective (12): $C_{d_o} \leq 0.007$ for $M \leq M_{DD} - 0.1$

This requirement implies the elimination of drag creep and other sources of drag degradation. Creep can occur at low-lift drag levels on sections with excessive leading edge camber. The drag required by Objective (12) is quite low, and it implies laminar flow on both surfaces to an extent which is not compatible with the higher priority $C_{\ell|max}$ objectives. An additional difficulty to overcome is the presence of some trailing edge separation due to pitching-moment compensation requirements.

SURVEY OF EXISTING AIRFOILS

Before attempting to design an airfoil to meet the criteria in table I, it was essential to establish how existing airfoils rate against the complete set of proposed design objectives. Table II shows the characteristics of five rotor airfoils compared against all 12 design objectives. Table III shows a more extensive but less detailed survey covering the first seven objectives for 35 airfoils. Most of the data was obtained from the Helicopter Airfoil Datcom, reference (4). The NLR 7223-62 data is from reference (16), and the VR-1 is from an unpublished report.

The plots in figures 3 and 4 display the data pattern for two key parameters. These parameters are the maximum lift at M=0.4 and M=0.5, respectively, and the zero-lift drag divergence Mach number for the airfoils in table III (Objectives (2) and (3), and (6) and (3)). In both figures the design objective appears to stand well out of reach of all known sections. At M=0.4, the airfoils on the boundary are the VR-7, the NACA 23012, the V23010-1.58, the V(1.9) 3009-1.25, the V13006-0.7 and the NACA 0006. The NLR 7223-62 is the only section outside of the boundary, even though it has a low maximum lift capability. For $C_{\ell max}$ at M=0.5 and M_{DD_o}, figure 4 shows the VR-7 at the high lift and lower M_{DD} end. The FX69-H-098, the NACA 64A(4.5)04 and the VR-8 are close to each other in the middle of the boundary while the V13006-0.7 and the NACA 0006 are at the high M_{DD} and low $C_{\ell max}$ end. Again the NLR 7223-62 stands out of the general trend. All other airfoils in figures 3 and 4 fall inside the "optimum boundary" and are quite far from the design objectives.

The pitching-moment values of tables II and III have not been presented graphically because there is no useful way to do so. An inspection of the pitching-moment values shows that, making an exception for the NACA 64-xxx airfoils, most of the sections have small pitching-moments near if not within Design Objective (1). In most of the cases for which the pitching-moment is not too negative, compensation is possible by

means of trailing-edge devices. Reference (4) describes pitching-moment compensation methods and related side effects, some of which can be also deduced by inspection of the data in table III. Practically any airfoil with a low speed $C_{m_o} \approx -0.02$ can be corrected to $C_{m_o} \approx -0.01$ with a small penalty in maximum lift, drag divergence and profile drag, but to quantify this penalty it would be necessary to review the turbulent boundary-layer separation sensitivity of each contour.

Design Objective (4), requiring slow growth of the zero-lift pitching moment with increasing Mach number, can be met by most of the airfoils satisfying the first objective. In few cases where some compensation is necessary and possible, it can be achieved with the T.E. devices discussed in the previous paragraph. However, a nose-up correction in the pitching moment causes a reduction in the maximum lift capability and a reduction in drag divergence Mach number. For instance, changing the V23010-1.58 from a 0° T.E. tab angle to -3° results in a $\Delta C_{\ell_{max}} = -0.04$ and a $\Delta M_{DD_o} = -0.02$ penalty. For other examples see table III.

The drag requirement for hover, Objective (5), is met by very few airfoils. Of these few, most would require additional pitching moment compensation at some cost in drag performance. As mentioned before, the low-drag potential of airfoils for helicopter rotors is a somewhat controversial issue, but the general consensus is that while some laminar flow is likely and possible, extensive laminar boundary layers have little probability of surviving the combination of the adverse flow in the rotor environment and the surface conditions of the blades. The hover drag objective is achievable theoretically, but some consideration will be necessary to determine the final drag of the contours implemented on an actual rotor.

The pitching-moment objective at $C_\ell = 1.0$ and M=0.3 (Number 7) is met, or is within reach with small T.E. corrections, for all airfoils satisfying the zero-lift pitching-moment objective at low speeds (Design Objective (1)).

The eighth objective, $C_{d_o} \leq 0.01$ at $M=M_{DD} + 0.02$, is out of reach of all the airfoils reviewed so far. The only section offering some promise is the FX69-H-098, table II, with $C_{d_o}=0.0125$ at M=0.82. However any contour change to increase the maximum lift at M=0.4 above the present $C_{\ell_{max}} = 1.25$ value would result in degradation of both the drag divergence boundary and the drag beyond drag divergence.

Of the third-priority objectives, (9) and (10) present no particular problems. The VR-8 with 0° T.E. Tab would not meet the Mach-tuck-after-drag-divergence requirement, but the VR-8 is used with additional nose-up compensation (-4.5° to -6° T.E. tab angle), so that Mach tuck is delayed with only a small penalty in drag divergence.

The requirement that the stall for $0.3 \leqslant M \leqslant 0.4$ be gradual is not met by most of the sections in table III, and by most of the airfoils related to the NACA 230-series documented in reference (4). The problem is particularly significant for airfoil sections with thickness varying from t/c=0.09 to t/c=0.12, because thinner sections display "thin" airfoil stall, i.e., gradual stall with poor maximum lift capability, while sections with thickness above 12% generally display trailing-edge stall behavior. The tendency of airfoils to separate from the trailing edge can be predicted quite reliably with present potential flow/boundary layer interaction methods.

The last design objective (12), requiring $C_{d_o}=0.007$ or better at $M=M_{DD}-0.1$, is not met by most of airfoils considered. The very few which do have such low drag do not meet the maximum lift objective at M=0.4, e.g., the FX69-H-098. Increasing camber would cause transition at the leading edge on the lower surface, thus increasing the profile drag well beyond the $C_{d_o}=0.007$ level.

In conclusion, it appears that five key design objectives have never been attained simultaneously with existing helicopter airfoil sections. Such objectives are:

- $C_{\ell_{max}} \geqslant 1.5$ at $M = 0.4$ (2)
- $M_{DD_o} \geqslant 0.81$ (3)
- $C_{\ell_{max}} \geqslant 1.5$ at $M = 0.5$ (6)
- $C_{d_o} \leqslant 0.01$ at $M = M_{DD} + 0.02$ (8)
- $C_{d_o} \leqslant 0.007$ at $M = M_{DD} - 0.1$ (12)

Of these, the last three (6, 8 and 12) seem to be the least likely to be achieved given the relative importance of Objectives (2) and (3). Other ways of presenting and comparing airfoil characteristics are discussed in references (2) and (4), but such comparisons would not help in interpreting the significance of the design objectives of this study.

DESIGN APPROACH

Design Logic

To define an airfoil optimization procedure should be a relatively simple matter, but in fact it is not. The problem is that, within every cycle of rotation, airfoils employed on a rotor experience most of the flow conditions ever considered for fixed wings.

Definition of the Problem

The priority assigned to the characteristics selected for improvement is an integral part of the design logic. The selection of the two-dimensional airfoil characteristics necessary to improve helicopter performance has already been the topic of many reports, e.g., references (1), (2), (13), (15), (17), so that the subject will not be covered again. The relative importance of each objective determines the procedure for the selection and modification of possible airfoil contours. The design objectives in table I, for instance, emphasize the low-speed pitching moments, the maximum lift capability at M=0.4, the drag rise Mach number at zero lift and, to a moderate extent, compressibility effects on low-lift pitching moments. The fact that the profile drag objectives are second and third order priorities is very significant. This allows the freedom to explore contours with high lift and extended drag-divergence boundaries, at the expense of marginal trailing edge separation characteristics.

An example of different design requirements is the development of the VR-7 and VR-8 airfoils, references (2) and (13). The VR-7 and VR-8 were designed mainly for low drag at conditions of interest for hover performance, and for a maximum lift capability at M=0.4 at least as good as that of the V23010-1.58 airfoil. Provisions were also to be made for pitching-moment compensation to nose-up C_{m_o} values ($C_{m_o} > 0$). No drag-divergence objectives were imposed on the VR-7, and the VR-8 was obtained by decambering and reducing the thickness of the VR-7 to the extent necessary for the application of the VR-8 at the tip of the Heavy Lift Helicopter (HLH) rotor blades. The V23010-1.58 section, which was the "reference" airfoil, was replaced by two airfoils which had to be appropriately distributed along the span of the blade to improve performance independently of twist and planform effects. Subsequent optimization efforts along the design guidelines which lead to the VR-7 and VR-8 proved to be generally unsuccessful: any contour changes to improve the drag-divergence boundary reduced the maximum-lift capability or caused a deterioration in pitching-moment characteristics. The design objectives of table I include sufficiently significant differences from the

VR-7/8 objectives to allow the investigation of entirely new combinations of airfoil contour elements.

To start any optimization effort, it is necessary to select no more than two or three characteristics which:

1) have the highest priority,

2) can be predicted with confidence and without unreasonable complexity,

3) have a beneficial effect on some of the lower priorities.

As verified by correlation with available test data, reference (4), the following quantities can be predicted with a good degree of confidence:

- The low speed zero-lift pitching-moment
- The maximum lift coefficient at M=0.4
- The zero lift drag divergence Mach number
- The drag coefficient at M=0.6, C_ℓ=0.6
- The type of stall

The VR-7 airfoil was designed with the maximum lift at M=0.4, and the drag at M=0.6 and C_ℓ=0.6 as primary objectives. The primary objectives in the VR-11X design are the maximum lift at M=0.4, and the zero-lift drag divergence Mach number.

The survey of existing airfoil data provided a quantitative assessment of the difficulty in defining contours which would satisfy all the design objectives. Figure 3 illustrates how the characteristics of existing airfoils compare to design objectives (2) and (3) while generally satisfying, i.e., being within reach of pitching moment objective (1).

Summary of Key Trends

The airfoil contour optimization process is based on the following qualitative trends:

1) As camber is increased, the maximum lift capability increases, but the zero-lift drag-divergence Mach number decreases.

2) With constant mean-line, a reduction in thickness will result in an improvement in the drag-divergence Mach number.

3) Changes in thickness between 11% and 15% typically cause small variations in maximum lift at M<0.4. A reduction in thickness below the 11% level causes a substantial deterioration in maximum lift capability.

4) Small, $|\Delta C_{m_o}| \leq 0.005$, pitching moment adjustments can be achieved with negligible lift and drag penalties by means of trailing edge contour changes. Even small T.E. changes, however, can cause premature turbulent separation, if applied to trailing-edge configurations already including significant surface curvature.

5) Within the same family of airfoils and for a constant low-speed C_{m_o}, camber and thickness variations will improve either the maximum lift or the drag-divergence Mach number, but will not improve both. To improve both, the airfoil loading would have to be redistributed more efficiently along the chord, at the cost of increased nose-down pitching moments.

6) To have high drag divergence characteristics at low lift, an airfoil must be "peaky" and/or have surfaces with very large curvature about maximum thickness.

7) T.E. cusp and reflexed (nose-up) mean-lines move the aerodynamic center back, closer to the T.E., at a possible cost in premature turbulent separation.

8) On airfoils with low trailing-edge loading, breaks in lift, drag and pitching moment will occur within a small Mach number excursion of each other ($\Delta M \approx 0.05$).

Contour Variation Logic

Figure 5 illustrates the process of contour selection and modification used to design airfoils with emphasis on the first three design objectives. The method is not entirely suited for an automated optimization procedure. If the prescribed contour changes fail to modify the starting contour to meet the objectives, the method relies on the experience of the designer to provide a new starting configuration. However, this procedure would work well in modifying known airfoil contours to meet some specific sectional requirements. In absence of an automated airfoil modification and analysis procedure, the comparison of airfoil characteristics with all the design objectives was carried out only for a few intermediate contours. A fully automated design path would require provisions for the reassignment of priorities, or for some

modification of the objectives in the event that some of the objectives cannot be met (e.g., the maximum lift requirement at M=0.5).

Table IV lists several of the key characteristics of most of the airfoils and contour variations examined during the design study leading to the definition of the VR-11x, mod. 5, figure 6. Since most of the sections considered do not fit the standard NACA definitions, arbitrary designations were selected which bear no relation to any airfoil characteristics. A few of the contours have been included in figure 1A in the Appendix.

As illustrated in figure 7, the design procedure used to define the airfoils in the present report is based on limited contour variations starting from a known contour. This procedure offers the additional advantage of allowing continous correlation with some experimental data base. Basically, four well-documented airfoils were used as starting points:

- the V23010-1.58
- the VR-7, related to a NACA 62A512 (a=0)
- the VR-8, related to a NACA 62A208 (a=0)
- the NLR 7223-62 (or NLR-1)

The data on the first three sections is presented in reference 4. The NLR 7223-62 is documented in references 16 and 17. For each airfoil, selected modifications were carried out to determine whether the design objectives were within the range of the approach considered. The initial selection of starting contours was guided by the survey of maximum-lift and drag-divergence data shown in figure 3, thus eliminating nearly all existing airfoils as likely candidates for improvement. The only direct emphasis on unsteady aerodynamic effects was to require predominatly trailing-edge stall characteristics while searching for contour modifications which would improve the maximum lift at M=0.4.

Table IV, listing the candidate contours in the order in which they were considered, illustrates the overall design logic. It was verified that the V23010-1.58, the VR-7 and the VR-8 airfoils could not be altered to improve the maximum lift and drag divergence characteristics within the contour modification guidelines of figure 5. As shown in figure 3, the NLR 7223-62 airfoil is the only section with unusually high drag-divergence characteristics. The maximum lift capability of the NLR 7223-62 at M=0.4 is low compared to most current helicopter rotor airfoils, but it is higher than that of thin airfoils with comparable drag-divergence characteristics.

Successive, separate variations were made in thickness, camber and trailing edge curvature. The maximum lift capability of the NLR 7223-62 was increased to near the $C\ell_{MAX}$ = 1.5 objective at M=0.4, while the pitching moment level was maintained within design requirements. The zero-lift drag divergence characteristics were considerably reduced with respect to the level of the original thin section, but the final VR-11x configurations all have a drag-divergence Mach number above 0.8. The VR-11X, mod.5, is the first contour to come close to meeting the first four design objectives.

Since the starting airfoil-modification process involves mainly mean-line and thickness changes, no attempt was initially made to refine the VR-11x, mod. 5. Instead, this airfoil was analyzed in detail over the entire range of Mach numbers from M=0.3 to M=0.95 to determine its limitations and to verify whether such contour would also meet the second and third order priorities. As already pointed out, this was not the case. The process, however, led to the identification of the problems associated with a contour over-optimized for $C\ell_{max}$ and M_{DD_O}. Subsequently, contour modifications 6 through 10 were defined and analyzed at key conditions to determine the feasibility and direction of additional improvements.

The optimization process is not yet completed. Further sectional performance gains are possible through:

- Wind tunnel tests of means to delay turbulent separation and reduce lower surface leading edge velocities.
- Analysis methods including separated wake modeling.
- Use of direct and inverse airfoil solutions to carry out small contour changes on the basis of local flow requirements.

Design Methods and Correlation

The theoretical tools available to the airfoil designer can be separated into two categories: (a) subcritical, and (b) supercritical flow analyses. Viscous and inviscid flow solutions have been defined for each case. Such solutions are valid only in absence of separated flow, but the validity of the methods can be extended to small separated regions through careful correlation with test data. Since the present methodology does not account for shock/boundary-layer interaction effects, the techniques described in this report cannot be used in the exact evaluation of any of the high speed design objectives.

The airfoil solutions available to date are summarized in reference (4). A new development in separated flow analysis, which will have a significant impact on airfoil design methods, is presented in reference (18). The airfoil solutions used in carrying out the work described in this report are the subcritical potential-flow/boundary-layer interaction method of reference (11), and the viscous transonic flow analysis of reference (12). Both computer codes are available through NASA.

The following text describes how existing methods can be used to predict the airfoil characteristics required by each of the design objectives. Where meaningful, numerical examples and correlation with test data will be presented. A summary of theoretical values for several known airfoils is shown in table V. Such values should be compared with the test levels of table II to understand the limitations of the theoretical prediction techniques.

1. Low-Speed Pitching Moments. Design objective (1) requires a specific zero-lift pitching-moment level at M=0.3. The zero-lift level is a convenient reference value because at $C_\ell=0$ the pitching moment is a pure couple. Thin airfoil theory can be used very effectively to predict the low-speed pitching moments. It has been used extensively in the past in conjunction with superposition methods, such as described in reference 19, to evaluate combinations of NACA mean-line and thickness shapes. At present, such a method is used less frequently.

Potential-flow/boundary-layer methods can accurately predict the low speed pitching moments of airfoils as long as no separation is present. In presence of separation theory overpredicts the pitching moments by an error as large as $\Delta C_m = 0.01$ (although generally the error is less than $\Delta C_m = 0.005$). The NLR 7223-62 displays the worst correlation between theory and test, but in this case the test level is probably slightly off because of instrumentation limitations in the model, as reported in reference (16). An improvement in correlation will be possible when separated flow methods, reference (18), are available. Until then, some improvement in correlation could be obtained by assuming that the pressure inside a small separated region is constant and identical to the value at separation. A separated region can be assumed to be small (for purposes of maximum lift prediction) if it does not extend forward of the x/c = 0.85 to 0.9 chordwise location; however, in order to be acceptable an airfoil must not display any separation at low lift.

2. Maximum Lift at M=0.4. As discussed in references (2) and (13), the ability to predict the maximum lift of an airfoil at M=0.4 has been a crucial requirement in helicopter airfoil design efforts. On Boeing Vertol rotor systems, for example, the maximum lift at M=0.4 has been shown to be a necessary, but not sufficient, prerequisite for rotor improvement through airfoil modification.

The identification of the type of stall cannot be considered independently of the efforts to improve the maximum-lift characteristics of a section. This is necessary because the lifting capability of an airfoil can only be improved through a detailed knowledge of the separated flow phenomena which limit its useful range. The three basic types of stall possible at subcritical flow conditions are:

- Trailing-edge stall
- Leading-edge stall
- Thin-airfoil stall

Of the three types, trailing-edge stall can be predicted with the greatest confidence, although such prediction is based on observations of incipient flow separation and present analysis methods do not include a separated wake model. The possibility of leading-edge stall and the resulting maximum lift level have been correlated with the attainment of a maximum value of the local Mach number at the leading edge. Test data on airfoils reported in reference (4) and the observations of reference (20) indicate that a good approximation of such critical value is $M_{\ell}=1.4$.

Thin airfoil stall and the maximum lift associated with it cannot be predicted because an adequate representation of the laminar separation bubble typical on thin airfoils has not been yet defined. At present, airfoil analysis methods including boundary-layer calculations predict the conditions for separation of the laminar boundary layer, but then zero bubble-length is assumed and empirical information is used to determine whether reattachment is likely or not. In the event that reattachment is expected, the calculations are continued downstream of the laminar separation point with a turbulent boundary layer. However, since thin airfoils do not have a high maximum lift capability, the proper assessment of thin airfoil stall is not critical to the attainment of present design objectives.

Some methods of predicting maximum lift relate the maximum local Mach number and the turbulent separation point to stall. Figures 8 and 9 show the lift characteristics of the VR-7 airfoil, with 0° and -6° T.E. tab angles respectively, as measured in a test and as calculated with the method in reference (11), at M=0.4. The theoretical data shown include the maximum attained local Mach number and the location of the upper-surface turbulent separation point. The maximum lift levels measured in the two-dimensional test section of BSWT can be matched on the theoretical lift curve by assuming that $C_{\ell_{max}}$ has been reached when

- the maximum local Mach number reaches a value of $M_\ell = 1.4$, or
- the turbulent separation point reaches the $x/c = 0.85$ chordwise station.

This approach obviously does not predict the correct stall angle, as it does not predict the changes in lift curve slope leading to maximum lift and stall. However, extensive correlation has been carried out with airfoils tested in the BSWT test section, and this simple approach correlates very well with experimental maximum lift values defined for $dC_\ell/d\alpha = 0.0$ or $C_d = 0.05$.

3. Drag Divergence Boundaries. The experimental drag-divergence Mach number boundary of an airfoil is determined by observation of the rate of change of the profile drag with free-stream Mach number at constant incidence. A generally accepted definition is the Mach number for which $dC_d/dM = 0.1$. The outboard portion of the advancing blade of a helicopter rotor in forward flight experiences low to negative lift at conditions near and beyond the drag divergence boundary of the blade sections. Therefore, the drag divergence Mach number at zero lift has been selected as a measure of the usefulness of an airfoil at blade tip.

The drag-divergence Mach number can be evaluated in two different ways:

1) by crest-line theory, using an incompressible and inviscid flow solution, reference (14).

2) by viscous transonic flow methods, reference (12).

Both methods yield answers which are conservative by approximately $\Delta M_{DD} = 0.02$, and such a value has been used to correct the theoretical levels to the level of data in the BSWT test section. Of the two methods, crest-line theory is by far simpler. Although it offers much less insight into the details of the flow, it is better suited for preliminary work requiring the evaluation of a substantial number of profiles. Crest-line theory is based on extensive correlation between incompressible/inviscid airfoil solutions and test data, as reported in reference (14). The key to the method is the observation that there is a predictable correspondence between experimental drag divergence boundaries and the free-stream Mach number for which the velocity at the crest of an airfoil in an inviscid flow solution first reaches the sonic condition (M_ℓ=1.0).

However, the drag-divergence Mach number boundary alone is not a sufficient measure of the performance of an airfoil at the onset of severe compressibility due to drag "creep". Profile drag can experience a form of drag "creep" at a rate dCd/dM<0.1 before the dCd/dM=0.1 level is reached. Drag creep can arise from two areas:

1) premature, slow growth of wave drag
2) premature trailing-edge separation.

The conditions for drag creep arising from premature wave drag can be predicted empirically by examining the shape of the incompressible/inviscid suction loops of an airfoil, obtained as illustrated below.

$$y'/c = (y/c)\cos\alpha + (1-x/c)\sin\alpha.$$

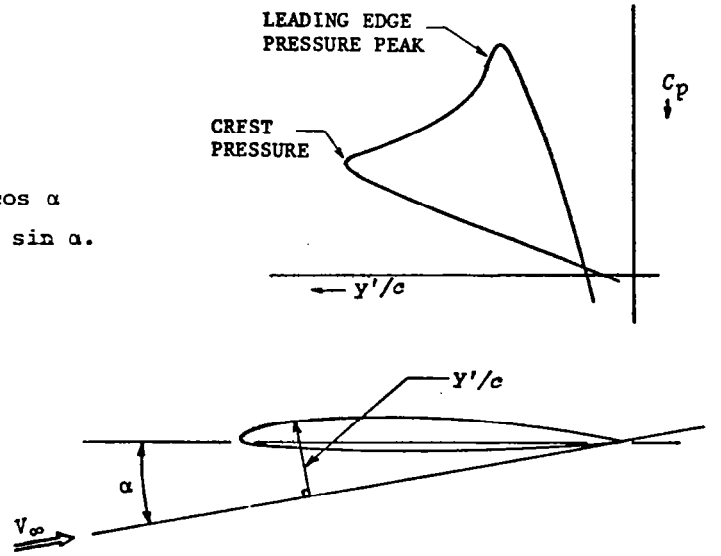

Reference (14) discusses in detail the guidelines through which drag creep and drag rise can be estimated. The key parameter is the rate of change of C_p with y'/c between the leading edge and the crest. At zero lift, the VR-11x, mod. 5, displays a "peaky" lower-surface suction loop, but the theoretical rate of recompression upstream of the crest is approximately $dC_p/d(y'/c)=12$, in excess of the recommended value of 10, which indicates that mod.5 is at best marginal in drag creep suppression at zero lift. At this time, it is not known whether drag creep on the VR-11x, mod. 5, can be eliminated without a penalty in maximum lift or drag-divergence Mach number. In fact, it might be desirable to accept some drag penalty in exchange for lift capability. As discussed later, it appears that some of the problems arising from the leading edge contour of the VR-11x, mod. 5, can be alleviated by increasing the lower-surface leading edge radius.

4. Compressibility Effects on the Pitching Moment at Subcritical Conditions. The fourth design objective of table I requires that the zero-lift pitching moment be restricted to $|C_{m_o}| \leq 0.015$ at Mach numbers up to M=0.7. Figure 10 shows a comparison between test and theoretical predictions for the reference airfoils of tables II and V. At Mach numbers below M=0.6, the recommended method is the potential-flow/boundary-layer analysis of reference (11). At Mach numbers above $M_\infty=0.6$, the subcritical flow solution is still applicable provided that the local Mach number is $M_\ell \leq 1.0$ everywhere, or at least that it does not exceed $M_\ell=1.0$ at the crest and $M_\ell=1.4$ at the leading edge. At zero lift, airfoils with camber and thickness comparable to the VR-11x can become limited by local Mach number criteria shortly beyond M=0.6, in which case it becomes necessary to use a transonic flow approach. However, the viscous transonic flow analysis of reference (12) has been only partly correlated with test data, and it is hard to use in predicting pitching moments. Difficulties in its use arise from the sensitivity of calculated pitching moments on a number of factors, ranging from the location of stimulated transition to control variables related to criteria built in the code. The presence of separated flow adds to the existing correlation difficulties.

During the present design study, the potential-flow/boundary-layer interaction analysis has been used up to M=0.7. At zero lift, the analysis showed local Mach numbers in excess of M_ℓ =1.4 within 0.5% of chord from the leading edge (compared to about 0.2% for the viscous transonic analysis). Pitching moment values from the subcritical analysis have been used to compare to this design objective because the overall level of the subcritical predictions agreed more consistently with the level of test data. It is possible that some airfoils

might suffer of a deterioration in pitching moment at Mach numbers below M_{DD} because of the same flow mechanism which produces drag creep.

5. Profile Drag at M=0.6, C_ℓ=0.6. From the point of view of viscous analysis methods, this flow condition does not involve any conceptual difficulties. At present, the potential-flow/boundary-layer interaction analysis is probably better suited for the task because of its versatility in boundary-layer transition options. Unfortunately, airfoils with the camber and T.E. contours required by the first priority design objectives have a strong predisposition for early T.E. separation. The drag coefficient values calculated by conventional boundary-layer analysis methods do not include the base drag arising from the separated portion of the airfoil surface. As long as the separated region is not so large that it would influence the velocity distribution upstream, it is a simple matter to correct the theoretical drag by an empirical drag increment. In reference (4), Hoerner suggests

$$\Delta C_d = k(C_d)^{-1/3} (h/c)^{4/3},$$

where C_d is the uncorrected drag coefficient, h/c is the thickness of a blunt trailing edge or the thickness of an airfoil at separation, and k is a constant which takes into account the character of the shed wake. Without a vortex street, which is generally the case at a lifting condition or at transonic speeds, a value of k=0.1 is recommended. In presence of organized vorticity, k=0.14.

A comparison of drag levels for a rotor airfoil, presented in figure 11, shows the predicted and measured lift-drag polars for the VR-7 with a 6° T.E. tab. The drag correction was estimated with a value k=0.1. The comparison of test levels and theoretical values for the drag coefficients in tables II and V is not meaningful without an insight into the sources of data. For example, figure 11 shows data for the VR-7 from two different tests run in wind-tunnels with a different level of turbulence in the test section. The drag increment due to separation accounts for the difference between theory (with natural transition) and the test data from the wind tunnel with the lower free-stream turbulence (BTWT). No verified methods are available at present to account theoretically for free-stream turbulence or surface roughness. The test data for the four reference airfoils considered in this study were obtained from one wind-tunnel facility (BSWT), and, therefore, the drag levels are directly comparable.

The theoretical drag values at subcritical flow conditions shown in this report have been calculated with the method of reference (11) prescribing natural transition from the laminar to the turbulent boundary layer. While airfoils can be best compared on the basis of natural boundary layer transition, the designer of helicopter airfoils is left with the burden of deciding how much laminar flow is possible on an actual rotor blade, so that performance calculations can be carried out with realistic profile drag values.

6. Maximum Lift Coefficient at M=0.5. Some airfoils with thickness ranging between 9% and 12% display an improvement in the maximum lift capability at M=0.5 over the M≤0.4 level. Before efficient transonic-flow analysis techniques became more generally available, Dr. Wortmann, reference (15), observed that airfoils taking advantage of beneficial transonic flow effects at high lift have an upper surface with a characteristics curvature distribution, although generally conforming to such distribution does not guarantee high lift.

In order to determine whether an airfoil can take advantage or not of beneficial transonic effects at high lift, it is necessary to evaluate the flow using both a subcritical and a transonic analysis. Table V shows the two estimated lift levels for airfoils such as the VR-7 and the NLR 7223-62 (NLR-1). A detailed comparison of the lift predictions for the VR-7 is shown in figure 12 together with test data from BSWT, reference (4). The subcritical analysis underpredicts the test level by a very considerable margin ($C_{\ell max}$=1.275 instead of 1.65), while the transonic flow analysis improves the prediction, $C_{\ell max}$=1.44, at least in part. The theoretical predictions for the NLR-1, in table V, show no benefit due to transonic effects, and such relatively low maximum lift, table II, was confirmed by test, reference (16). The maximum lift values from both subcritical and transonic flow analysis have been correlated with test data for:

- the attainment of a maximum local Mach number value of M_ℓ=1.4, and/or
- turbulent separation moving upstream to x/c=0.85 with increasing lift.

Initial correlation work shows that the maximum lift requirements at M=0.4 and M=0.5 are incompatible of each other, unless pitching moment and drag divergence requirements can be considerably reduced.

7. Effect of Lift on Low-Speed Pitching-Moment Characteristics. Objective (7) requires that

$$|C_m| \leqslant 0.02 \text{ at } M=0.3 \text{ and } 0 \leqslant C_\ell \leqslant 1.0$$

The comments made for the zero lift pitching moment (objective 1) apply here as well, except that greater em- emphasis must be placed on separation effects. Separation at the trailing edge is expected to be small at low lift levels. It will generally be more pronounced as the lift is increased because of the pitching-moment compensation techniques employed on helicopter airfoils. The discrepancy between theory and test can be $\Delta C_m < 0.01$ in absence of significant separation, but it can be much greater if the location of a turbulent separation is upstream of $x/c=0.95$. While the exact pitching-moment level in presence of lift is subject to some uncertainty, the pitching-moment band of objective (7) is sufficiently generous to make up for the lack in a more rigorous approach.

8. Drag Above Drag Divergence. The evaluation of the drag at conditions beyond the drag-divergence boundary requires transonic flow analysis. Although some empirical observations have been made, the guidelines for such observations remain largely qualitative. Figure 13 compares the drag of several airfoils at Mach number levels through and above drag divergence. The correlation between test and theory for the drag beyond M_{DD} is not yet well-documented and firm guidelines on the use of the viscous, transonic-flow analysis are not available at this time.

Part of the problem in evaluating the drag coefficient at a Mach number increment over drag divergence is the establishment of a reference level. As previously discussed, and as noted in reference (12), present methods to estimate drag divergence are conservative by $\Delta M_{DD} \approx 0.02$.

There are additional discrepancies in the level of drag between theory and test caused by differences in fixed transition locations. Transition for the test data in table II is now known.

9. Estimate of the Pitching Moment Break Boundary (Mach "tuck"). Design objective (9) restricts the onset of compressibility effects on the zero-lift pitching moments until after drag divergence. The growth of pitching moments at supercritical conditions can be evaluated only by means of a transonic flow analysis, such as the method of reference (12). Test and theory are compared in some detail in figure 10 for

the four reference airfoils. The pitching moment break, defined by the Mach number for which $dCm_o/dM = 0.25$, is subject to the same correlation problems as the drag divergence Mach number. The discrepancy between theory and test, (tables II and V) is also approximately $\Delta M_T = 0.02$.

Separation over the aft portion of airfoils influences the absolute pitching moment level before and after the onset of significant compressibility effects. The data shown in figure 10 for the NLR-1 indicate a nose-up peak in the pitching moment at $M \approx 0.86$. Such peak is probably due to the redistribution of upper and lower surface supersonic regions with increasing free-stream Mach number. This effect is hardly noticeable at all in the theoretical predictions, leaving some questions as to the significance of wind-tunnel wall effects, and as to the influence of a number of empirical control constants in the transonic analysis. The overall trends with present predictive methods seem to be correct, but considerable correlation work is necessary.

10. Zero Lift Pitching Moment Variation at Mach Numbers Below Drag Divergence. The evaluation of this objective presents no serious problems, but both subcritical and supercritical methods are necessary to cover the Mach number range from low speed to drag divergence. In comparing experimental and theoretical data it must be remembered that present theoretical methods yield drag divergence Mach number values which are conservative by $\Delta M_{DD} \approx 0.02$ with respect to test levels.

11. Gradual Stall Requirement for $0.3 \leq M \leq 0.4$. The original correlation work by Gault, reference (21), does not apply too well because at $M > 0.3$ compressibility effects are significant. The requirement for a specific stall character cannot be carried out separately from the contour modifications for maximum lift improvements and the comments in the section on maximum lift at $M = 0.4$ are applicable to the definition of stall requirements.

The importance of gradual stall characteristics is further emphasized by the data presented in figures 26 and 27, illustrating the relationship between quasi-steady stall and aerodynamic damping during forced-pitch oscillation. The test evidence indicates that when the quasi-steady stall characteristics are associated with substantial hysteresis effects, the aerodynamic damping can grow to large negative values during dynamic stall.

12. Profile Drag at $\Delta M = 0.1$ Below Drag Divergence. No difficulties, except for the comments on transition and separation already reported while discussing drag prediction at other conditions.

DESCRIPTION OF THE NEW AIRFOIL

As previously noted, the VR-11X, mod.5, contour has been defined through a series of contour modifications utilizing the NLR 7223-62 airfoil, reference (7), as the starting point. This airfoil is shown in figure 6. The theoretical predictions for the VR-11X, mod.5, are shown in table VI. The coordinates are shown in table VII, and table VIII lists the mean line and thickness distribution. The predictions have been carried out at two Reynolds number levels to explore Reynolds number sensitivity and to provide a basis for the evaluation of the potential of the new section with intermediate (0.43 m or 17 in) and large (0.68 m or 27 in) chords.

Since the definition of the VR-11X was carried out at the limit of the validity of presently available methods, several critical characteristics, such as $C_{\ell_{max}}$, M_{DD}, T.E. separation sensitivity, and drag-creep effects must be quantified experimentally. Test verification is necessary before the VR-11X can be utilized on helicopter rotor blades, and before further airfoil design work can be undertaken.

An outline of the airfoil design procedure has been presented in the section on design logic. The airfoil contours taken into consideration during the optimization process are listed in table IV, while figure 7 shows how several candidate airfoils approached two of the first priority objectives.

The following sections compare the predicted VR-11X characteristics to the design objectives, and then show the results of local and overall (thickness and camber) contour variations. Such variations were examined to determine contour sensitivity and to place the VR-11X, mod.5., within a family of affinely related airfoil shapes.

First Priority Objectives
(Objectives 1 through 4)

The first priority objectives have been met fairly closely at both Reynolds number levels (0.43m and 0.68m chords). Since the maximum lift objective at M=0.4 has been probably exceeded when the estimated test/theory correction is applied, the VR-11x, mod.5, could be slightly decambered to reduce the excess $C_{\ell_{max}}$ by -0.025 to -0.03. Such reduction would benefit the other three priorities, but this was not attempted because the changes involved are small and within possible test/theory correlation error.

Second Priority Objectives (Objectives 5 through 8)

Priority (5), dealing with the profile drag at lift and Mach number levels for hover, cannot be assessed accurately. Limited knowledge of the extent of trailing edge separation and of the impact of separation on drag introduce uncertainty. At Rn = 6 x 10^6, the profile drag not including separation effects is C_d = 0.0078. By including the effect of turbulent separation at x/c = 0.944 with previously described methods, the profile drag estimate is increased to C_d = 0.0102. However, the final drag values can be verified only experimentally because theory does not take into account the influence of separated flow on conditions upstream of separation. With increasing Reynolds number, the theoretical profile drag is reduced to C_d = 0.007 without separation, and to C_d = 0.0094 including separation. This illustrates the fact that the performance of airfoils such as the VR-11X, mod.5, is strongly influenced by the Reynolds number, so that a careful verification of separation effects must be carried out for each application.

Design objective (6), requiring a maximum lift coefficient of 1.5 at M=0.5, cannot be achieved. $C_{\ell_{max}}$ = 1.3 is probable, and such a value is an improvement over most of the airfoils listed in table III. Theory indicates moderate gains in lifting capability attributable to beneficial transonic flow effects but in this case an accurate maximum lift value can be determined only in a wind tunnel.

The trend of the data shown in figure 4 indicates that the present maximum lift requirement at M=0.5 is totally incompatible with the drag-divergence and low-speed pitching-moment objectives.

The seventh objective ($|C_m| \leq 0.02$ at C_ℓ=1.0 and M=0.3) can be easily achieved because the VR-11X, mod.5, has the low-speed aerodynamic center ahead of the quarter chord ($x_{a.c.}/c$= 0.23 to 0.24). The forward aerodynamic center location in all probability cannot be avoided, although this is generally considered an undesirable design feature because of the stability requirement that the center of gravity be located forward of the aerodynamic center. The problems associated with the weight penalties due to a forward c.g. placement on a conventional rotor blade and the load, stability, and control problems arising for the a.c./c.g. relationship are beyond the scope of this study, but they remain a serious issue.

The drag beyond drag divergence, objective (8), could not be met. Existing sections (see table III) and the sections reviewed during the present study, table V, cannot meet it.

Third Priority Objectives
(Objectives 9 through 12)

Delaying the pitching-moment break (Mach tuck) until after drag divergence, objective (9), can be easily achieved. If necessary, final adjustments can be made during two-dimensional testing through small trailing-edge contour changes. The same applies to the pitching-moment levels of objective (10).

The requirement for graudal stall at M=0.3 and 0.4, objective (11), has been met because the VR-11X, mod.5, develops trailing edge separation at high lift levels before leading-edge velocities become critical. An analysis covering all the elements of the flow,including the separated wake, is not available at this time. Therefore, the stall character can only be judged from the theoretical trends as the analysis is carried to high lift levels, at the limit of the range of validity of present methods.

The analysis used in this study (reference 11) predicts a significant predisposition for turbulent separation by the VR-11X, mod.5. However, the extent to which the prediction is quantitatively accurate remains to be verified. By unseparated flow analysis, the velocities at the trailing edge and the location of turbulent separation can be changed significantly with small T.E. contour changes, but such changes cannot be as large in real flow because of the shielding effect of the boundary layer and of separated flow regions.

Design objective (12) quite probably cannot be met with airfoils employing T.E. reflex or other T.E. devices. Such devices produce drag penalties due to separated flow. An additional obstacle is that airfoils optimized for high lift typically develop high lower surface velocities near the leading edge which do not allow the drag to remain small at low, or negative, lift conditions.

CONTOUR MODIFICATIONS

There are two reasons to study the effect of possible airfoil modifications. First, because an airfoil should be viewed as a shape representative of an entire family of affinely related shapes; second, as a review of the weaknesses of a contour leading to the definition of airfoils with improved characteristics.

Basic Airfoil Variations

An approximate mean-line and a thickness shape are defined in table VIII. Thickness and camber have been derived by

assuming that the thickness is distributed along constant x/c lines and not along lines locally perpendicular to the mean-line. Such approximation is satisfactory as long as a mean-line does not display large variations in curvature, as is the case with either substantial camber or very blunt leading edges. Unfortunately, "peaky" airfoils have blunt leading edges, and in such case variations in thickness and camber require the verification and maybe the adjustment of the leading edge curvature on the basis of "suction loop" considerations, reference (14).

Simple modifications are possible by direct scaling of camber and thickness. Airfoils affinely related to the VR-11x (mod.5) can be obtained by scaling and thickness by:

$$Y_t/c = (Y_t/c)_1 \ (t/c)/0.11$$

where t/c is the new required thickness, and $(y_t/c)_1$ is the thickness distribution of the VR-11x, mod. 5, airfoil.

A new camber can be defined by:

$$Y_c/c = (Y_c/c)_1 \ Y_{c_{max}}/0.024165$$

expressed in terms of a new maximum camber as a fraction of chord, $Y_{c_{max}}$, where $(Y_c/c)_1$ is the mean-line of the VR-11x, mod. 5.

The effect of concurrently scaling the mean-line and thickness of the VR-11x, mod. 5 from 8% to 13% is shown in table IX. Only the low speed C_{m_o}, $C_{\ell_{max}}$ at M=0.4 and MDD_o have been evaluated. The coordinates are listed in Tables I-A and II-A in the Appendix. The thin versions of the VR-11x, closely related to the NLR 7223-62, have attractive drag divergence characteristics which make them suitable for use at the tip of rotor blades.

Local Contour Changes

The VR-11x, mod. 5, was defined to determine how closely it is possible to meet the design objectives in table I, while retaining most of the originally assigned order of design priorities. Since the hover drag requirements were among the second order priorities, the emphasis of the design was focused on maximum lift and drag divergence characteristics. Nevertheless, some effort was devoted to reducing premature turbulent separation since it caused a small but significant drag penalty at all but the lowest lift levels.

The VR-11x, mod. 6, with coordinates in table X, was defined to delay turbulent separation from the trailing edge without a significant penalty in first-order priority characteristics. The contour modification was achieved by filling in some of the

upper-surface T.E. cusp of the VR-11x, mod. 5, and by adding some lower-surface curvature to maintain most of the pitching moment compensation. The characteristics of the VR-11x, mod. 6, are compared to those of mod. 5 in table XI. As it can be seen, the zero-lift pitching moment grew to a larger nose-down value than for mod. 5.,also, although the theoretical value is still within the objective, the test level is probably below $C_{m_o} = -0.01$. The corrected maximum lift at M=0.4 is acceptable and the drag divergence is only slightly changed. Objective (4) is not entirely met by the VR-11x, mod. 6, but the discrepancy, if confirmed, is within correctable range. The significant difference between mod. 5 and mod. 6 is in the drag level at the hover conditions. The turbulent separation over the VR-11x, mod. 6, has been substantially delayed so that the drag level is $C_d = 0.0078$ instead of $C_d=0.0094$ for mod. 5, at the hover point, for $Rn=9x10^6$. No improvement was obtained at $Rn=6x10^6$.

The study of other small T.E. variations was not carried out at this time. Since small T.E. contour changes cause theoretically large effects of dubious physical significance, the final T.E. configuration cannot and should not be defined entirely through analysis. The only theoretical method to meaningfully continue the study along this line would be the analysis of reference (18), but such method is not presently available.

Future work with the VR-11x, mod. 5, should attempt to deal with upper-surface separation. The upper surface is flat over an extensive portion of the chord, and it is deflected abruptly at about 75% of chord to meet trailing-edge thickness requirements. This causes the flow to slow down at too fast a rate before reaching the T.E., with the resulting premature turbulent separation. The approach tried in mod. 6 was to reduce the upper-surface cusp at the trailing edge. A better method would be to give up some of the flat upper surface and cause the flow to slow down more gradually. This can be accomplished at some cost in M_{DD} and maximum lift capability, as demonstrated by the VR-11x modifications 8 and 10.

A second area of potential problems is the very small radius on the lower-surface leading edge. This causes severe separation effects at negative lift levels, particularly at supercritical flow conditions. As pointed out in reference (22), this could also cause severe impulsive noise in high speed forward flight. The VR-11x, mod. 5 or mod. 6 airfoils are not recommended for use at the rotor tip, although they might be adequate up to 85% or 90% of span. A lower-surface modification of the leading edge has been examined through the VR-11x, mod. 9 and mod. 10, as part of the assessment of the impact of contour errors.

The coordinates of VR-11x mods. 8, 9 and 10 are shown in table XII. Key characteristics of mods. 5 through 10 are compared in table XIII for Rn = 10^7 x M. A detailed comparison at selected angles of attack for M=0.4, Rn = 4 x 10^6 is shown in table XIV.

The upper surface modification between x/c = 0.60 and 0.88, mod. 8, illustrates the effect of prescribing a more gradual transition from the upper surface to the trailing edge. Mod. 8 produced no beneficial effects at the Rn = 10^7 x M level, at some cost in drag divergence; it was considerably less successful than mod. 6 in delaying trailing-edge separation at $C_\ell \simeq 0.6$. Mod. 9 increases the lower surface radius at the leading edge of the VR-11x, mod. 5 with small overall results. Mod. 10 is a combination of mod. 8 and mod. 9. This contour change is moderately successful in delaying separation at M = 0.4, although it is not useful at M = 0.6.

A wind tunnel test comparison of the VR-11x, mod. 5 and mod. 10 airfoils would provide the experimental evidence necessary (a) to quantify the weaknesses of the mod. 5 contour, and (b) to determine the feasibility of improving the sectional performance of mod. 5 with the least compromise in the first priority objectives.

EFFECT OF CONTOUR ERRORS

Two leading-edge contour error conditions have been examined at M = 0.4 and M = 0.6. These representing additional upper and lower surface leading edge bluntness. The aerodynamic characteristics of the VR-11x, mod. 5, with and without such deviations are summarized in table XV. The modified leading-edge coordinates describing these contour errors are listed in table XVI. The errors involve an additional buildup of material at the leading edge amounting to 0.38 mm, for a chord of 0.432 m, at the point of maximum deviation, and they caused no detrimental effects to the VR-11x, mod. 5, performance. In one case, the maximum lift capability at M=0.4 was actually slightly improved.

The effect of trailing-edge contour errors can be deduced from a comparison between the VR-11x, mod. 5, and mod. 6. At least theoretically, these airfoils appear to be quite sensitive to trailing-edge contour variations because of their pre-disposition for the separation of the turbulent boundary layer, but theory overpredicts both the sensitivity to separation and the effect of small contour changes on the pitching moment.

The effect of a small surface disturbance which would cause premature transition is shown in table XVII. Such data was obtained by prescribing the transition from laminar to turbulent flow to take place no further downstream than 30% of chord. Such condition is representative of the surface discontinuities which often take place between the leading edge spar and the trailing edge elements on production rotor blades.

ESTIMATED CHARACTERISTICS OF THE NEW AIRFOIL

Plots of lift, drag and pitching moment coefficients of the VR-11x, mod. 5 and mod. 6 airfoils are presented in figures 14 through 24. The data was estimated using the methods of references (11) and (12) at two Reynolds number levels, $Rn=10^7 \times M$ and $Rn=1.5 \times 10^7 \times M$, over a Mach number range from M=0.3 to M=0.95. All relevant comments are shown in the figures. At M=0.95 the viscous transonic analysis for the VR-11x, mod. 5, contour did not converge at $Rn=9.5 \times 10^6$, while no problems were encountered at $Rn=14.2 \times 10^6$. No difficulties were encountered in the calculation of the characteristics of the VR-11x, mod. 6, but complete data were evaluated only for the $Rn=10^7 \times M$ level. Typical pressure distributions for the VR-11x, mod. 5, are shown in figure 19.

CONCLUSIONS AND RECOMMENDATIONS

1) The first priority objectives can be met, though marginally.

2) The maximum lift requirement at M=0.5 is incompatible with the drag-divergence and pitching-moment objectives.

3) The profile drag characteristics of the VR-11x, mod. 5, are adversely influenced by a small amount of premature T.E. separation. The true extent of such separation and the means to suppress it cannot be established analytically.

4) The lower-surface L.E. radius on the VR-11x, mod. 5, is too small and should be modified to reduce L.E. velocities at small positive and negative lift levels.

5) Theory is optimistic in predicting nose-up pitching moment corrections, although a large discrepancy with test data is probably due to test problems.

6) Although the viscous, transonic flow analysis appears to give excellent overall results, more detailed correlation work is necessary before it can be clearly used as an airfoil design tool at conditions of interest in helicopter applications.

7) Additional contour changes should be derived through pressure distribution modification by inverse airfoil solutions.

8) The maximum lift boundaries, the drag-divergence characteristics, the premature separation and drag creep problems should be quantified and, where necessary, improved upon experimentally.

REFERENCES

1) Davenport, F. J., and Front, J. V.; Airfoil Sections for Rotor Blades - A Reconsideration. Presented at the 22nd Annual Forum of the American Helicopter Society, Washington, D.C., May 12, 1966.

2) Dadone, L. U., and Fukushima, T.; A Review of Design Objectives for Advanced Helicopter Rotor Airfoils. Presented at the AHS Symposium on Helicopter Aerodynamic Efficiency, (Hartford, Connecticut), March 1975.

3) Sloof, J. W., Wortmann,F. X., Duhon, J. M.; The Development of Transonic Airfoils for Helicopters. Presented at the 31st Annual National Forum of the American Helicopter Society, Washington, D.C., May 1975.

4) Dadone, L. U.: U.S. Army Helicopter Design Datcom, Volume I - Airfoils. NASA CR-153247, 1976.

5) Tetervin, N.; Tests in the NACA Two-Dimensional Low-Turbulence Tunnel of Airfoil Sections Designed to Have Small Pitching Moments, and High Lift-Drag Ratios, NACA Report L-452, originally issued in September 1943 as C.B. 3I13.

6) Stivers, L. S., Jr., and Rice, F. J., Jr.; Aerodynamic Characteristics of Four NACA Airfoil Sections Designed for Helicopter Rotor Blades. NACA Report L-29, originally issued as R.B. L5K02, February 1946.

7) Gross, D. W., and Harris, F. D.; Prediction of Inflight Stalled Airloads from Oscillating Airfoil Data. Presented at the 25th Annual National Forum of the American Helicopter Society, May 1969.

8) Liiva, J., Davenport, F. J., Gray, L., and Walton, I.D.; Two-Dimensional Tests of Airfoils Oscillating Near Stall. U.S. Army AVLABS TR 68-13, 1968.

9) Gray, L., Liiva, J., and Davenport, F. J.; Wind Tunnel Tests of Thin Airfoils Oscillating Near Stall. USAAVLABS TR 68-89A, 1969.

10) Gray, L., Dadone, L. U., Gross, D. W., and Child, R. F.; Wind Tunnel Investigation of Airfoils Oscillating in Reverse Flow. USAAVLABS TR 70-4.

11) Stevens, W. A., Goradia, S. H., and Braden, J. A.; Mathematical Model for Two-Dimensional Multi-Component Airfoils in Viscous Flow. NASA CR-1843, July 1971.

12) Bauer, F., Garabedian, P., Korn, D., and Jameson, A.; Supercritical Wing Sections II. Lecture Notes in Economics and Mathematical Systems, Volume 108, Springer-Verlog (New York), 1975.

13) Benson, R. G., Dadone, L. U., Gormont, R. E., and Kohler, G.R.; Influence of Airfoils on Stall Flutter Boundaries of Articulated Helicopter Rotors. Presented at the 28th Annual Forum of the American Helicopter Society, Washington, D.C., May 1972.

14) A Method for Estimating Drag-Rise Mach Number for Two-Dimensional Aerofoil Sections. R. Ae. S. T.D. Memo 6407, 1964.

15) Wortmann, F. X., and Drees, J. M.; Design of Airfoils for Rotors. Paper presented at CAL/AVLABS 1969 Symposium on Aerodynamics of Rotary Wing and VTOL Aircraft.

16) Dadone, L. U.; Two-Dimensional Wind-Tunnel Test of an Oscillating Rotor Airfoil. NASA CR 2914 and 2915, September 1977.

17) Kemp, L. D.; An Analytical Study for the Design of Advanced Rotor Airfoils. B.H.C: Report No. 299-099-635, NASA CR-112297, March 29, 1973.

18) Maskew, B., and Dvorak, F. A.; Investigation of Separation Models for the Prediction of $C_{\ell max}$. Presented at the 33rd Annual National Forum of the American Helicopter Society, Washington, D.C., May 1977.

19) Abbott, I. H., vonDoenhoff, A. E.; Theory of Wing Sections. Dover Publications, Inc., New York, New York, 1958.

20) Lindsey, W. F., and Johnston, P.J.; Some Observations on Maximum Pressure Rise Across Shocks Without Boundary-Layer Separation on Airfoils at Transonic Speeds. NACA TN 3820, November 1956.

21) Gault, D. E.; A Correlation of Low-Speed, Airfoil-Section Stalling Characteristics with Reynolds Number and Airfoil Geometry. NACA TN 3963, March 1957.

22) Tangler, J. L.; Schlieren and Noise Studies of Rotors in Forward Flight. Presented at the 33rd Annual National Forum of the American Helicopter Society, Washington, D.C., May 1977.

Table I. Priority List od Aerodynamic Characteristics.

	FIRST PRIORITY	SECOND PRIORITY	THIRD PRIORITY
LIFT	2.) $C_l \geq 1.5$ AT M = 0.4 $\frac{dC_l}{d\alpha} = 0$	6.) $C_l > 1.5$ AT M = 0.5 $C_d = 0.05$	11.) GENTLEST POSSIBLE STALL AT $0.3 \leq M \leq 0.4$
DRAG	3.) $M_{DD} \geq 0.81$ AT $C_l = 0$	5.) $C_d \leq 0.008$ AT M = 0.6 $C_l = 0.6$ 8.) $C_d \leq 0.01$ AT $M = M_{DD} + 0.02$ $C_l = 0$	12.) $C_d \leq 0.007$ AT $M \leq M_{DD} - .1$ $C_l = 0$
PITCHING MOMENT	1.) $C_m \leq 0.010$ AT M = 0.3 $C_l = 0$ 4.) $C_m \leq 0.015$ AT $M \leq 0.015$ $C_l = 0$	7.) $C_m \leq .02$ AT M = 0.3 $0 \leq C_l \leq 1.0$	10.) $.01 \geq M^2 C_m \geq -0.04$ AT $M \leq M_{DD}$ $C_l = 0$ 9.) $M_T \geq M_{DD}$

NOTE: M_T = M at $\frac{dC_m}{dM} = 0.25$, $C_l = 0$

M_{DD} = M at $\frac{dC_d}{dM} = 0.1$, constant C_l

Table II. Complete Review of the Performance of Five Rotor Airfoils.

#	OBJECTIVE	TEST DATA V23010-1.58 0° TAB	VR-7 -6° TAB	VR-8 0° TAB	NLR-1	FX69-H -098
1	Cm_o at M=0.3	-.009	+.009	-.011	-.02	-.01
2	$C\ell_{MAX}$ at M=0.4	1.46	1.41	1.04	1.1	1.25
3	M_{DD_o}	0.79	0.731	0.811	0.85	0.80
4	Cm_o at M=0.7	-.007	+.003	-.013	-.02	-.026
5	Cd for $C\ell$=.6 and M=.6	0.0104	0.0085	0.0070	0.008	0.007
6	$C\ell_{MAX}$ at M=0.5	1.22	1.51	1.060	1.08	1.33
7	Cm at $C\ell$=1.0 and M=0.3	-.021	-.020	-.024	-.010	-.020
8	Cd_o at $M=M_{DD}+0.02$	0.0165	0.020	0.0204	0.018 (0.015)	0.0125
9	M_T at $C\ell$=0	0.795	0.77	0.79	>0.85(?)	.825
10	M^2Cm_o at M_{DD_o}	-.0081	0.0	-.0191	.014	-.0225
11	Type of Stall at M=0.3 M=0.4	L.E. L.E./T.E.	Weak L.E. T.E.	Thin Airf. Thin Airf.	L.E. T.E.	L.E. L.E.
12	Cd_o at M_{DD}-0.1	0.0098	0.0085	0.0076	0.0078	0.007

Table III Test Levels.

Ref. No.	Airfoil	C_{m_o} at M = 0.3	$C_{\ell,max}$ at M = 0.4	M_{DD_o}	C_{m_o} at M = 0.7	C_d for C_ℓ = 0.6 M = 0.6	$C_{\ell,max}$ at M = 0.5	C_m at C_ℓ = 1.0 M = 0.3
1	NACA 0006	0.0	0.96	0.875	0.0	0.015		-0.13
2	NACA 0012	0.0	1.08	0.765	0.0	0.0122	0.967	+0.01
6	NACA 0015	0.0	0.99	0.740	0.0	0.0132	0.920	+0.005
7	NACA 23012	-0.01	1.38	0.795	-0.013	0.029	1.22	0.004
8	NACA 23012 .043c T.E.TAB	-0.0075	1.42	0.780	-0.010	0.029	1.28	-0.008
9	NACA 23012 .087c T.E.TAB	-0.005	1.42	0.780	-0.009	0.029	1.28	-0.009
10	NACA 23015	-0.01	1.30	0.720	-0.008	0.0138	1.08	0.0
11	NACA 63A009	0.0	0.87	0.805	0.0	0.0137	0.70	--
12	NACA 63A012	0.0	0.85	0.770	0.0	0.011	0.78	--
14	NACA 63A015	0.0	1.01	0.740	0.0	0.011	0.9	0.002
15	NACA 63A018	0.0	1.00	0.725	0.0	0.015	0.87	0.022
16	NACA 64A(4.5)08	-0.095	1.23	0.752	-0.126	0.007	1.15	-0.092
17	NACA 64A608	-0.13	1.4	0.755	-0.212	0.006	1.37	-0.129
18	NACA 64A312	-0.065	1.29	0.758	-0.085	0.0074	1.21	-0.066
19	NACA 64A(4.5)12	-0.095	1.43	0.735	-0.13	0.0085	1.38	-0.095
20	NACA 64A612	-0.125	1.45	0.69	-0.17	0.0080	1.50	-0.122
21	NACA 64A516	-0.102	1.47	0.685	-0.139	0.0089	1.41	-0.10
23	V13006-0.7	-0.012	0.97	0.865	-0.012	0.0075	0.97	-0.012
24	V(1.9)3009-1.25	-0.012	1.225	0.815	-0.015	0.0084	1.12	+0.002
25	V23010-1.58 0° T.E.TAB	-0.009	1.46	0.79	-0.007	0.0104	1.22	-0.021
26	V23010-1.58 -3° T.E.TAB	0.006	1.42	0.77	0.008	0.011	1.18	-0.006
30	V43012-1.58 0° T.E. TAB	0.001	1.665	0.65	0.0		1.21	-0.033
31	V43012-1.58 -6° T.E.TAB	0.022	1.55	0.639	---		1.145	-0.004
32	SA13109-1.58	0.0	1.05	0.825	0.005	0.0102	0.96	0.001
33	NPL9615	-0.009	1.17	0.785	-0.012	0.0116	1.10	-0.001
36	NPL9660	-0.006	1.18	0.792	-0.008	0.0114	1.15	-0.011
37	NACA CAMBRE'	-0.012	1.26	0.79	-0.015	0.011	1.14	0.0
38	VR-7(0° TAB)	-0.025	1.50	0.742	-0.04	0.0081	1.65	-0.048
39	VR-7(-3° TAB)	-0.007	1.46	0.7365	-0.0175	0.0084	1.57	-0.035
40	VR-7 (-6° TAB)	+0.009	1.41	0.731	+0.003	0.0085	1.51	-0.02
41	VR-8 (0° TAB)	-0.011	1.04	0.811	-0.013	0.007	1.060	-0.024
43	FX69-H-098	-0.01	1.25	0.80	-0.026	0.007	1.33	-0.020
	NLR7223-62	-0.02	1.10	0.85	-0.02	0.008	1.08	-0.010
	VOO11		1.26	(0.80)			1.07	
	VR-1	-0.035	1.2	0.792	-0.046	0.0074	1.04	-0.022
	DESIGN OBJECTIVE	-.01 to .01	1.5	0.81	-0.015	0.008	1.5	-0.02

Table IV Theoretical Predictions (Not Corrected).

Ref. No.	Airfoil	C_{m_o} at M = 0.3	C_{ℓ} max at M = 0.4	M_{DD_o}	C_{m_o} at M = 0.7	C_d for C_{ℓ} = 0.6 M = 0.6	C_{ℓ} max at M = 0.5	C_m at C_{ℓ} = 1.0 M = 0.3
70	62-410 (a = 0) 0° TAB	-.02	1.26	.741				-.022
71	62-410-1.0 0° TAB	-.02	1.23					-.023
72	62-410 1	-.01	1.25					-.0123
73	62-410 2	-.014	1.25					-.018
74	62-410 3	-.006						-.0126
75	B1	-.025	1.445	.752				-.034
76	B2 (0° TAB)	-.0053	1.36	.761		.0071	1.155 1.29*	-.012
77	B3	-.035	1.475	.738				
78	12% NLR-1	-.0152	1.445	.783	-.023	.009	1.162 1.2*	-.011
79	VAR-A-8.3	-.014	1.06	.803				-.015
80	VAR-A-10	-.017	1.21	.779		.0075	1.025	-.02
81	VAR-A-12	-.0208	1.375	.751		.0075	1.13	-.0248
82	NLR-1 (10.2%)	-.013	1.265			.008	1.050	-.011
83	VAR-B-10.2	-.0108	1.330			.008	1.075	-.0135
84	78-T.E. Mod. 1	+.0085	1.435		+.0101	.0074	1.145	+.002
85	11% Incr.Camb	-.037	1.530					-.035
86	85-T.E. Mod.	-.013	1.530			.007	1.27	-.021
87	78-T.E. Mod. 2	-.0116	1.437	.787		.009	1.147	-.0043
88	85-Mod. 2	-.0063	1.518	.783	-.01	-.007	1.242	-.013
89	85-Mod. 3	-.0105	1.495	.787	-.0156	.0072	1.23	-.009
90	VR-11X, Mod. 2	-.003	1.445	.794	-.006	.007	1.190	-.009
91	85-Mod. 4	-.029	1.605	.789				-.044
92	VR-11X-1	-.0256	1.605	.789				-.04
93	VR-11X, Mod. 5	-.007	1.492	.785	-.0113	.007	1.225 1.280*	-.0053
93A	VR-11X, Mod. 5	-.0079	1.485	.785	-.015	.0078	1.225	-.0042
94	VR-11X, Mod. 6	-.0085	1.47	.786	-.017	.007	1.20	-.006
94A	VR-11X, Mod. 7 VR-11X, Mod. 8 VR-11X, Mod. 9 VR-11X, Mod. 10	-.01	1.47	.786	-.022	.0078	1.20	-.0025

(*) Viscous Transonic Flow Solution

FEDD DOCUMENT

Note that this document bears the label "FEDD," an acronym for "FOR EARLY DOMESTIC DISSEMINATION." The FEDD label is affixed to documents that may contain information having high commercial potential.

The FEDD concept was developed as a result of the desire to maintain U.S. leadership in world trade markets and encourage a favorable balance of trade. Since the availability of tax-supported U.S. technology to foreign business interests could represent an unearned benefit, research results that may have high commercial potential are being distributed to U.S. industry in advance of general release.

The recipient of this report must treat the information it contains according to the conditions of the FEDD label on the front cover.

Table V Theoretical Predictions for Four Rotor Airfoils. (Levels of data not corrected)

#	OBJECTIVE	THEORETICAL PREDICTION V23010-1.58 0° TAB	VR-7 -6° TAB	VR-8 0° TAB	NLR-1
1	C_{m_o} at M=0.3	-.0093	.02	-.00865	-.01
2	$C_{\ell_{MAX}}$ at M=0.4	1.4	1.37	.965	1.122
3	M_{DD_o}	0.77	0.707	.785	0.827
4	C_{m_o} at M=0.7	-.0133	≈ .023	-.013	-.016
5	Cd for M=0.6 and M=0.6	0.007	.007	.007	.0075
6	$C_{\ell_{MAX}}$ at M=0.5	1.15	1.2	.802	.965
7	Cm at C_ℓ=1.0 and M=0.3	-.015	.006	-.0145	-.009
8	Cd_o at $M=M_{DD}+0.02$	0.0175		0.0087	0.012
9	M_T at $C_\ell=0$	>.81		.81	.835 (>.85?)
10	$M^2 C_{m_o}$ at M_{DD_o}	-.0092		-.009	-.022
11	Type of Stall at M=0.3 M=0.4	Mostly L.E. L.E.	T.E. T.E./L.E.	Thin Airf. L.E. Thin	L.E. L.E. Thin
12	Cd_o at $M_{DD}-0.1$		~.006	.006	.0066

Table VI Theoretical Predictions for the VR-11X, mod. 5 Airfoil.

NOTE: Values in parenthesis are corrected to test level.

		VR-11X, MOD .5	
#	OBJECTIVE	$Rn=10^7 xM$	$Rn=1.5x10^7 xM$
1	C_{m_o} at M=0.3	-.0079	-.007
2	$C_{\ell_{MAX}}$ at M=0.4	1.485 (1.525)	1.492 (1.532)
3	M_{DD_o}	.785 (.805)	.785 (.805)
4	C_{m_o} at M=0.7	-.015	-.0113
5	C_d for C_ℓ=0.6 and M=0.6	.0078 (.0105)	.007 (.0094)
6	$C_{\ell_{MAX}}$ at M=0.5	1.225	1.225 1.280(*)
7	C_m at C_ℓ=1.0 and M=0.3	-.0042	-.0053
8	C_{d_o} at $M=M_{DD}+0.02$	Approx. .016	.016
9	M_T at C_ℓ=0	Approx. 0.795 (0.815)	0.795 (0.815)
10	$M^2 C_{m_o}$ at M_{DD_o}	Approx. -.029	-.029
11	Type of Stall at M=0.3 M=0.4	T.E. T.E.	T.E. T.E.
12	C_{d_o} at M_{DD} -0.1	.0065	.0065

(*) Viscous Transonic Flow Solution

Table VII. Coordinates of the VR-11x, mod. 5, Airfoil.

x/c	y_u/c	y_ℓ/c
0.00	0.0	0.0
0.002	0.0105	-0.00450
0.005	0.0160	-0.00670
0.0075	0.0193	-0.00780
0.0125	0.0242	-0.00940
0.025	0.0345	-0.01230
0.050	0.0481	-0.01600
0.075	0.0573	-0.01890
0.100	0.0636	-0.02110
0.150	0.07038	-0.02450
0.200	0.07453	-0.02692
0.250	0.07718	-0.02885
0.30	0.07832	-0.03000
0.35	0.07890	-0.03080
0.40	0.07861	-0.03110
0.45	0.07754	-0.03100
0.50	0.07575	-0.03035
0.55	0.07303	-0.02920
0.60	0.07016	-0.02770
0.65	0.06615	-0.02600
0.69	0.06257	-0.02450
0.73	0.05728	-0.02280
0.77	0.05004	-0.02085
0.81	0.04081	-0.01890
0.845	0.03220	-0.01690
0.88	0.02477	-0.01460
0.91	0.01800	-0.01210
0.935	0.01260	-0.01000
0.955	0.00820	-0.00800
0.97	0.00500	-0.00610
0.98	0.00430	-0.00460
0.99	0.00366	-0.00280
0.995	0.00333	-0.00160
1.00	0.00300	0.00

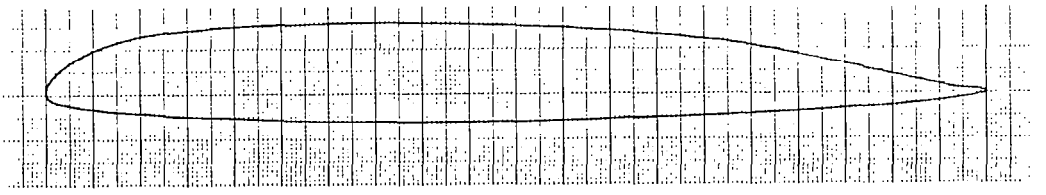

Table VIII. Mean Line and Thickness Distribution of the VR-11x, mod. 5, Airfoil.

x/c	y_c/c	y_t/c
0.00	0.0	0.0
0.005	0.00455	0.01145
0.0075	0.00575	0.01355
0.0125	0.00750	0.01670
0.025	0.01118	0.02333
0.05	0.01605	0.03205
0.075	0.01920	0.03810
0.10	0.02125	0.04235
0.15	0.02294	0.04744
0.20	0.02380	0.05072
0.25	0.02416	0.05301
0.30	0.02416	0.05416
0.35	0.02405	0.05485
0.40	0.02375	0.05485
0.45	0.02327	0.05427
0.50	0.02270	0.05305

x/c	y_c/c	y_t/c
0.55	0.02191	0.05111
0.60	0.02123	0.04893
0.65	0.02008	0.04608
0.70	0.01850	0.04250
0.75	0.01615	0.03785
0.80	0.01190	0.03120
0.845	0.00765	0.02455
0.88	0.00509	0.01969
0.91	0.00295	0.01505
0.935	0.00130	0.01130
0.955	0.00010	0.00810
0.97	-0.00055	0.00555
0.98	-0.00013	0.00446
0.99	0.00043	0.00323
0.995	0.00086	0.00246
1.00	0.00150	0.00150

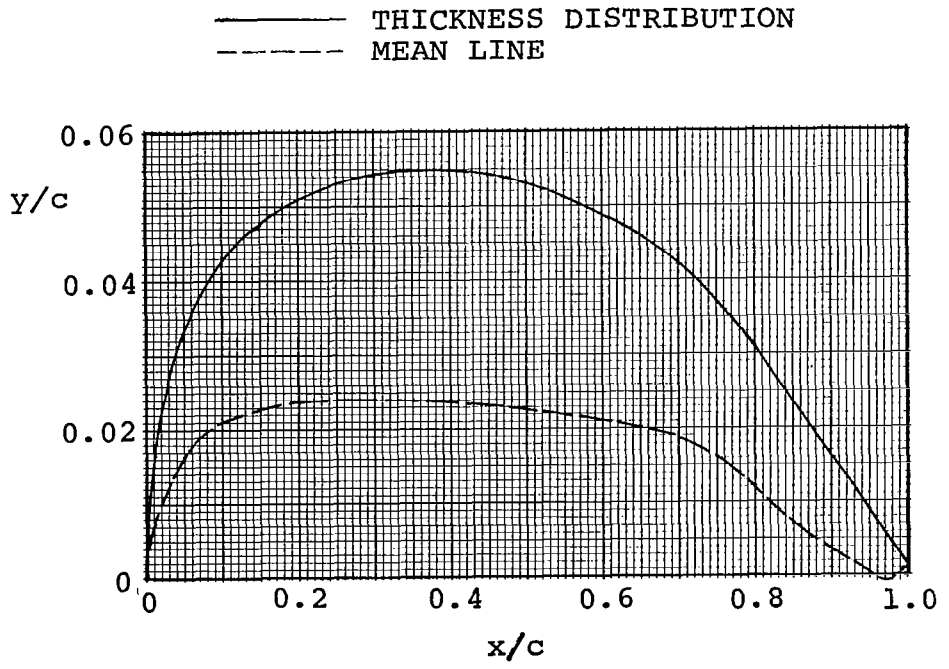

Table IX Aerodynamic Characteristics of Contours Obtained by Scaling the VR-11X, Mod. 5, Airfoil to Thicknesses Ranging from 8% to 13%.

t/c	c_{mo}	M=0.4, Rn=4X10^6		M_{DD_o} + 0.02	
		$C_{\ell_{max}}$	$x_{sep/c}$		
0.09	-0.0057	1.15	0.970	0.855	
0.09	-0.0073	1.26	0.950	0.834	
0.10	-0.0073	1.37	0.920	0.818	
0.11	-0.0079	1.485	0.900	0.805	VR-11X, Mod. 5
0.12	-0.0088	1.58	0.900	0.790	
0.13	-0.0093	1.68	0.875	0.773	

Table X Modification 6 of the VR-11X contour.

x/c	UPPER y/c	LOWER y/c
0.810	0.040809	-0.018900
0.845	0.033220	-0.016900
0.880	0.024772	-0.015000
0.910	0.018185	-0.013050
0.935	0.013173	-0.011600
0.955	0.009021	-0.009900
0.970	0.006850	-0.007700
0.980	0.005300	-0.005800
0.990	0.004000	-0.003300
0.995	0.003550	-0.001800
1.0	0.00300	0.0

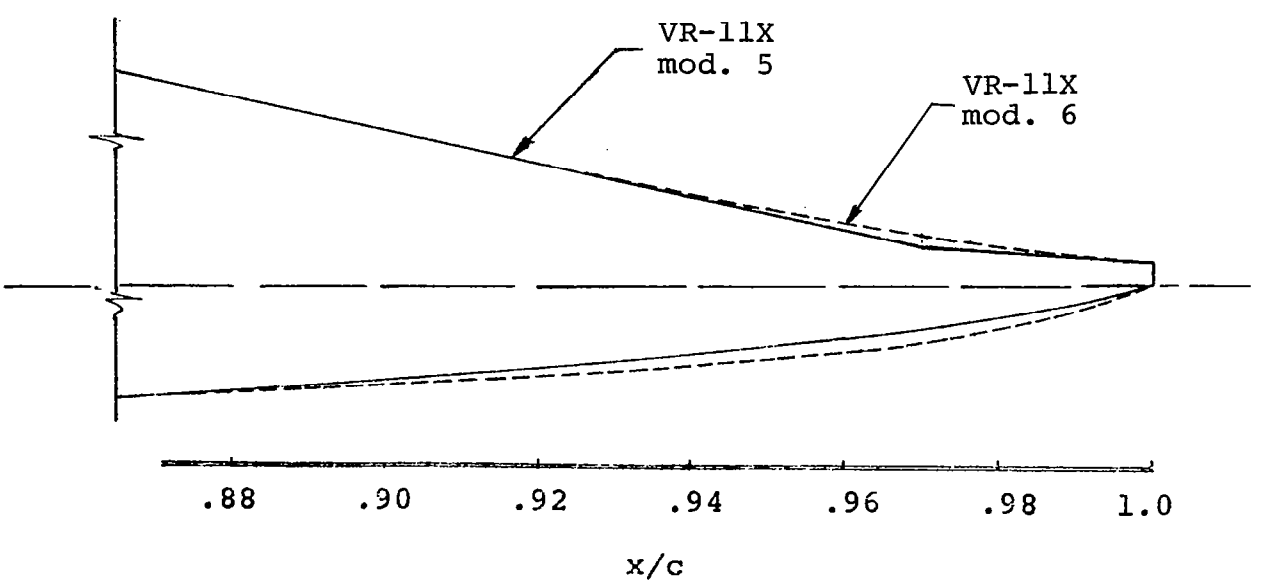

Table XI Comparison of the Theoretical Predictions for Modifications 5 and 6 of the VR-11X Airfoil.

		THEORETICAL PREDICTIONS			
		VR-11X, MOD .5		VR-11X, MOD .6	
#	OBJECTIVE	$Rn=10^7xM$	$Rn=1.5x10^7xM$	$Rn=10^7xM$	$Rn=1.5x10^7xM$
1	Cm_o at M=0.3	-.0079	-.007	-.01	-.0085
2	$C\ell_{MAX}$ at M=0.4	1.485 (1.525)	1.492 (1.532)	1.47 (1.51)	1.47 (1.51)
3	M_{DD_o}	.785 (.805)	.785 (.805)	.786 (.806)	.786 (.806)
4	Cm_o at M=0.7	-.015	-.0113	-.002	-.017
5	Cd for $C\ell$=0.6 and M=0.6	.0078 (.0105)	.007 (.0094)	.0078 (.0107)	.007 (.0078)
6	$C\ell_{MAX}$ at M=0.5	1.225	1.225 1.280(*)	1.20	1.20
7	Cm at $C\ell$=1.0 and M=0.3	-.0042	-.0053	-.0025	-.006
8	Cd_o at $M=M_{DD}+0.02$	Approx. .016	.016	.0165	Approx. .0165
9	M_T at $C\ell$=0	Approx. 0.795 (0.815)	0.795 (0.815)	0.81 (0.83)	Approx. 0.81 (0.83)
10	M^2Cm_o at M_{DD_o}	Approx. -.029	-.029	-.033	Approx. -.033
11	Type of Stall at M=0.3 M=0.4	T.E. T.E.	T.E. T.E.	T.E. T.E.	T.E. T.E.
12	Cd_o at M_{DD} -0.1	.0065	.0065	.0065	.0068

NOTE: Values in parenthesis are corrected to test level.

(*) Viscous Transonic Flow Solution

Table XII . Coordinates of the VR-11X, Modifications 8, 9 and 10.

Mod. 8

x/c	y_u/c
0.60	0.070163
0.65	0.066154
0.69	0.0609
0.73	0.0542
0.77	0.0469
0.81	0.0389
0.845	0.0319
0.88	0.024772

(All other coordinates are identical to the VR-11X, Mod. 5)

NOTE: The VR-11X, Mod 10 is the combination of Modifications 8 and 9.

Mod. 9

x/c	y_ℓ/c
0.0	-0.0
0.00055	-0.0025
0.002	-0.0050
0.004	-0.0072
0.0062	-0.0090
0.0086	-0.0103
0.0110	-0.0115
0.01465	-0.0128
0.01955	-0.0140
0.02615	-0.0154
0.0343	-0.0165
0.04449	-0.0177
0.0569	-0.01895
0.07245	-0.02
0.0924	-0.021
0.1185	-0.0225

(All other coordinates are identical to the VR-11X, Mod. 5)

Table XIII Effect of Modifications of the VR-11x Contour on First Priority Objectives

VR-11x Mod.	C_{m_o} at M=0.3	M=0.4, Rn=4x10^6		M_{DD_o} +0.02	C_ℓ=0.6, M=0.6, Rn=6x10^6		
		$C_{\ell max}$	x_{sep}/c		C_d	x_{sep}/c	CORR. C_d
5	-0.0079	1.485	0.900	0.805	0.0078	0.944	0.0105
6	-0.01	1.47	0.900	0.806	0.0078	0.947	0.0107
8	-0.0062	1.48	0.922	0.802	0.0076	0.933	0.0107
9	-0.0092	1.49	0.896	0.802	0.0077	0.944	0.0101
10	-0.0074	1.49	0.915	0.802	0.0078	0.934	0.0109

Table XIV Comparison of VR-11x Modifications 5 through 10 from Potential-Flow/Boundary-Layer Interaction Analysis.

M=0.4, Rn=4×10^6, Natural Transition

VR-11x Mod.	α (Deg)	C_ℓ	$C_{m_{.25}}$	C_d	SEPARATION CORRECTED C_d	MAX. M_ℓ	TRANSITION $X_{u/c}$	TRANSITION $X_{\ell/c}$	TURB. SEP. x/c
5	0	0.125	-0.0076	0.00731	0.00753	0.528	0.389	0.320	-
6		0.138	-0.0097	0.00750	0.00800	0.529	0.383	0.335	0.994
8		0.110	-0.0042	0.00796	0.00817	0.524	0.248	0.291	-
9		0.129	-0.0088	0.00748	0.00873	0.530	0.379	0.049	0.980
10		0.124	-0.0068	0.00760	0.00782	0.527	0.369	0.045	-
5	-2	-0.086	-0.0098	0.00758	0.00780	0.781	0.713	0.007	-
6		-0.068	-0.0127	0.00761	0.00788	0.768	0.712	0.007	0.998
8		-0.095	-0.0071	0.00775	0.00797	0.790	0.662	0.007	-
9		-0.088	-0.01108	0.00712	0.00740	0.705	0.712	0.014	0.997
10		-0.097	-0.0083	0.00757	0.00779	0.711	0.663	0.014	0.999
5	4	0.549	-0.0022	0.00714	0.01009	0.651	0.106	0.944	0.942
6		0.552	-0.0022	0.00724	0.00796	0.651	0.107	0.952	0.990
8		0.546	-0.0006	0.00713	0.00986	0.649	0.103	0.946	0.945
9		0.549	-0.0029	0.00721	0.01021	0.652	0.105	0.944	0.941
10		0.547	-0.0015	0.00740	0.01000	0.651	0.103	0.946	0.947
5	8	1.015	-0.0024	0.01127	0.01479	0.845	0.080	0.957	0.922
6		1.007	-0.0004	0.01114	0.01333	0.842	0.079	0.960	0.948
8		1.010	-0.0006	0.01126	0.01401	0.845	0.081	0.939	0.937
9		1.015	-0.0030	0.01140	0.01465	0.844	0.082	0.957	0.928
10		1.009	-0.0010	0.01165	0.01445	0.843	0.080	0.941	0.935
5	12	1.461	-0.0052	0.02031	0.02419	1.351	0.013	0.965	0.900
6		1.420	0.0033	0.02016	0.02409	1.312	0.014	0.969	0.903
8		1.458	-0.0038	0.02049	0.02321	1.350	0.013	0.965	0.926
9		1.461	-0.0057	0.02056	0.02458	1.336	0.013	0.965	0.896
10		1.458	-0.0042	0.02132	0.02400	1.336	0.013	0.965	0.926

Table XV. Summary of Leading Edge Contour Error Effects on Design Objectives 1, 2, 3 and 5.

AIRFOIL	C_{mo}	M=0.4, Rn=4X10^6		M_{DD_o} + .02	M=0.6, C_ℓ=0.6, Rn=6X10^6		
		$C_{\ell_{max}}$	$x_{sep/c}$		C_d	$x_{sep/c}$	Corr. C_d
VR-11X mod. 5	-.0079	1.485	.900	.805	.0078	.944	.0107
UPPER SURFACE DEVIATION	-.0083	1.475	.91	.806	.0078	.937	.0109
LOWER SURFACE DEVIATION	-.0083	1.495	.899	.805	.0077	.933	.0111
UPPER AND LOWER SURFACE DEVIATION	-.0083	1.475	.91	.805	.0079	0.943	.0108

Table XVI Leading Edge Contour Deviations of the VR-11x, mod. 5, Airfoil.

UPPER SURFACE

	VR-11X mod. 5	CONTOUR DEVIATION
x/c	y/c	y/c
0.0	0.0	0.0
0.00012	0.00365	0.00365
0.0008	0.00730	0.00800
0.00195	0.01052	0.01140
0.00340	0.01339	0.01440
0.00520	0.01611	0.01735
0.00700	0.01854	0.01990
0.00900	0.02083	0.02250
0.01105	0.02298	0.02450
0.01415	0.02599	0.02745
0.01860	0.02971	0.03110
0.02450	0.03415	0.03530
0.03205	0.03902	0.04000
0.04160	0.04425	0.0451
0.05350	0.04969	0.05050
0.06850	0.05534	0.05585
0.08800	0.06121	0.06125
0.11400	0.06608	0.06608

LOWER SURFACE

	VR-11X mod. 5	CONTOUR DEVIATION
x/c	y/c	y/c
0.0	0.0	0.0
0.00055	-0.00250	-0.00250
0.00200	-0.00450	-0.00480
0.00400	-0.00610	-0.00670
0.00620	-0.00720	-0.00780
0.00860	-0.00815	-0.00890
0.01100	-0.00895	-0.00980
0.01465	-0.01000	-0.01090
0.01955	-0.01120	-0.01205
0.02615	-0.01260	-0.01325
0.03430	-0.01400	-0.01440
0.04449	-0.01550	-0.01555
0.05690	-0.01700	-0.01700
0.07245	-0.01860	-0.01860
0.0924	-0.02045	-0.02045
0.11850	-0.02250	-0.02250

Table XVII Effect of stimulated transition at x/c=0.3 on both surfaces on the characteristics of the VR-11x, mod. 5 airfoil

TRANSITION	C_{m_o}	M=0.4, Rn=4x10^6		M_{DD_o} +0.02	M=0.6, C_ℓ=0.6, Rn=6x10^6		
		$C_{\ell_{max}}$	x_{sep}/c		C_d	x_{sep}/c	CORR. C_d
Natural	-.0079	1.485	0.900	0.805	0.0078	0.944	0.0105
at x/c=0.3 (upper and lower)	-.0055	1.490	0.910	0.805	0.0099	0.935	0.0128

Note: The increase in drag is due entirely to the lower surface, since in both cases the upper surface achieves natural transition at x/c≅0.10.

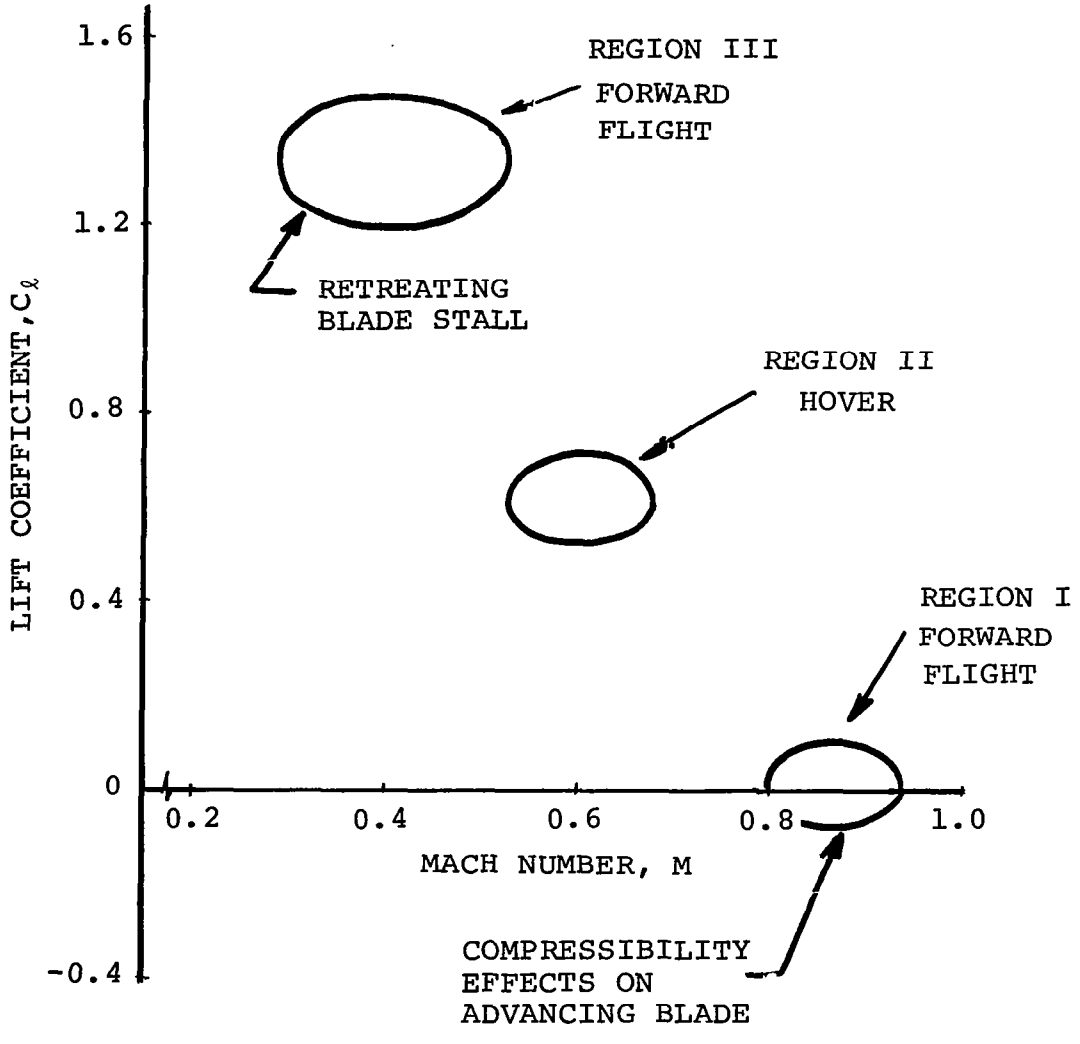

Figure 1. Rotor environment.

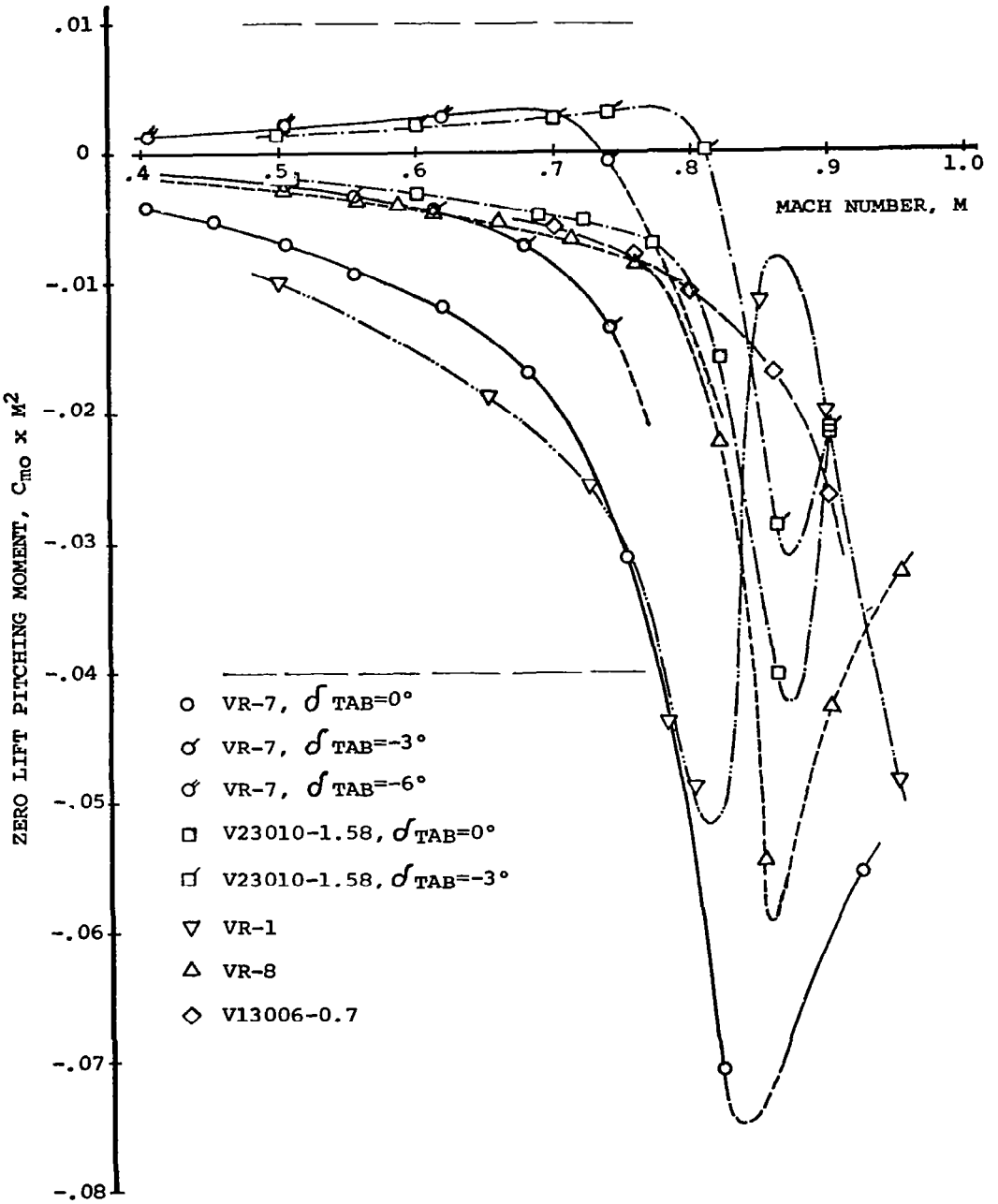

Figure 2. Compressibility effects on airfoil pitching moments at zero lift.

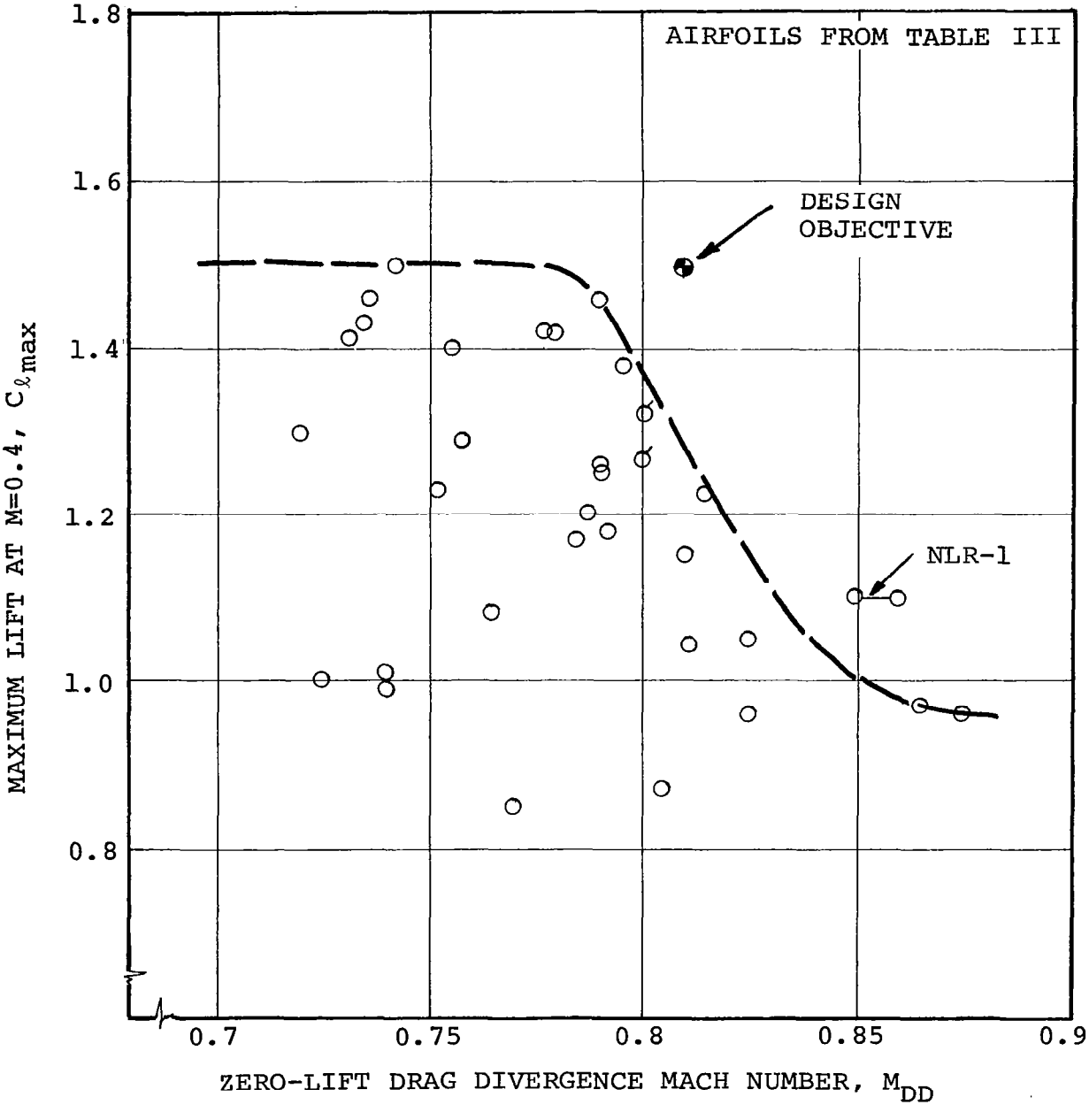

Figure 3. Survey of maximum lift and drag divergence characteristics.

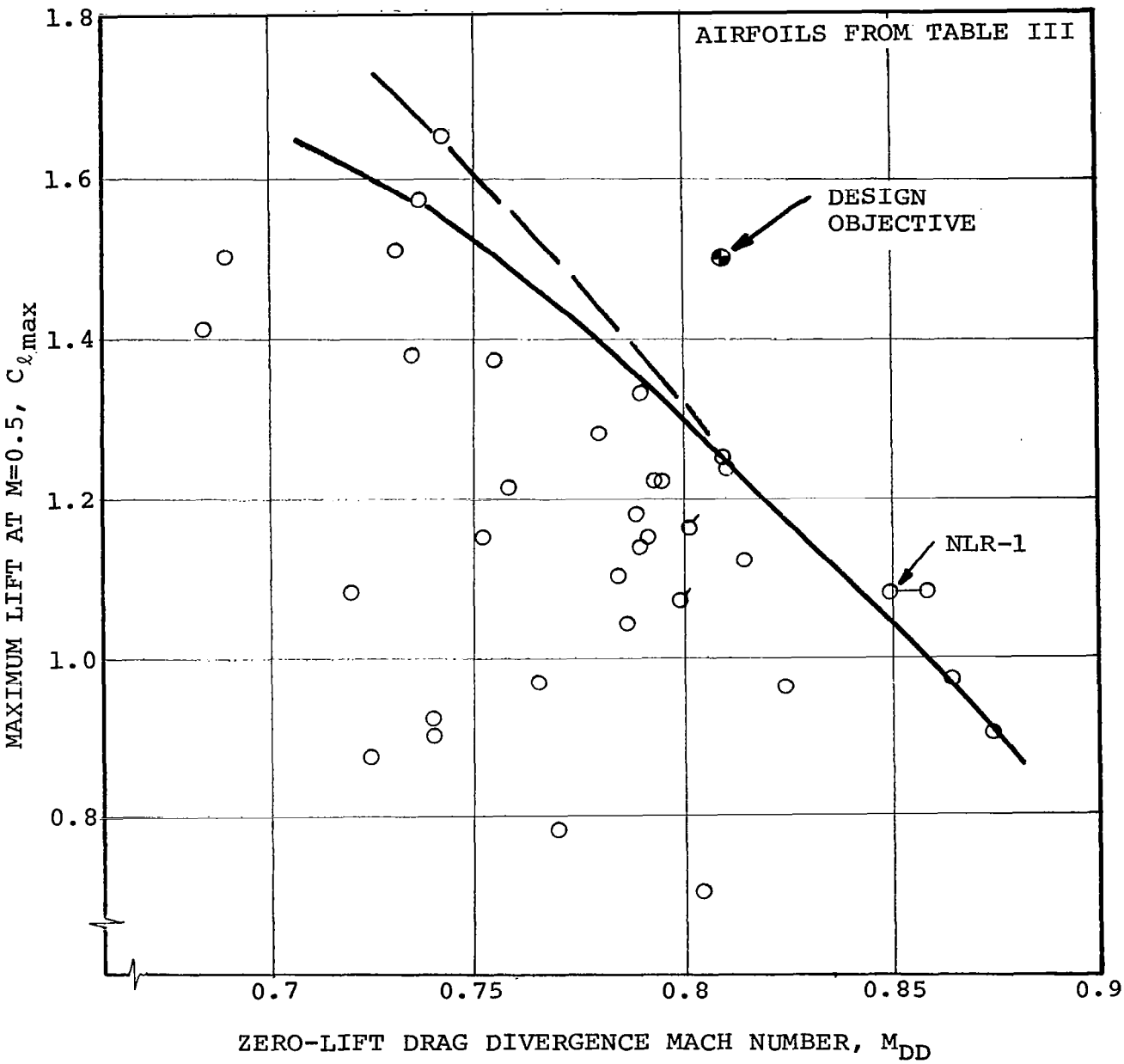

Figure 4. Survey of maximum lift and drag divergence characteristics.

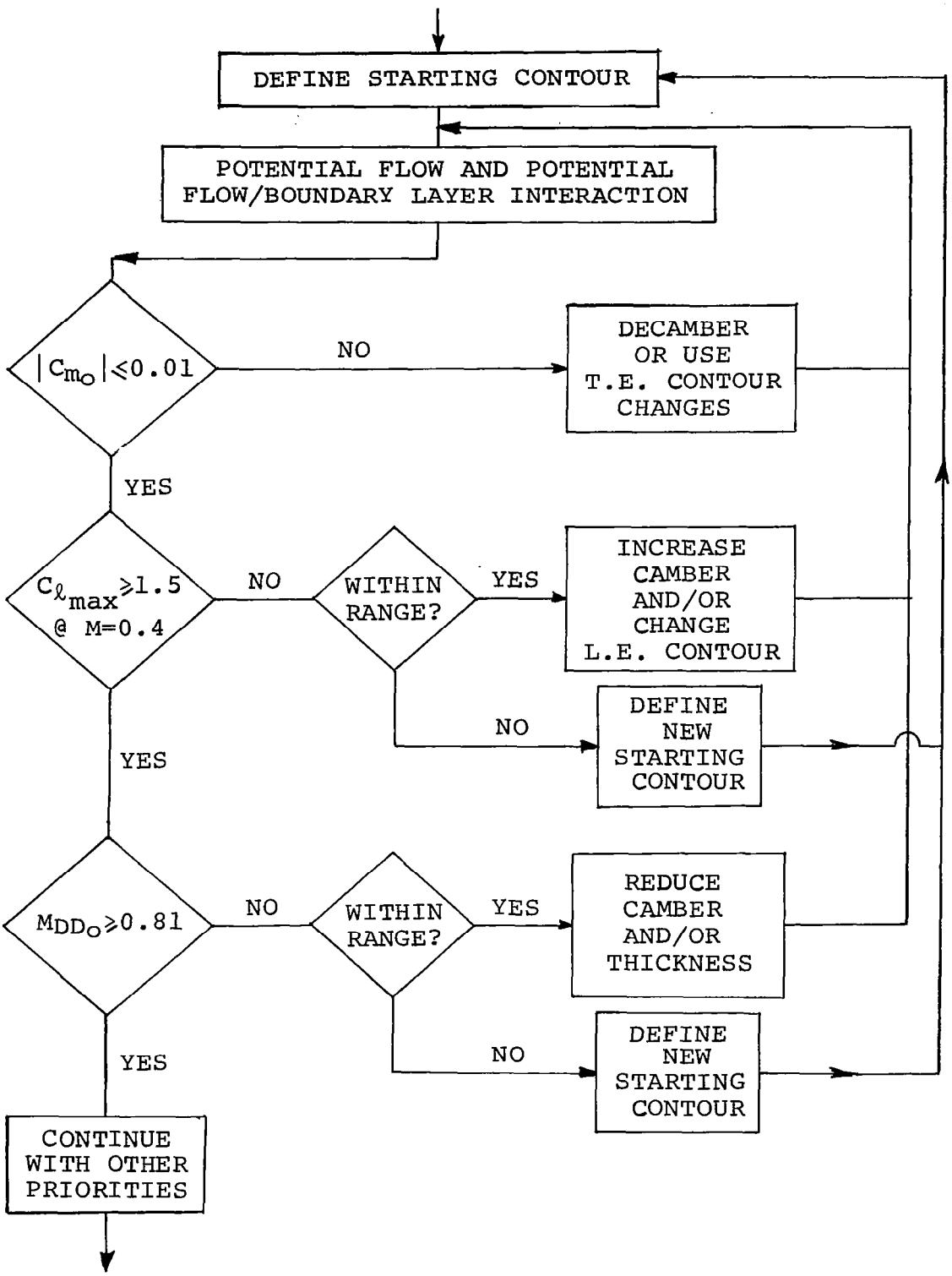

Figure 5. Outline of airfoil design logic for the first three design objectives

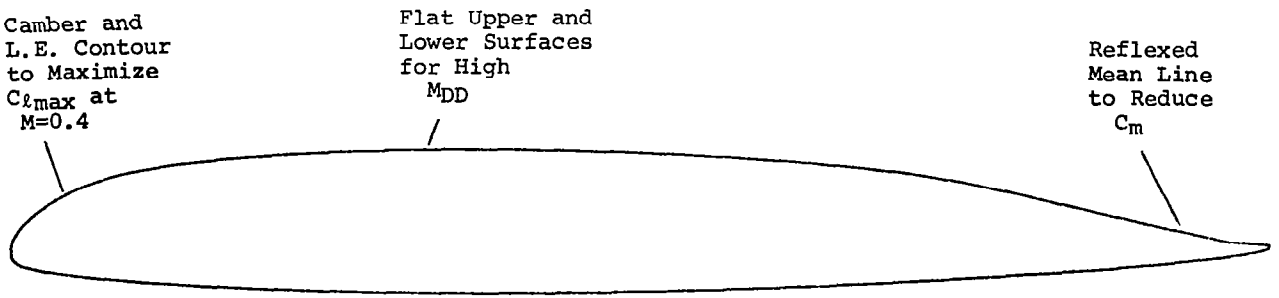

Figure 6. Airfoil VR-11X, mod. 5.

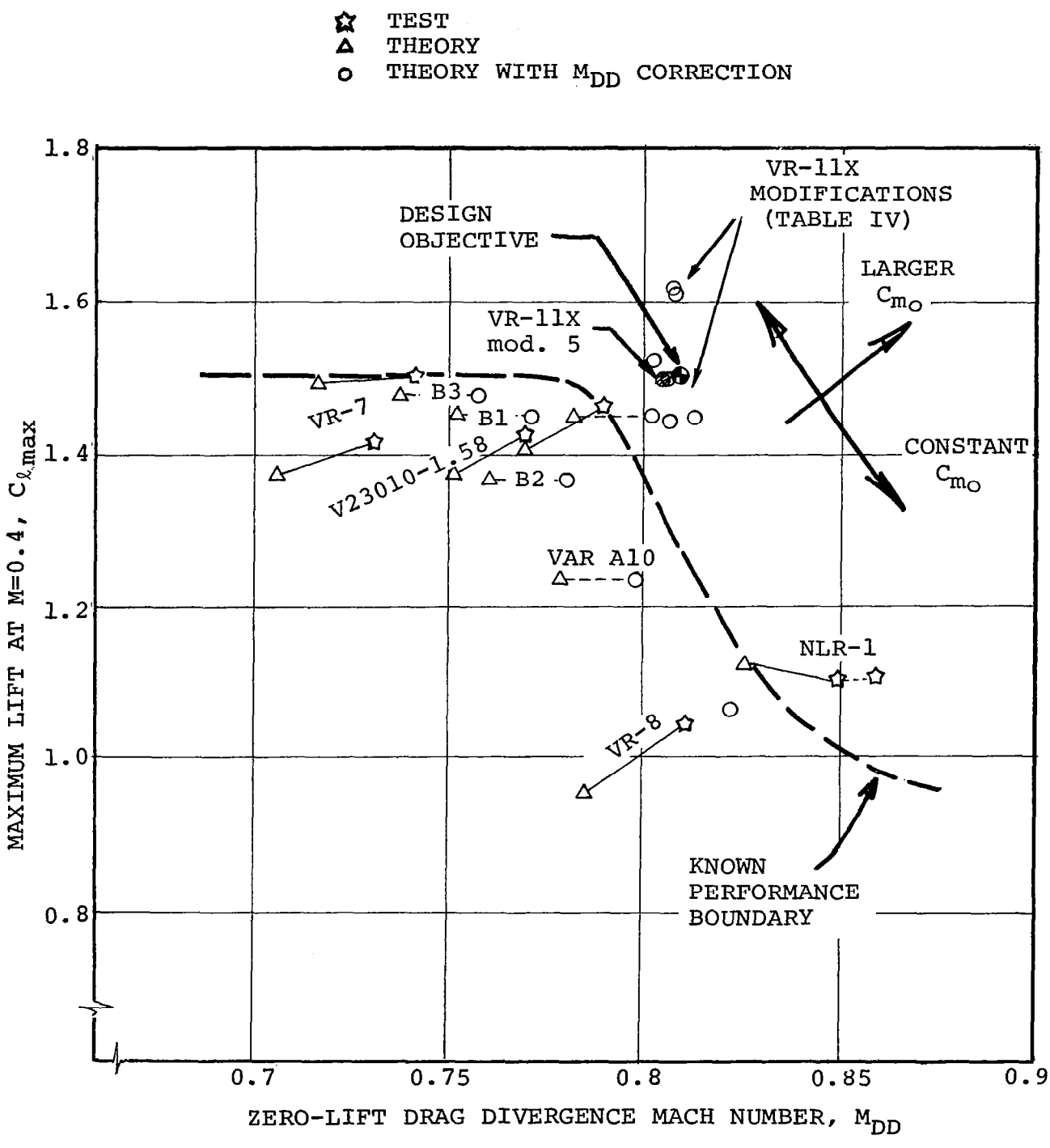

Figure 7. Airfoil design approach for the first three design objectives.

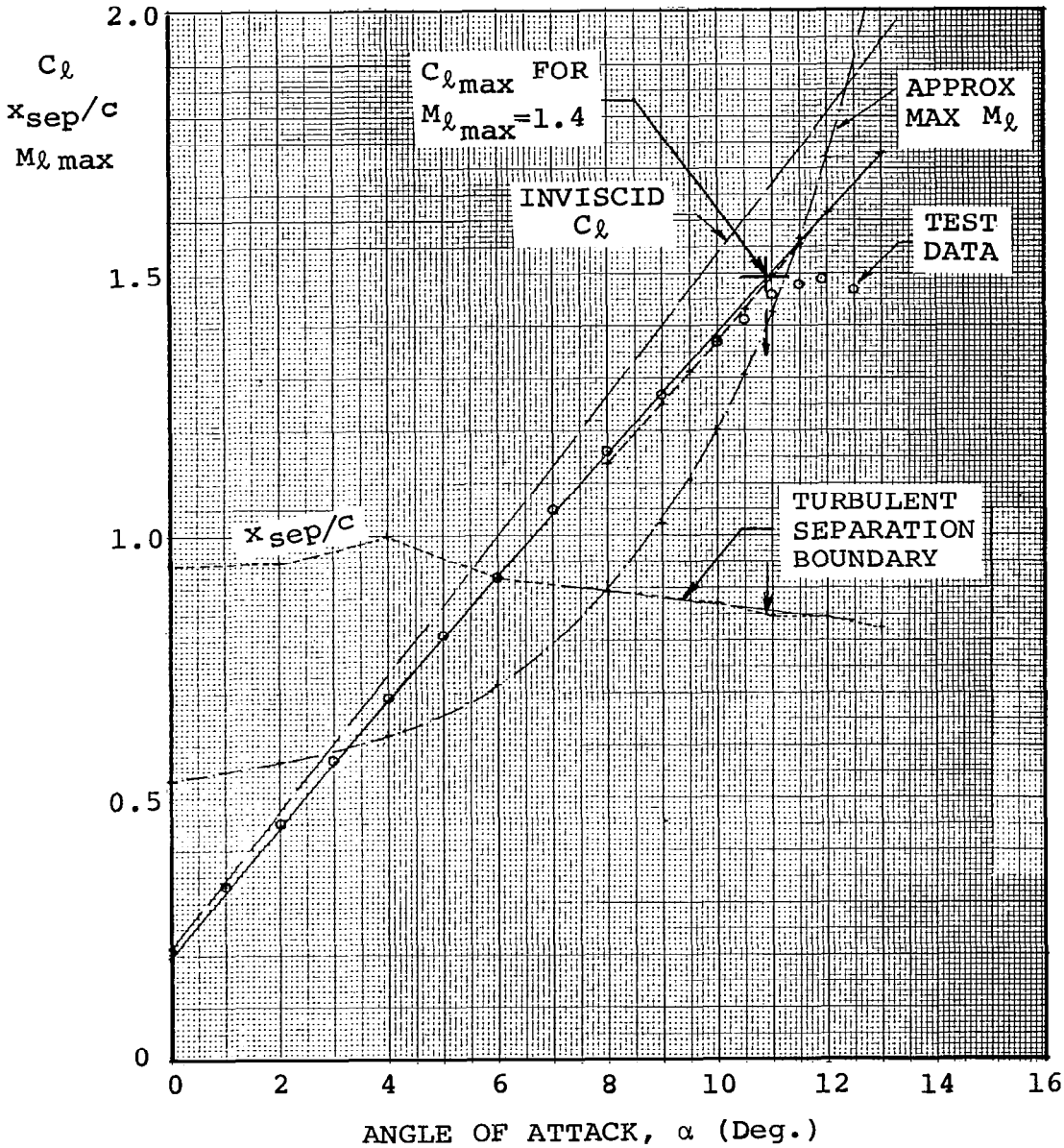

Method: Potential-flow/boundary layer interaction

Figure 8. Lift and maximum lift correlation between theory and test for the VR-7 airfoil with a 0° T.E. tab at M = 0.4, free transition, Rn = 7.4 x 10^6.

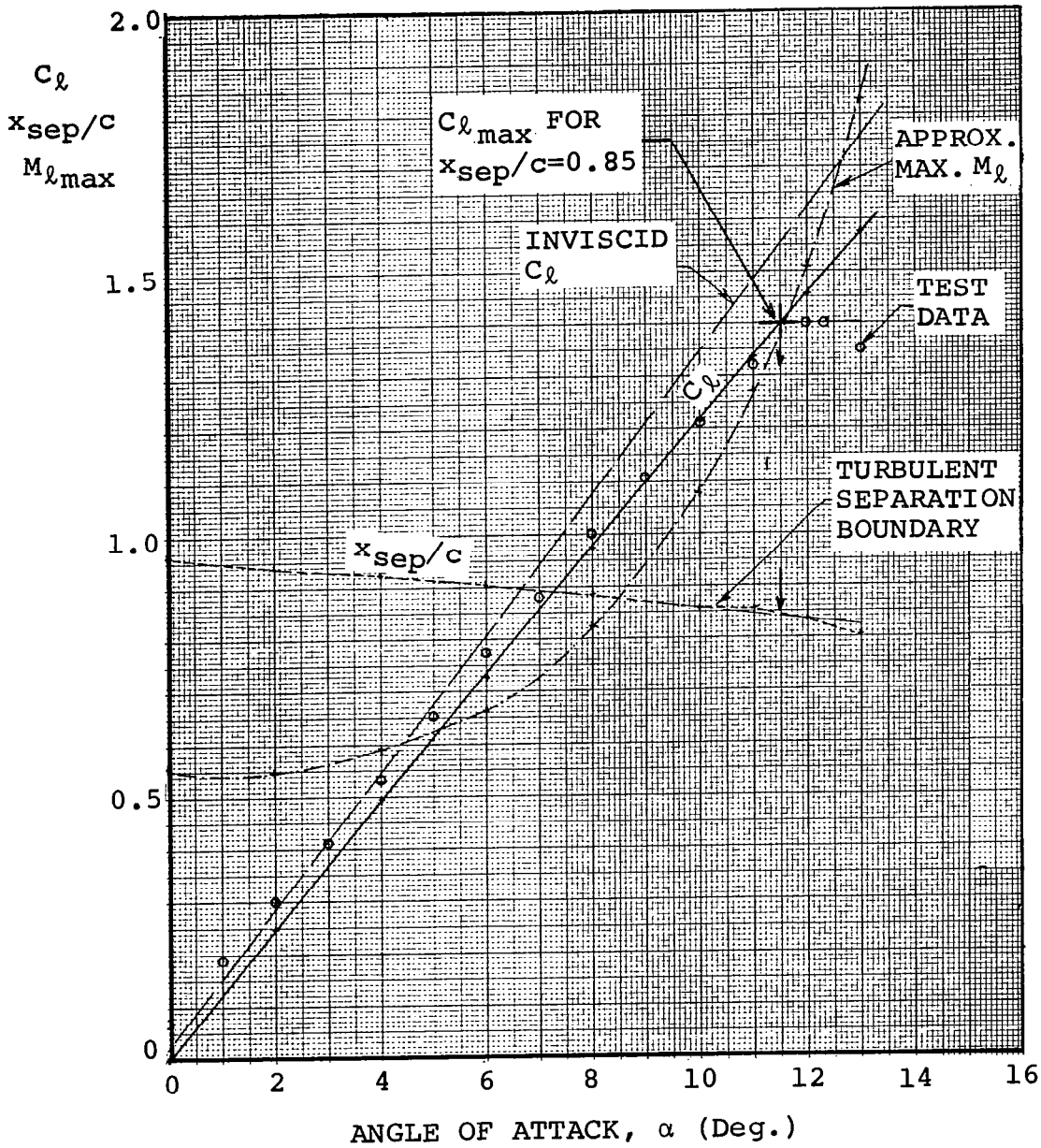

Method: Potential-flow/boundary layer interaction

Figure 9. Lift and maximum lift correlation between theory and test for the VR-7 airfoil with a -6° T.E. tab at M = 0.4, free transition, Rn = 7.4 x 10^6.

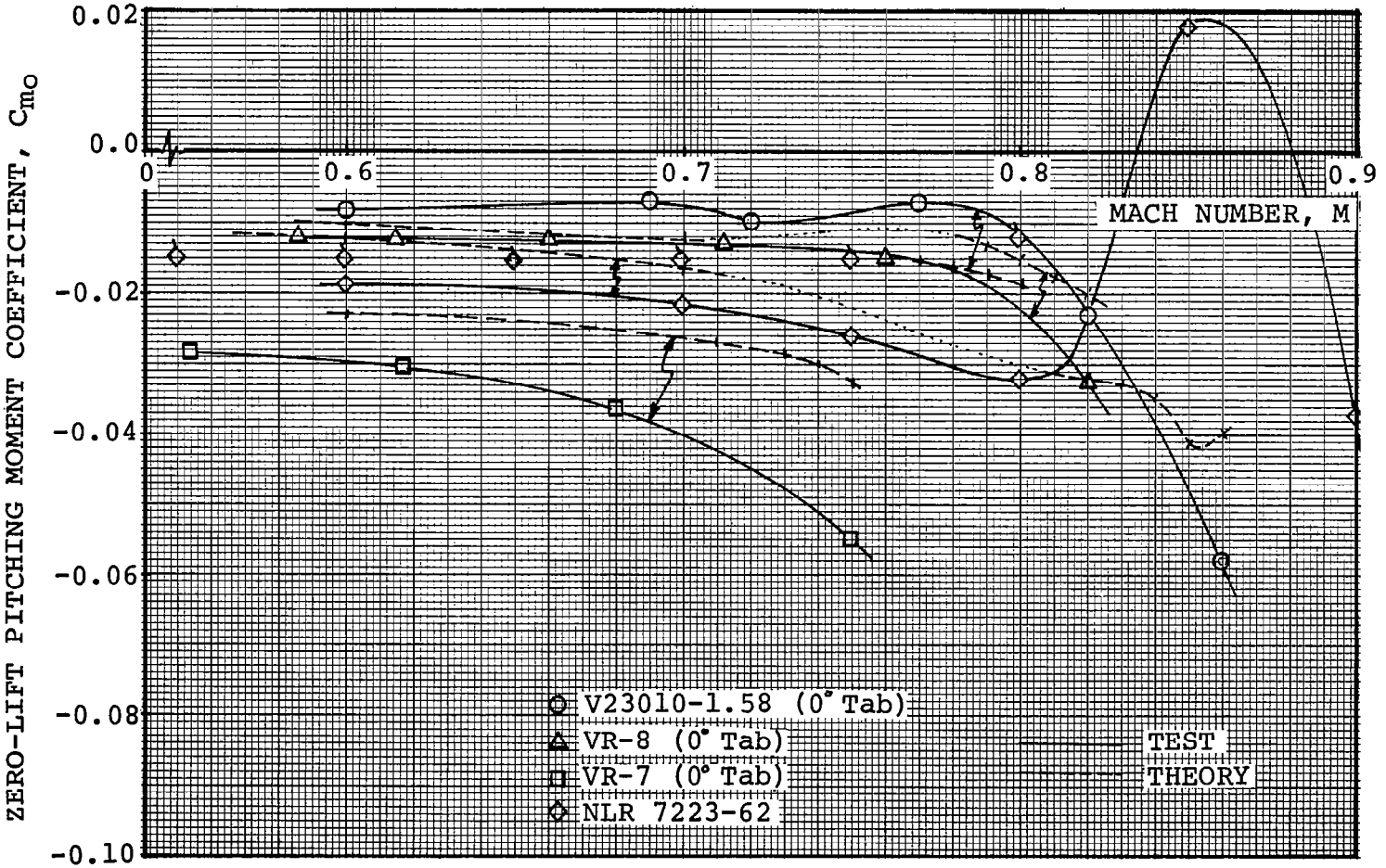

Figure 10. Compressibility effects on the pitching moment coefficients of several rotor airfoils, and comparison between test and theoretical predictions.

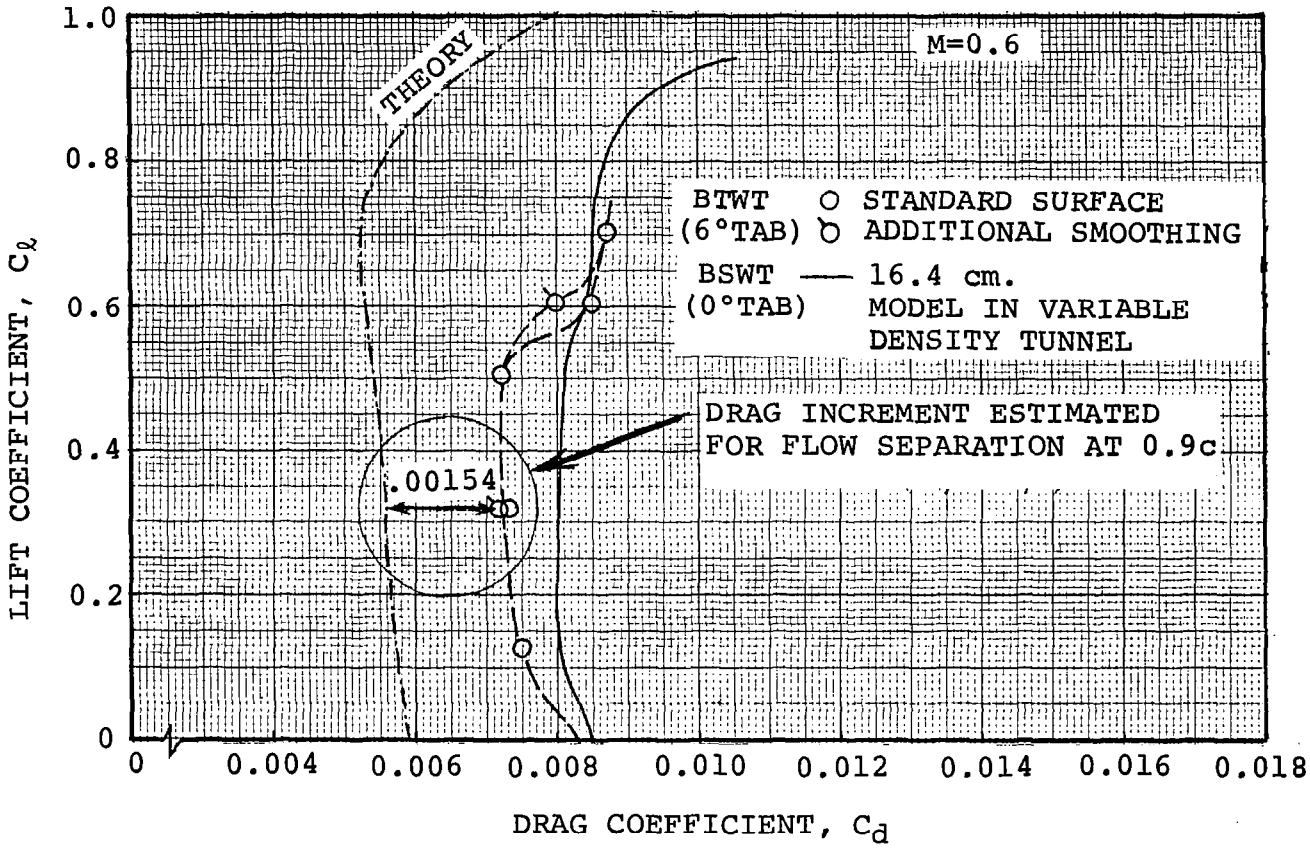

Figure 11. Drag coefficient of the VR-7 airfoil with a -6° T.E. tab - comparison between theory and test.

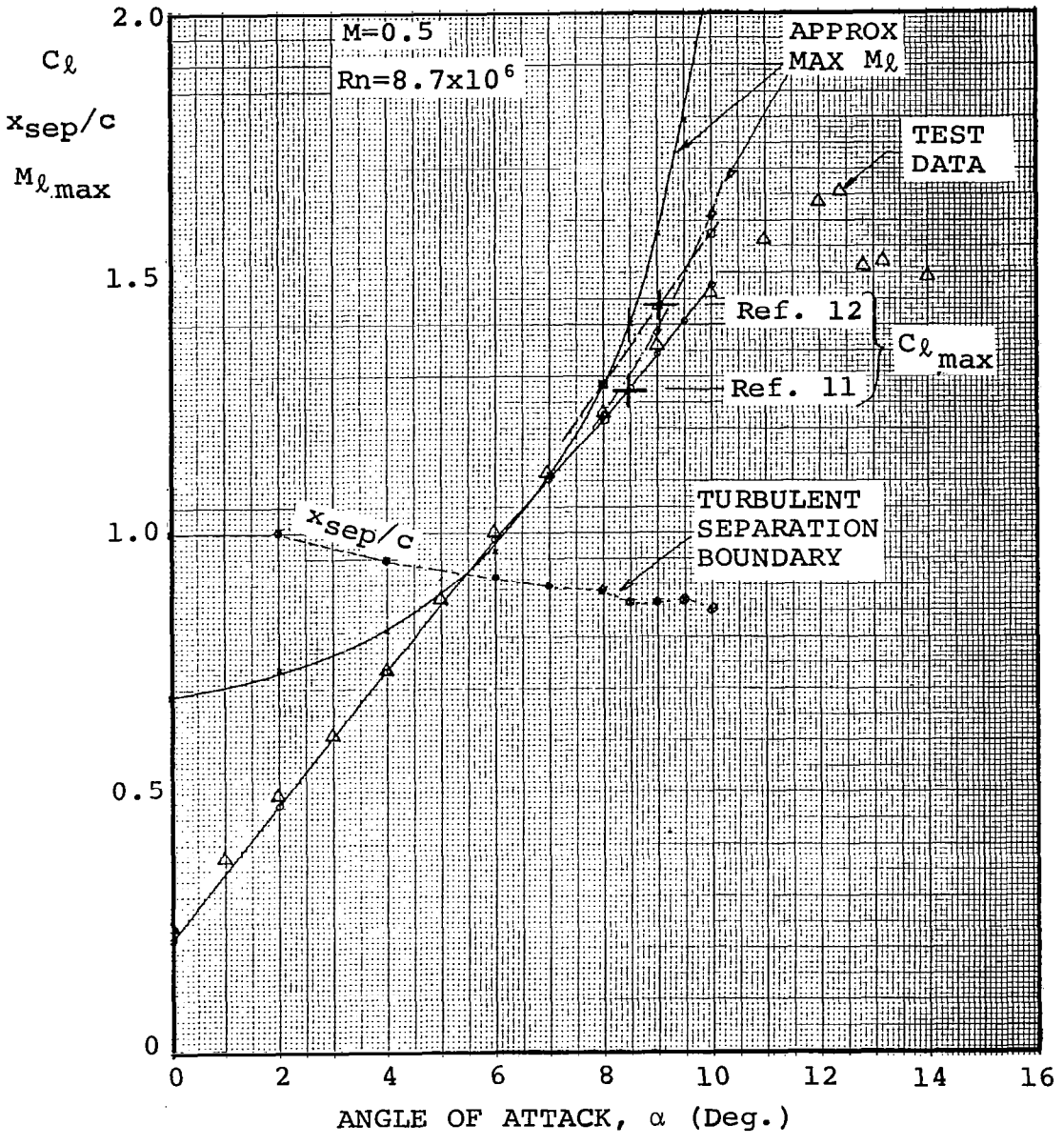

Methods: Potential-flow boundary layer interaction (ref. 11)
Viscous, transonic flow analysis (ref. 12)

Figure 12. Lift and maximum lift correlation between theory and test for the VR-7 airfoil with a 0° T.E. tab at M = 0.5.

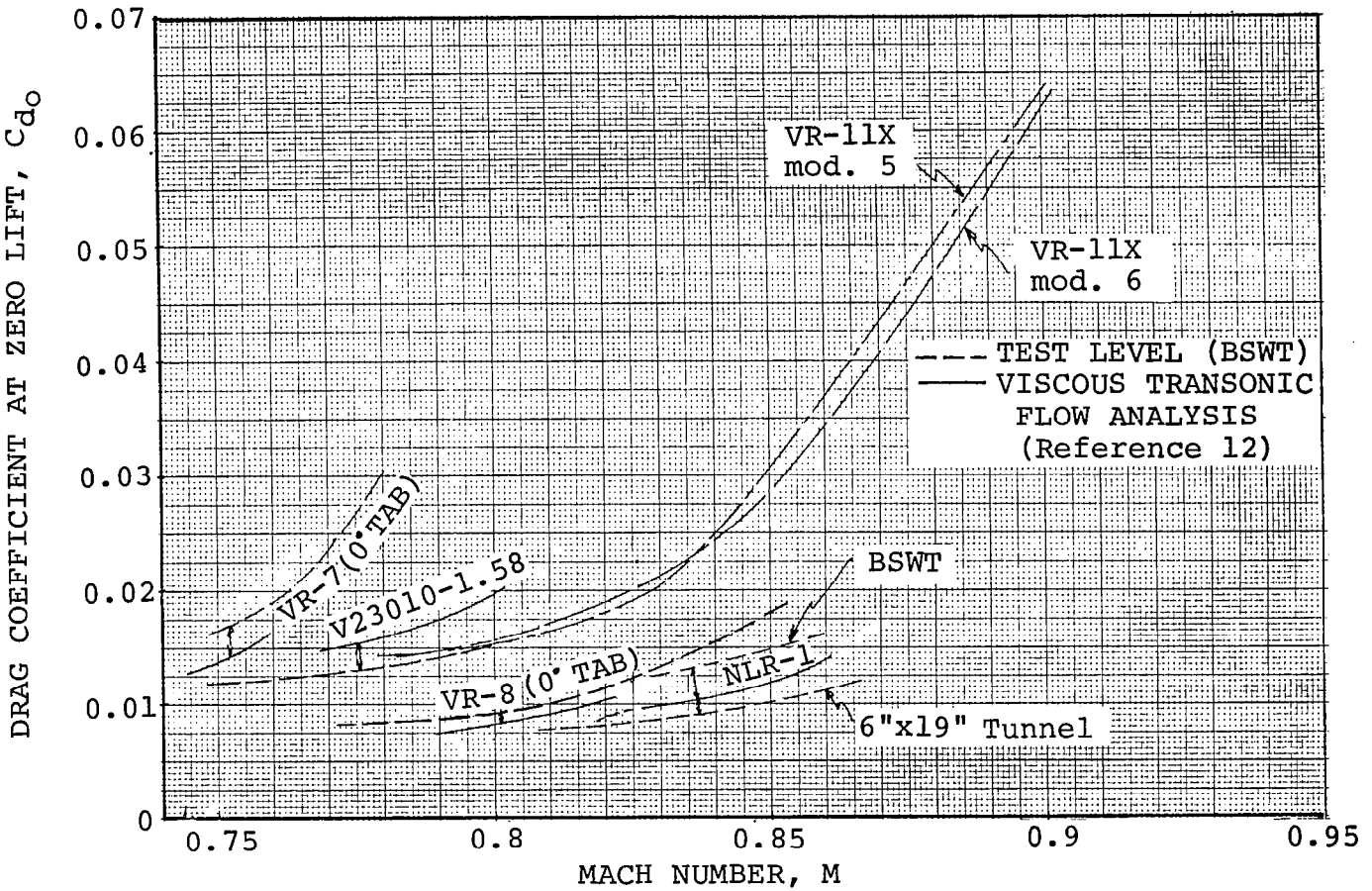

Figure 13. Comparison of measured and predicted drag levels near drag divergence.

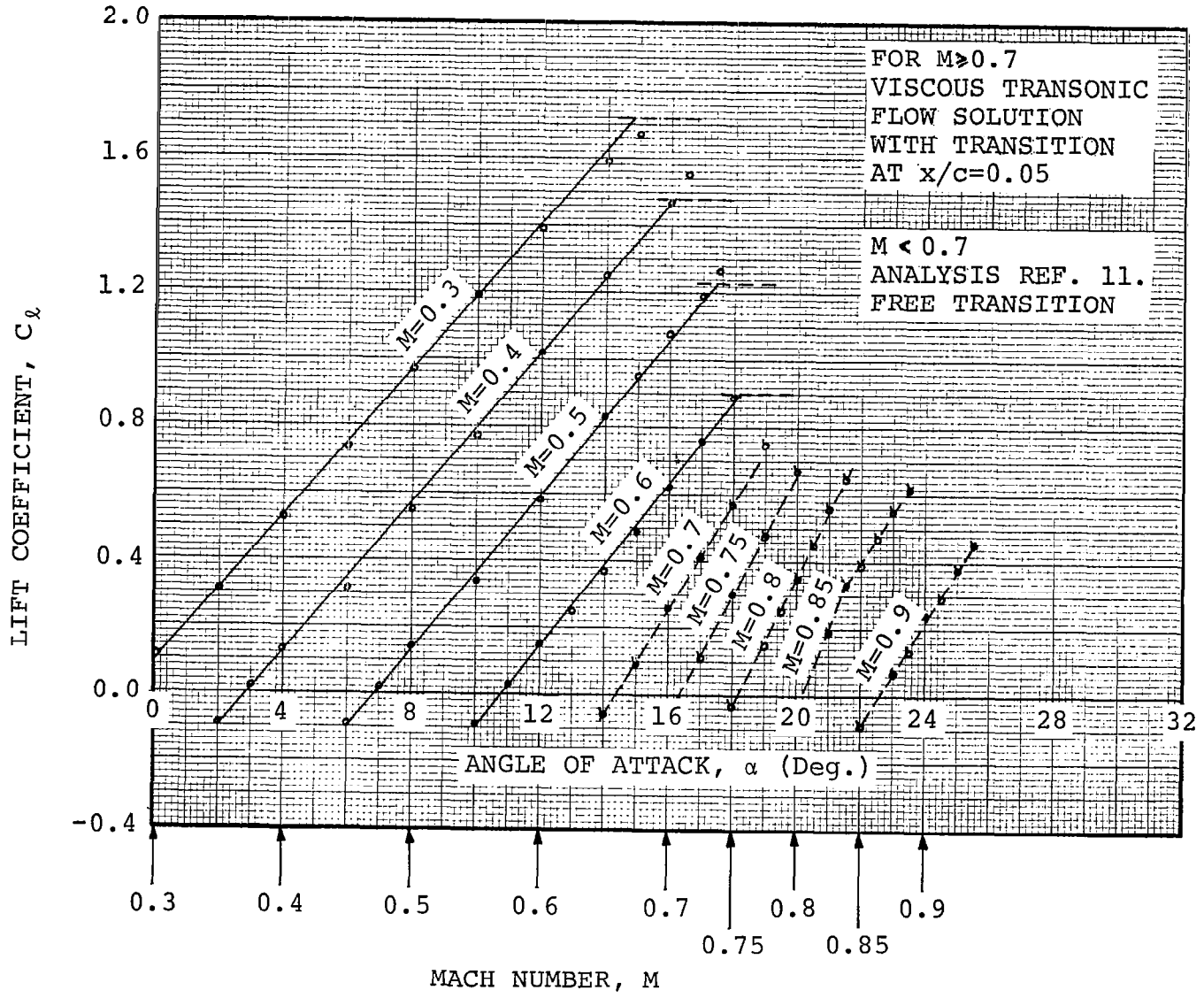

Figure 14. Estimated lift coefficients for the VR-11x, mod. 5 airfoil at $Rn=10^7 xM$.

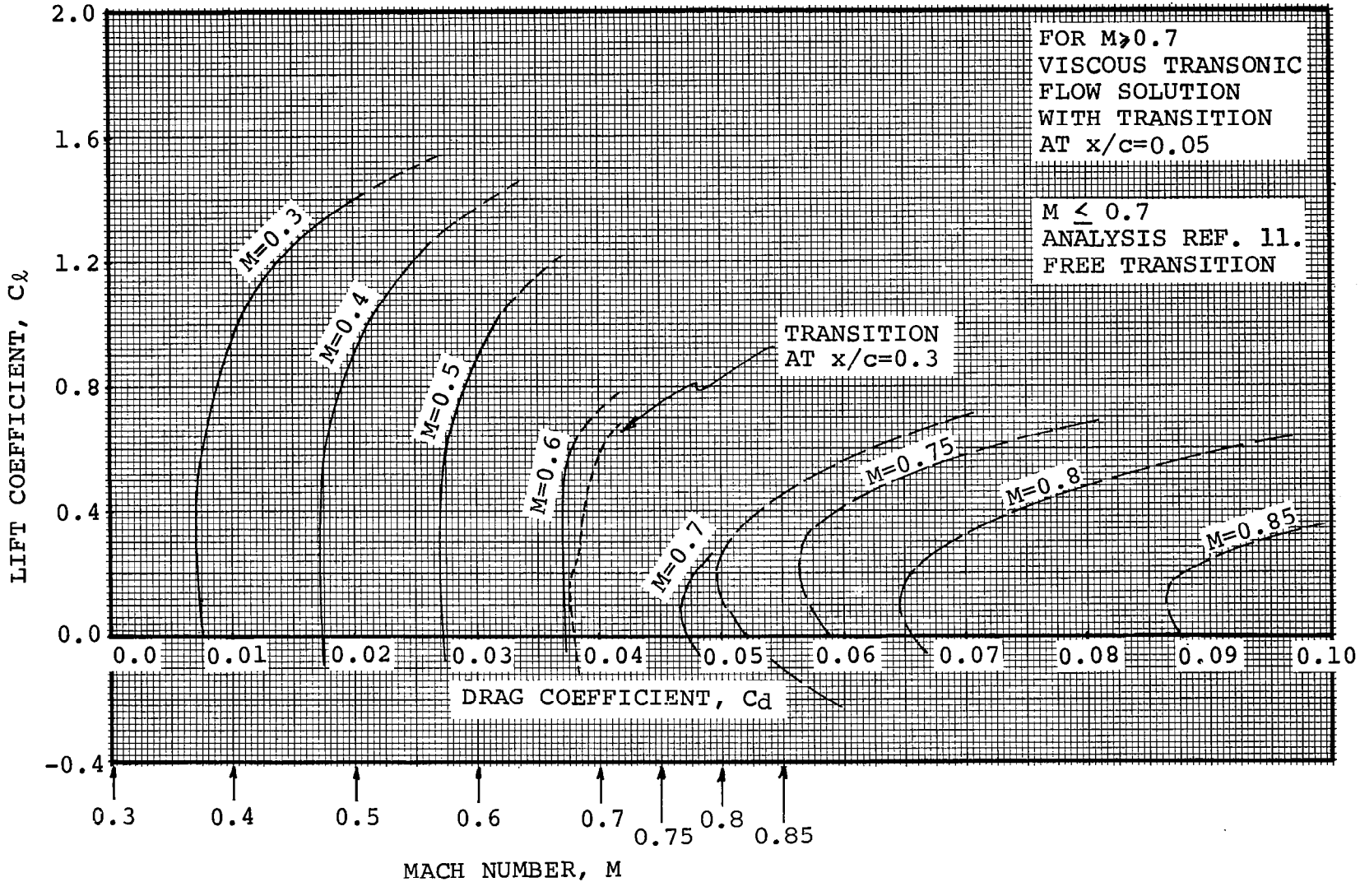

Figure 15. Estimated lift/drag polars for the VR-11x, mod. 5 airfoil at $Rn=10^7 xM$.

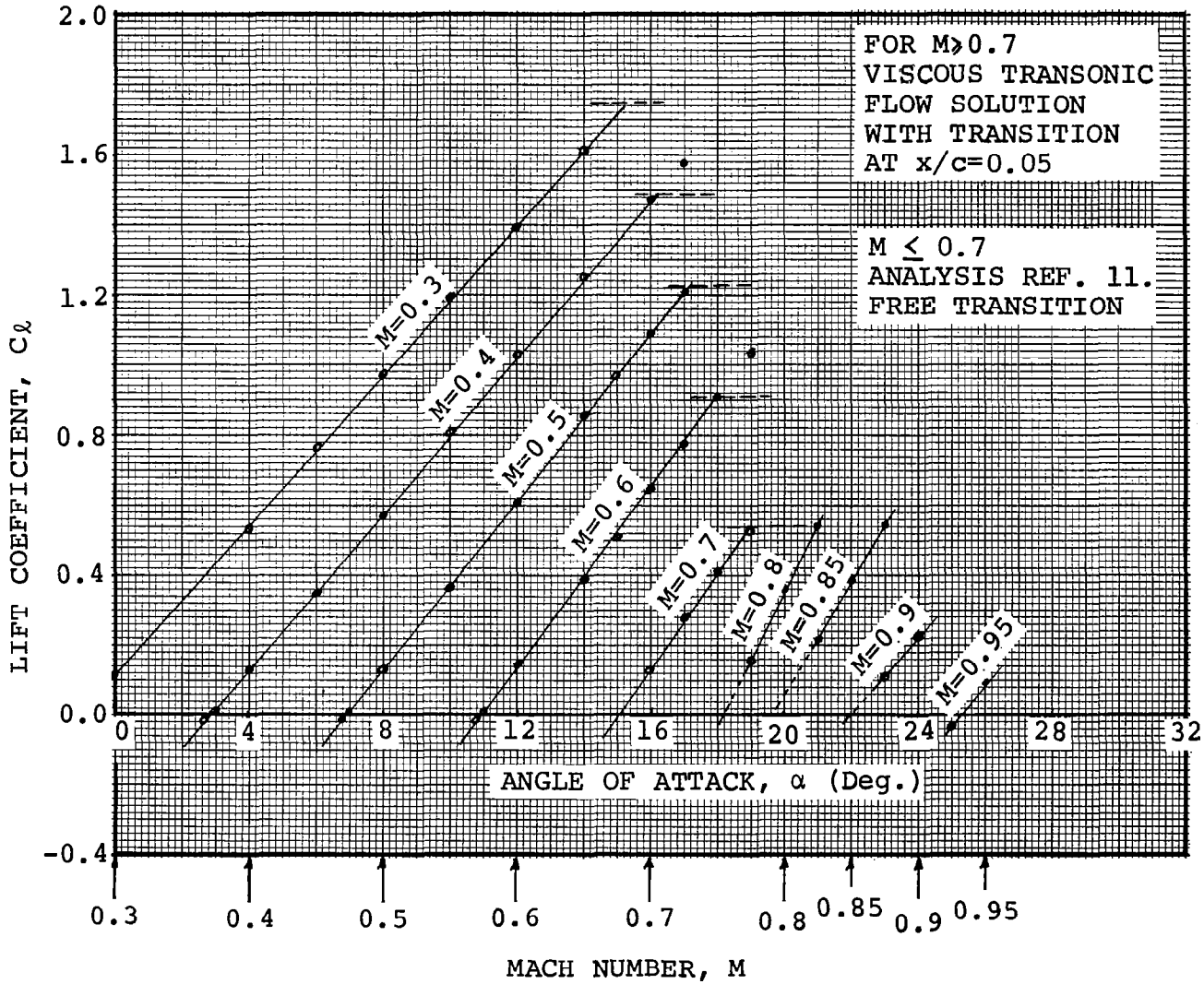

Figure 16. Estimated lift coefficients for the VR-11x, mod. 5 airfoil at Rn=1.5x10^{7}xM.

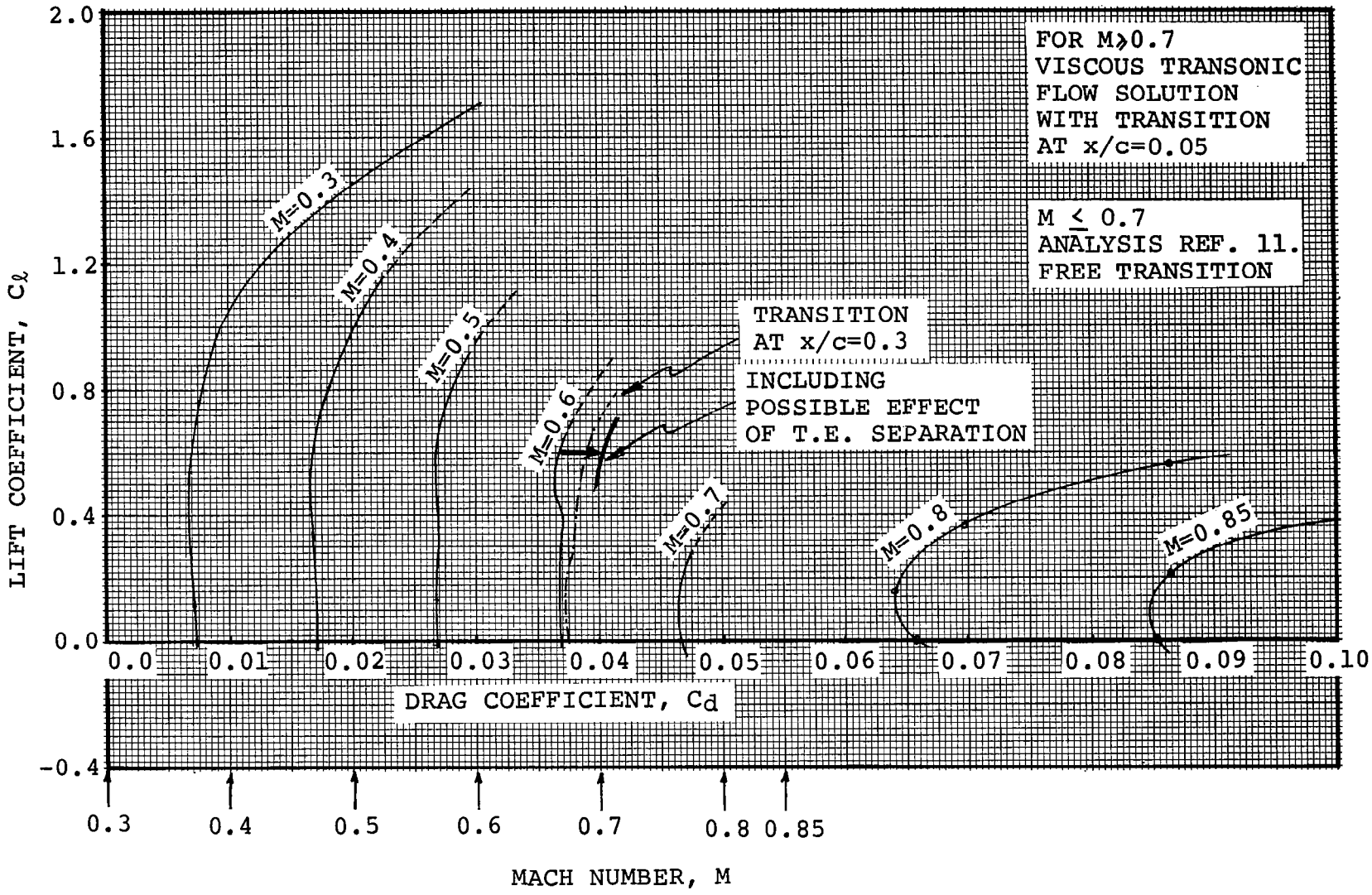

Figure 17. Estimated lift/drag polars for the VR-11x, mod. 5 airfoil at $Rn=1.5\times10^{7}\times M$.

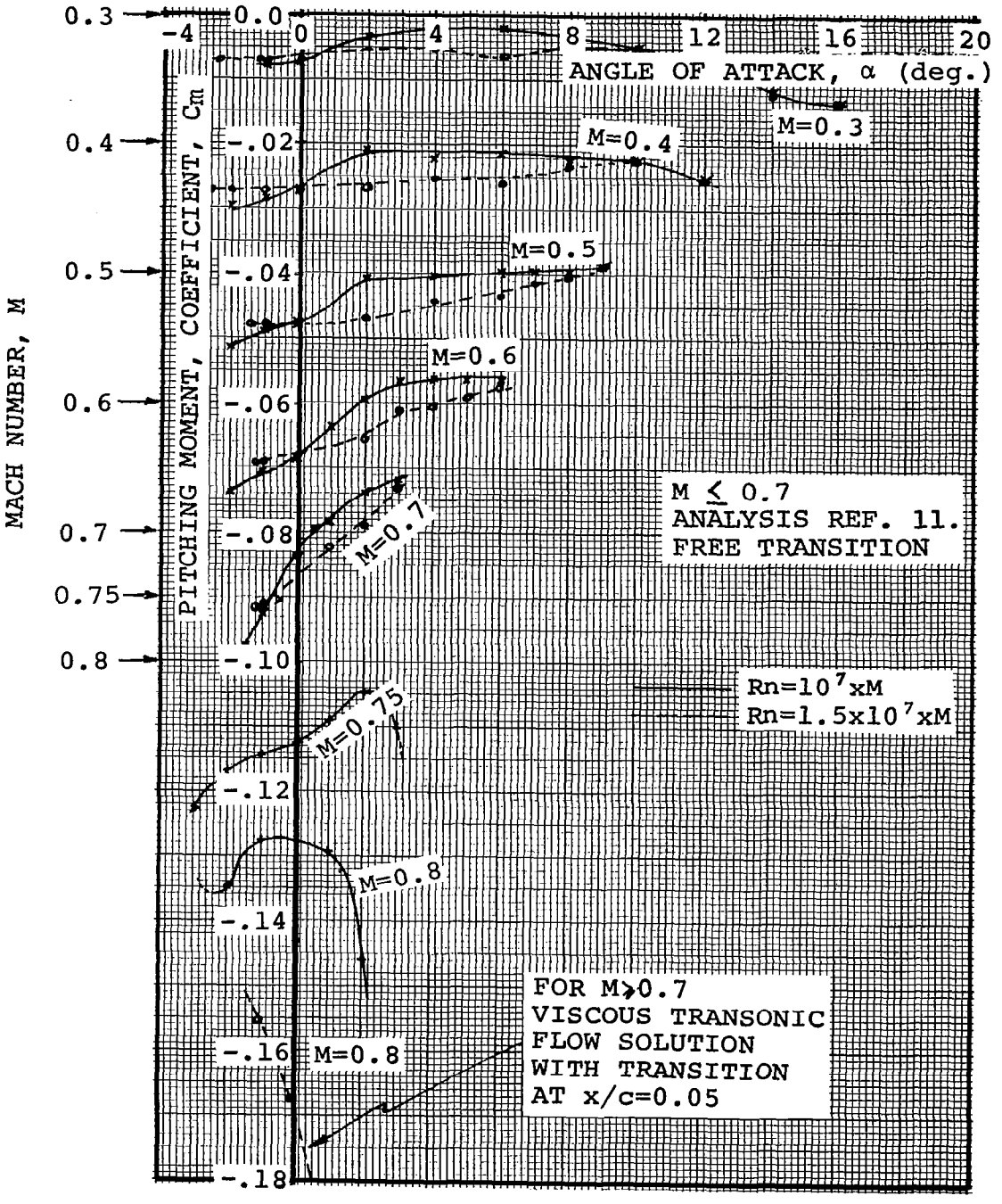

Figure 18. Estimated pitching moment coefficients for the VR-11x, mod. 5 airfoil at $Rn=10^7xM$ and $Rn=1.5x10^7xM$.

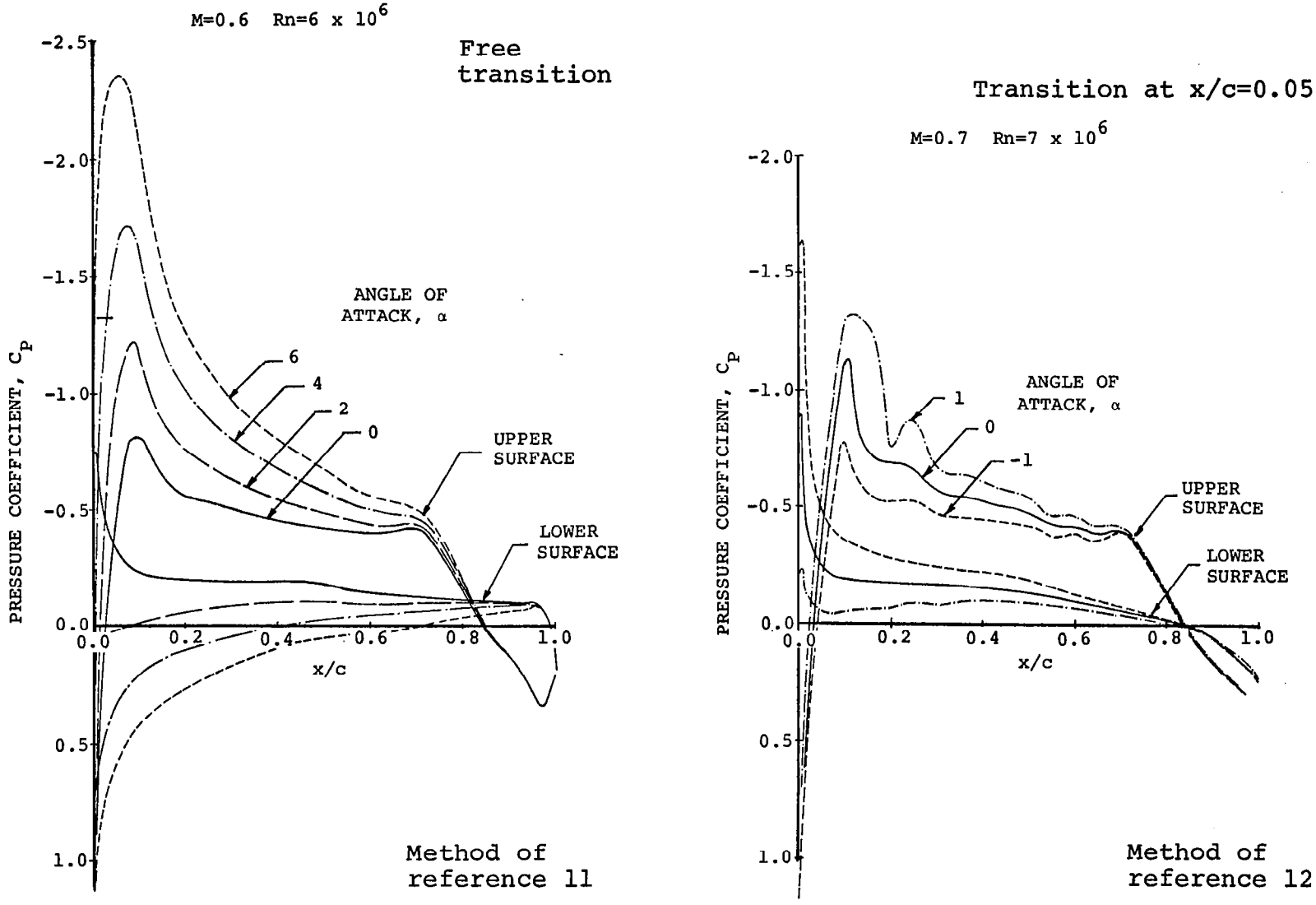

Figure 19. Typical pressure distributions for the VR-11x, mod. 5.

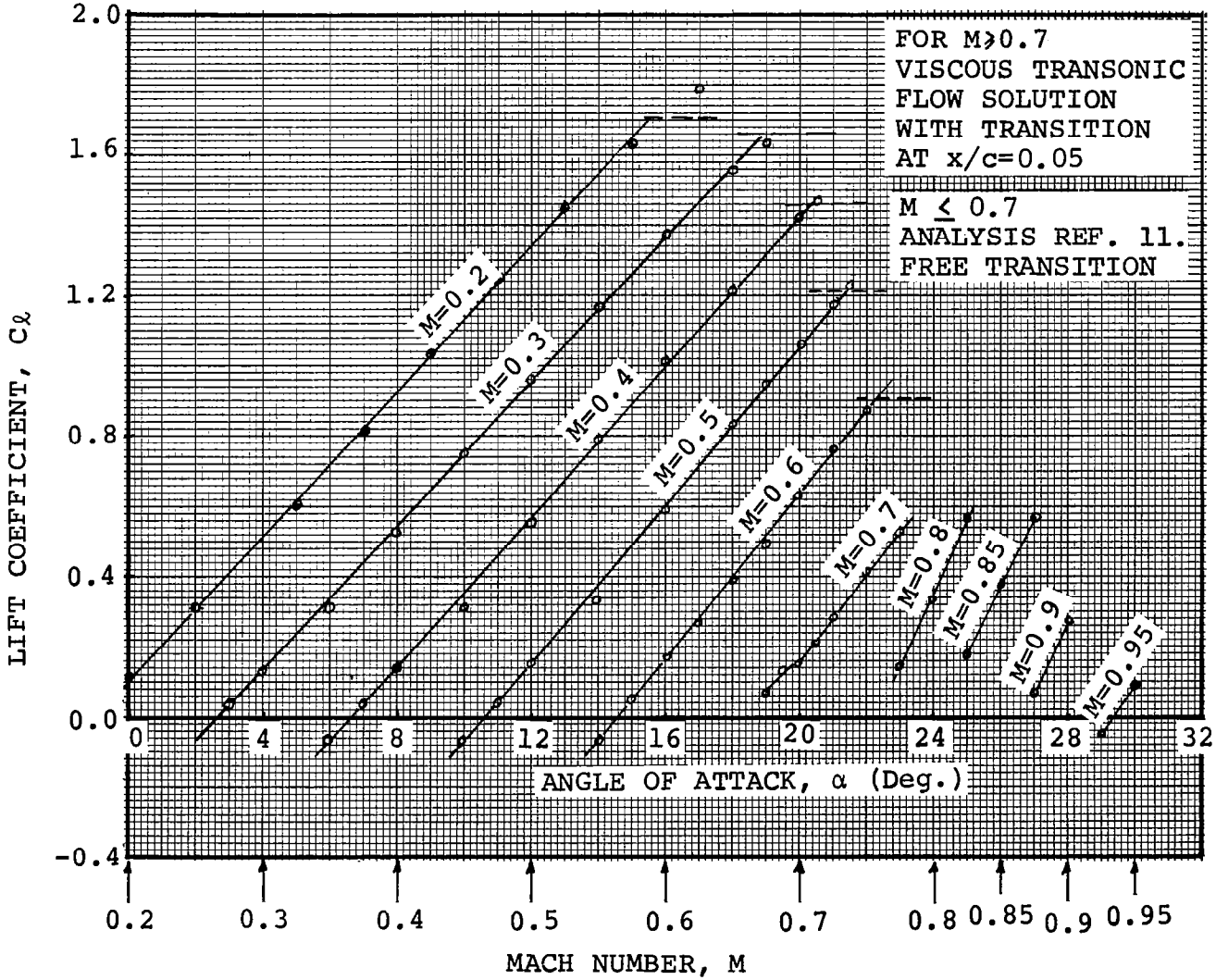

Figure 20. Estimated lift coefficients for the VR-11x, mod. 6 airfoil at $Rn=10^7 \times M$.

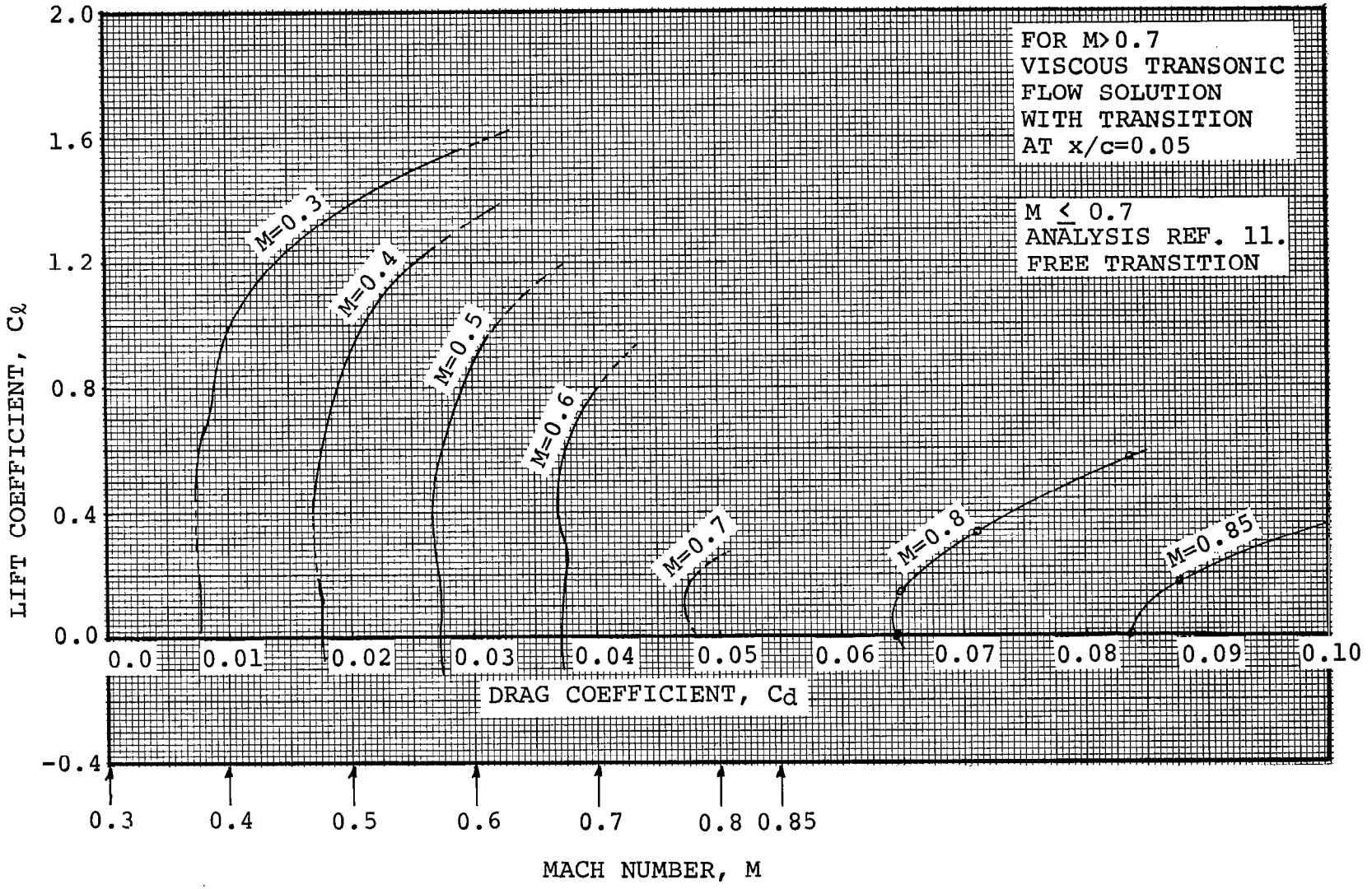

Figure 21. Estimated lift/drag polars for the VR-11x, mod. 6 airfoil at $Rn=10^7 xM$.

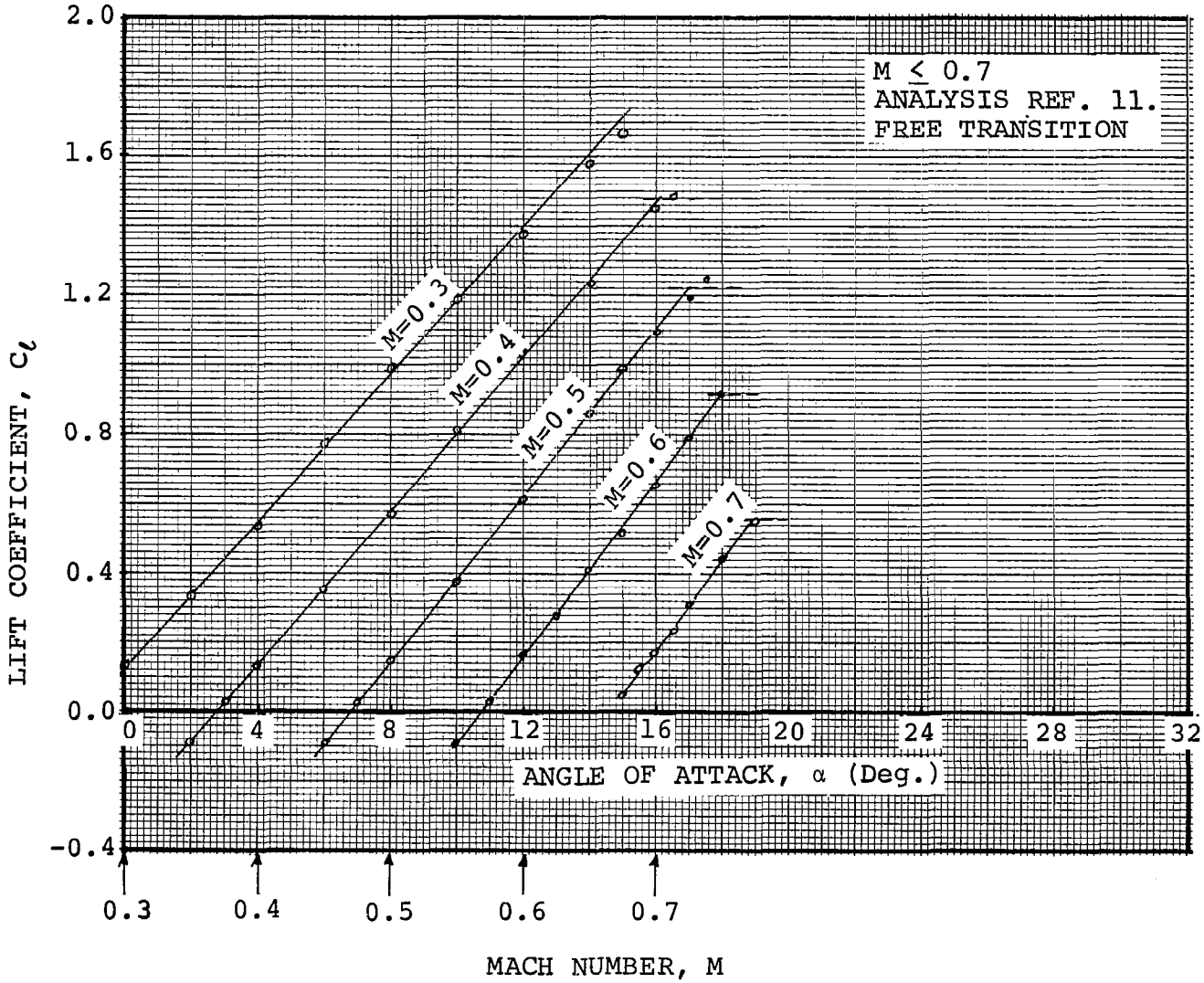

Figure 22. Estimated lift coefficients for the VR=11x, mod. 6 at $Rn=1.5x10^7xM$.

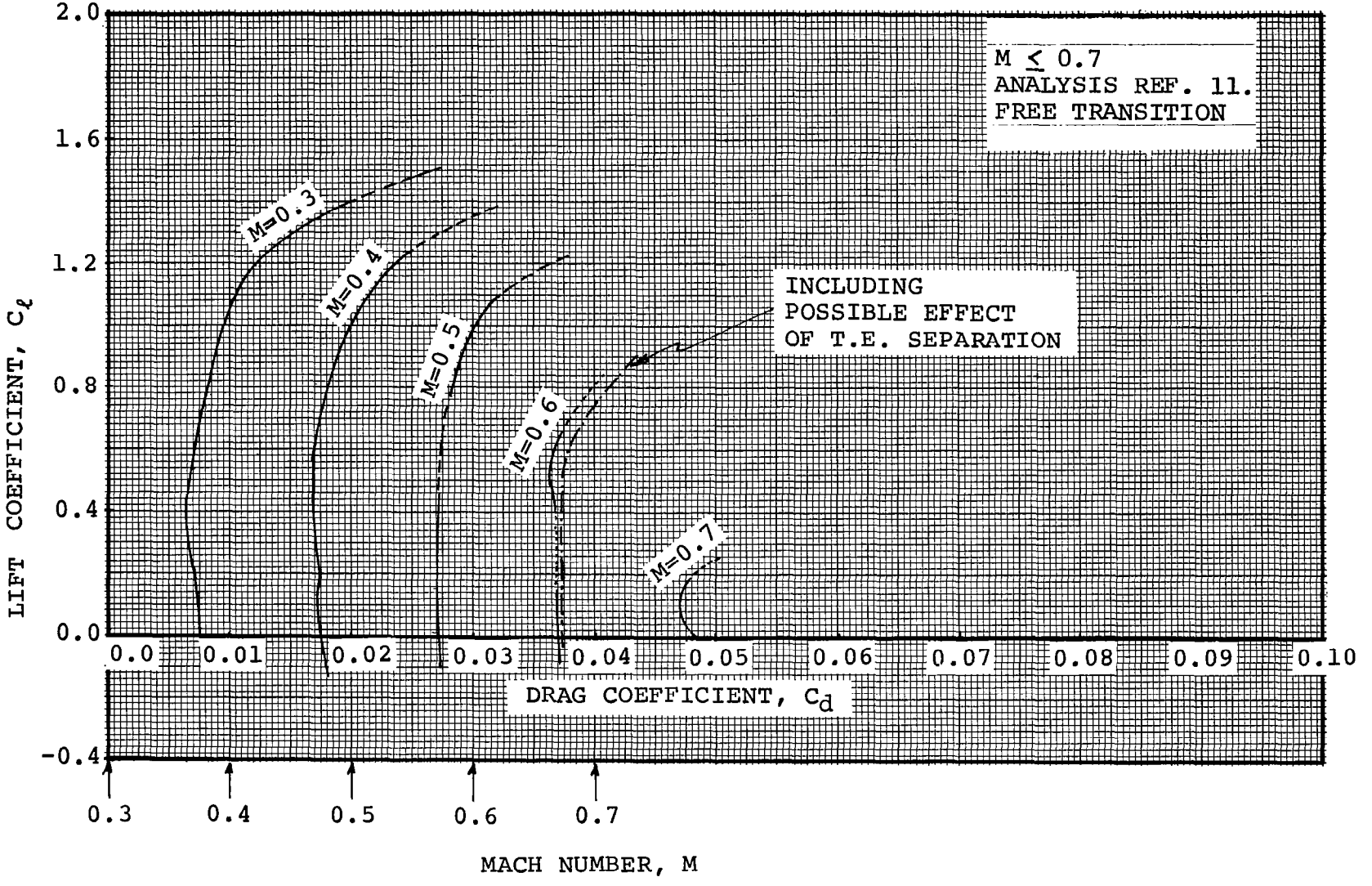

Figure 23. Estimated lift/drag polars for the VR-11x, mod. 6 at $Rn=1.5x10^7xM$.

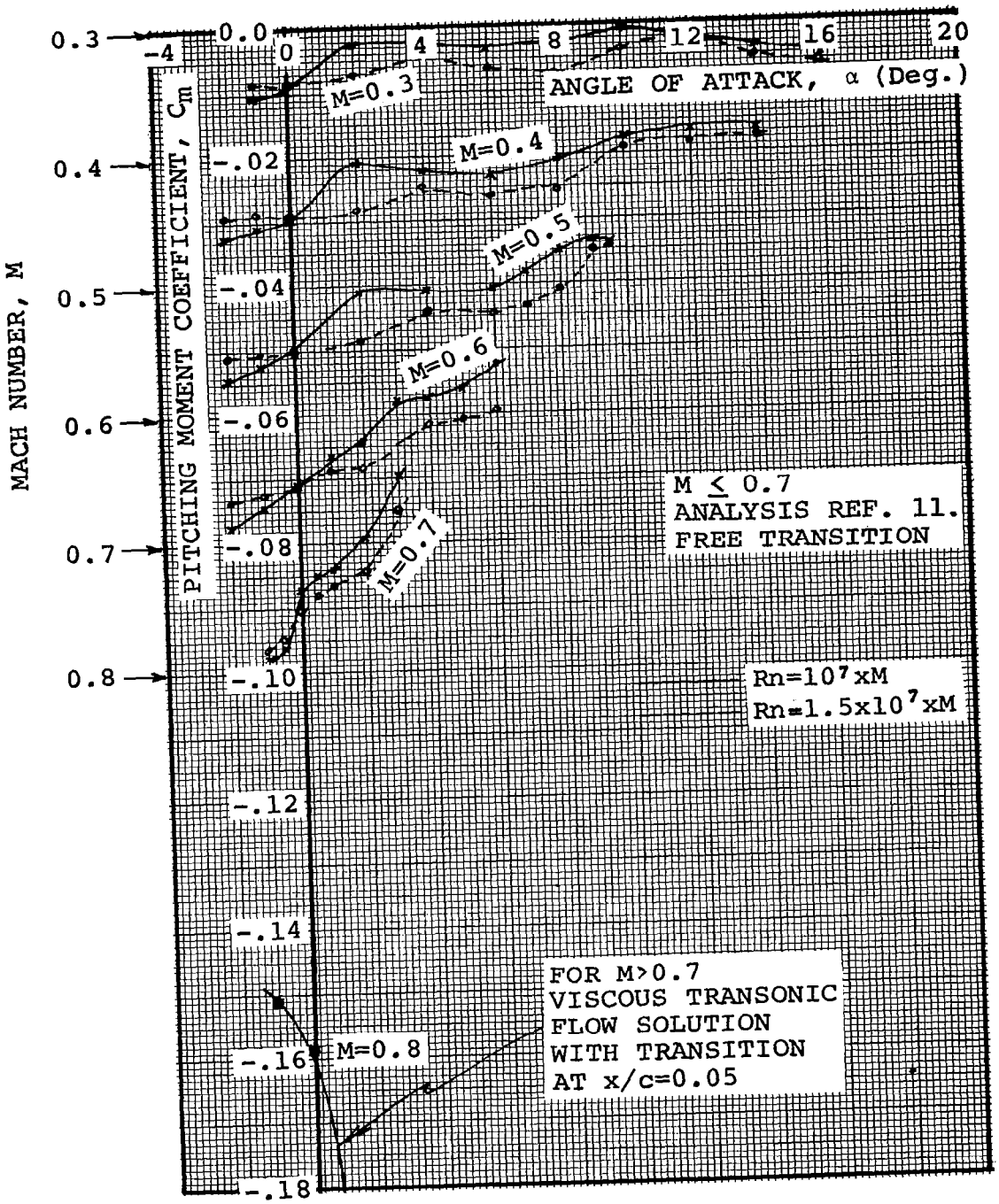

Figure 24. Estimated pitching moment coefficients for the VR-11x, mod. 6 at $Rn=10^7xM$ and $Rn=1.5x10^7xM$.

APPENDIX

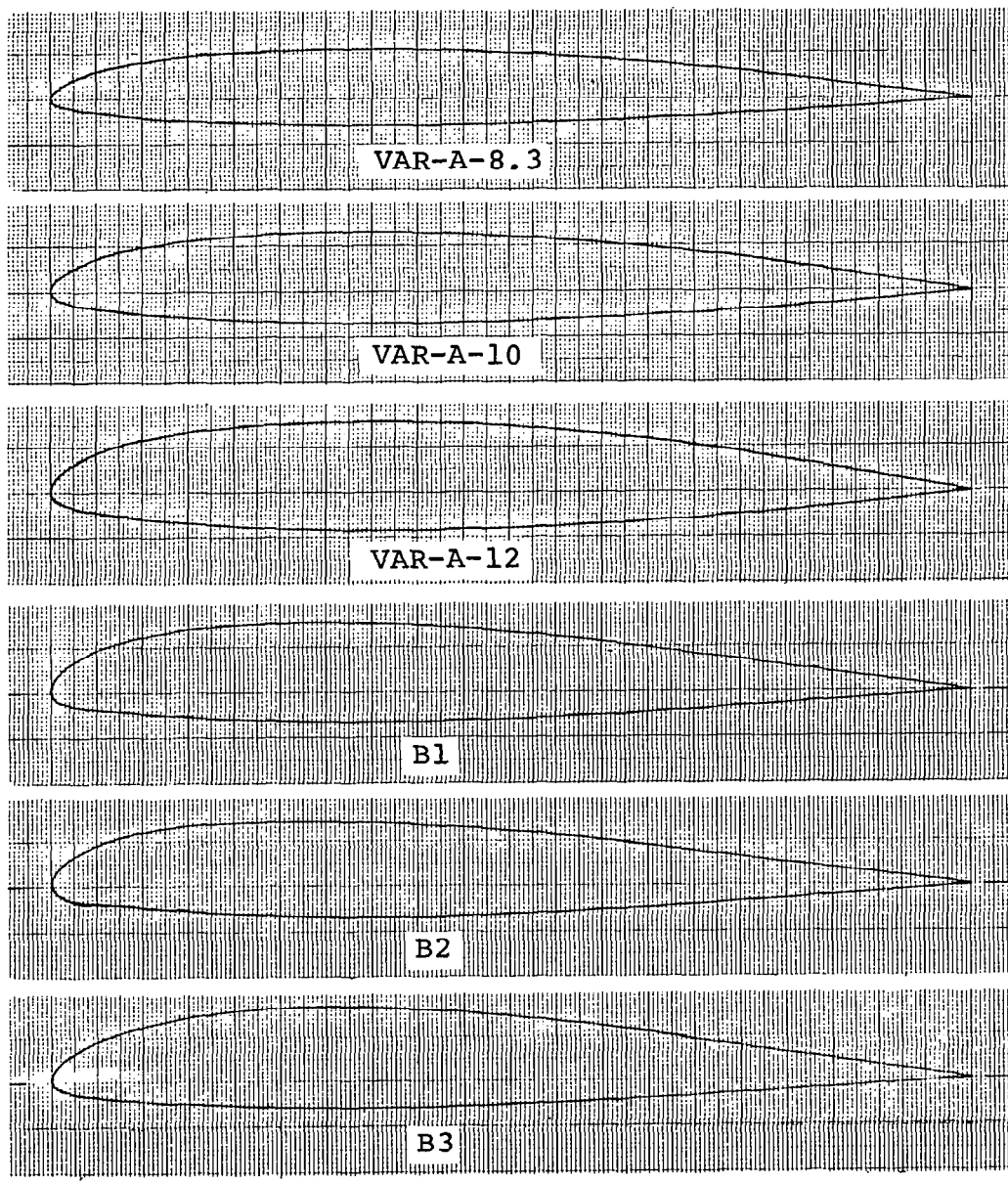

Figure 1A. Example of contours considered during airfoil design.

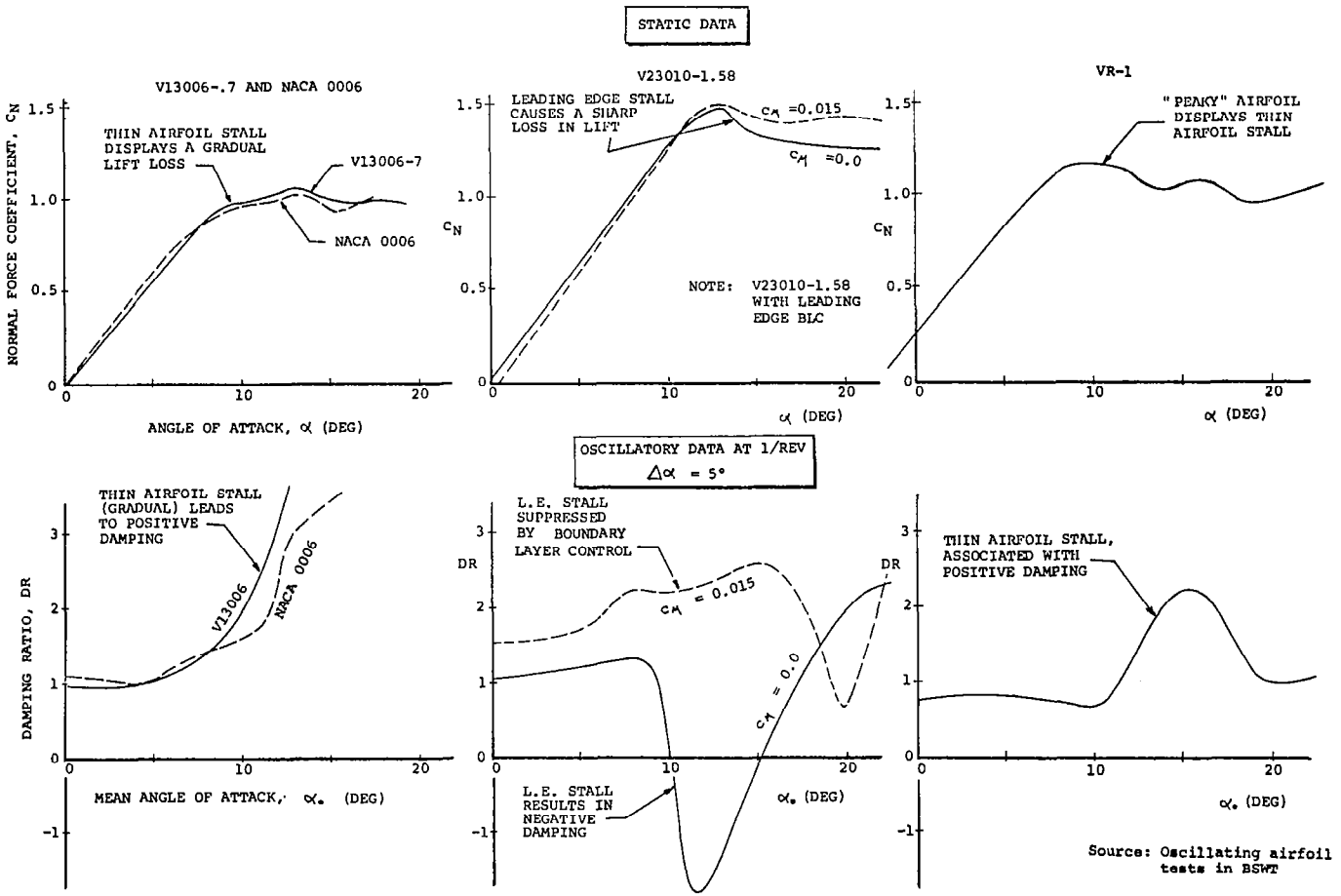

Figure 2A. Dependence of the aerodynamic damping on static stall characteristics

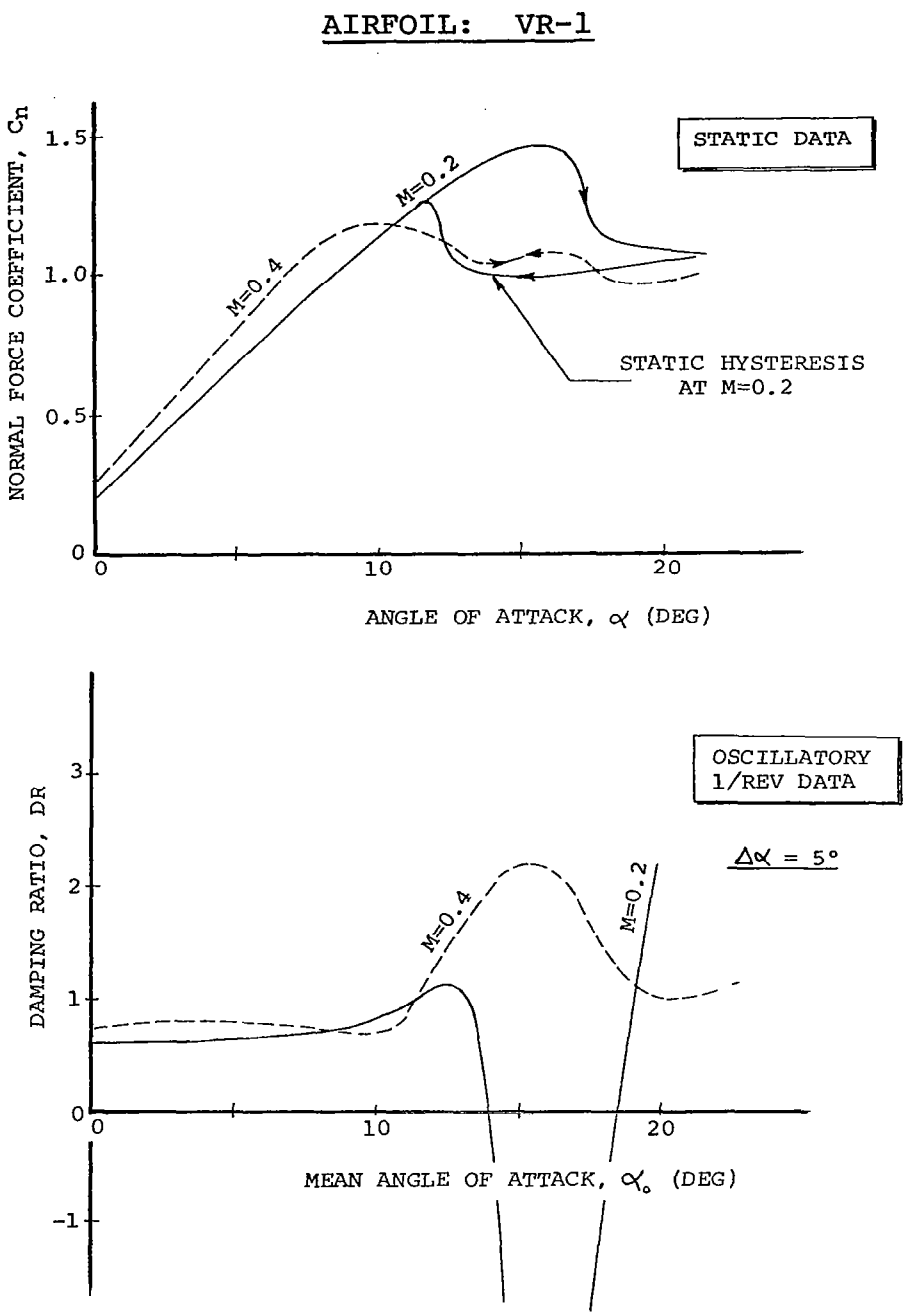

Figure 3A. Dependence of the aerodynamic damping on the static stall hysteresis

Table I-A Thickness Variations of the VR-11X (Mod. 5) Airfoil - Upper Surface Coordinates.

t/c	0.11	0.08	0.09	0.10	0.12	0.13
x/c	Y_u/c	Y_u/c	Y_u/c	Y_u/c	Y_u/c	Y_u/c
0.0	0.0	0.0	0.0	0.0	0.0	0.0
0.00012	0.003651	0.002655	0.002987	0.003191	0.003983	0.004315
0.00080	0.007303	0.005311	0.005975	0.006639	0.007967	0.008631
0.00195	0.010524	0.007654	0.008610	0.009567	0.011481	0.012437
0.0034	0.013388	0.009737	0.010954	0.012171	0.014605	0.015822
0.0052	0.016109	0.011716	0.013180	0.014644	0.017573	0.019038
0.007	0.018543	0.013486	0.015171	0.016857	0.020229	0.021914
0.009	0.020834	0.015152	0.017046	0.018940	0.022728	0.024622
0.01105	0.022982	0.016714	0.018803	0.020893	0.025071	0.027161
0.01415	0.025989	0.018901	0.021264	0.023626	0.028352	0.030714
0.0186	0.029712	0.021609	0.024310	0.027011	0.032413	0.035114
0.0245	0.034151	0.024837	0.027942	0.031046	0.037256	0.040360
0.03205	0.039019	0.028377	0.031925	0.035472	0.042566	0.046113
0.04160	0.044246	0.032179	0.036201	0.040224	0.048268	0.052291
0.05350	0.049687	0.036136	0.040653	0.04517	0.054204	0.058721
0.06850	0.055343	0.040249	0.045281	0.050312	0.060374	0.065405
0.08800	0.061214	0.044519	0.050084	0.055649	0.066779	0.072344
0.11400	0.066082	0.048060	0.054067	0.060074	0.072089	0.078097
0.15	0.070378	0.051184	0.057582	0.063980	0.076776	0.083174
0.2	0.074530	0.054204	0.060979	0.067754	0.081305	0.088081
0.25	0.077179	0.056130	0.063146	0.070163	0.084195	0.091211
0.3	0.078325	0.056964	0.064084	0.071204	0.085445	0.092566
0.35	0.078898	0.057380	0.064553	0.071725	0.086070	0.093243
0.4	0.078611	0.057172	0.064318	0.071464	0.085757	0.092904
0.45	0.077537	0.056390	0.063439	0.070488	0.084586	0.091635
0.5	0.075748	0.055089	0.061976	0.068862	0.082634	0.089520
0.55	0.073027	0.053110	0.059749	0.066388	0.079666	0.086305
0.60	0.070163	0.051028	0.057406	0.063784	0.076541	0.082920
0.65	0.066154	0.048112	0.054126	0.060140	0.072168	0.078182
0.69	0.062574	0.045508	0.051197	0.056885	0.068262	0.073951
0.73	0.057276	0.041655	0.046862	0.052069	0.062483	0.067690
0.77	0.050045	0.036396	0.040946	0.045495	0.054594	0.059144
0.81	0.040809	0.029679	0.033389	0.037099	0.044519	0.048229
0.845	0.032200	0.023418	0.026345	0.029272	0.035127	0.038054
0.88	0.024772	0.018016	0.020268	0.02252	0.027024	0.029276
0.91	0.0180	0.013091	0.014727	0.016364	0.019636	0.021273
0.935	0.0126	0.009164	0.010309	0.011454	0.013745	0.014891
0.955	0.0082	0.005964	0.006709	0.007454	0.008945	0.009691
0.97	0.0050	0.003636	0.004091	0.004545	0.005454	0.005909
0.98	0.00433	0.003149	0.003543	0.003936	0.004724	0.005117
0.99	0.00366	0.002662	0.002994	0.003327	0.003993	0.004325
0.995	0.00333	0.00242	0.002724	0.003027	0.003633	0.003935
1.0	0.0030	0.002182	0.002454	0.002727	0.003273	0.003545

Table II-A Thickness Variations of the VR-11X (Mod. 5) Airfoil - Lower Surface Coordinates.

t/c	0.11	0.08	0.09	0.1	0.12	0.13
x/c	$y_{1/c}$	$y_{1/c}$	$y_{1/c}$	$y_{1/c}$	$y_{1/c}$	$y_{1/c}$
0.0	0.0	0.0	0.0	0.0	0.0	0.0
0.00055	-0.0025	-0.001818	-0.002045	-0.002273	-0.002727	-0.002954
0.002	-0.0045	-0.003273	-0.003682	-0.004091	-0.004909	-0.005318
0.004	-0.0061	-0.004436	-0.004991	-0.005545	-0.006654	-0.007209
0.0062	-0.00720	-0.005236	-0.005891	-0.006545	-0.007854	-0.008509
0.0086	-0.00815	-0.005927	-0.006668	-0.007409	-0.008891	-0.009632
0.011	-0.00895	-0.006509	-0.007323	-0.008136	-0.009764	-0.010577
0.01465	-0.01000	-0.007273	-0.008182	-0.009091	-0.010909	-0.011818
0.019550	-0.01120	-0.008145	-0.009163	-0.010182	-0.012218	-0.013236
0.02615	-0.01260	-0.009164	-0.010309	-0.011454	-0.013745	-0.014891
0.0343	-0.01400	-0.010182	-0.011454	-0.012727	-0.015273	-0.016545
0.04449	-0.0155	-0.011273	-0.012682	-0.014091	-0.016909	-0.018318
0.05690	-0.017	-0.012364	-0.013909	-0.015454	-0.018545	-0.020091
0.07245	-0.0186	-0.013527	-0.015218	-0.016909	-0.020291	-0.021982
0.09240	-0.02045	-0.014873	-0.016732	-0.018591	-0.022309	-0.024168
0.11850	-0.02250	-0.016364	-0.018409	-0.020454	-0.024545	-0.026591
0.15000	-0.02450	-0.017818	-0.020045	-0.022273	-0.026727	-0.028954
0.20000	-0.02692	-0.019578	-0.022025	-0.024473	-0.029367	-0.031814
0.25000	-0.028850	-0.020982	-0.023604	-0.026227	-0.031473	-0.034095
0.30	-0.03	-0.021818	-0.024545	-0.027273	-0.032727	-0.035454
0.35	-0.0308	-0.0224	-0.0252	-0.0280	-0.0336	-0.0364
0.40	-0.0311	-0.022618	-0.025445	-0.028273	-0.033927	-0.036754
0.45	-0.0310	-0.022545	-0.025364	-0.028182	-0.033818	-0.036636
0.50	-0.03035	-0.022073	-0.024832	-0.027591	-0.033109	-0.035868
0.55	-0.0292	-0.021236	-0.023891	-0.026545	-0.031854	-0.034509
0.60	-0.0277	-0.020145	-0.022664	-0.025182	-0.030218	-0.032736
0.65	-0.026	-0.018909	-0.021273	-0.023636	-0.028364	-0.030727
0.69	-0.0245	-0.017818	-0.020045	-0.022273	-0.026727	-0.028954
0.73	-0.0228	-0.016582	-0.018654	-0.020727	-0.024873	-0.026945
0.77	-0.02085	-0.015164	-0.017059	-0.018954	-0.022745	-0.024641
0.81	-0.0189	-0.013745	-0.015464	-0.017182	-0.020618	-0.022336
0.845	-0.0169	-0.012290	-0.013827	-0.015364	-0.018436	-0.019973
0.88	-0.0146	-0.010618	-0.011945	-0.013273	-0.015927	-0.017255
0.91	-0.0121	-0.008800	-0.009900	-0.011000	-0.013200	-0.014300
0.935	-0.010	-0.007273	-0.008182	-0.009091	-0.010909	-0.011818
0.955	-0.008	-0.005818	-0.006545	-0.007273	-0.008727	-0.009454
0.970	-0.0061	-0.004436	-0.004991	-0.005545	-0.006655	-0.007209
0.98	-0.0046	-0.003345	-0.003764	-0.004182	-0.005018	-0.005436
0.99	-0.0028	-0.002036	-0.002291	-0.002545	-0.003054	-0.003309
0.995	-0.0016	-0.001636	-0.001309	-0.001454	-0.001745	-0.001891
1.0	0.0	0.0	0.0	0.0	0.0	0.0

1. Report No.	2. Government Accession No.	3. Recipient's Catalog No.
NASA CR-2988		

4. Title and Subtitle	5. Report Date
Design and Analytical Study of a Rotor Airfoil	May 1978
	6. Performing Organization Code

7. Author(s)	8. Performing Organization Report No.
Dadone, L. U.	D210-11239-1
	10. Work Unit No.

9. Performing Organization Name and Address	11. Contract or Grant No.
Boeing Vertol Company Boeing Center, P.O. Box 16858 Philadelphia, Pa. 19142	NAS1-14659
	13. Type of Report and Period Covered

12. Sponsoring Agency Name and Address	14. Sponsoring Agency Code
NASA Langley Research Center Hampton, Va. 23655	

15. Supplementary Notes

The contract research effort which has led to the results in this report was financially supported by USARTL (Structures Laboratory).
Langley Technical Monitor: Charles E. K. Morris, Jr. Final Report

16. Abstract

An airfoil section for use on helicopter rotor blades has been defined and analyzed by means of potential-flow/boundary-layer interaction and viscous transonic flow methods to meet as closely as possible a set of advanced airfoil design objectives.

The design efforts showed that the first priority objectives, including selected low-speed pitching-moment, maximum lift and drag-divergence requirements can be met, though marginally. The maximum lift requirement at M=0.5 and most of the profile drag objectives cannot be met without some compromise of at least one of the higher order priorities.

17. Key Words (Suggested by Author(s))	18. Distribution Statement
Airfoils Rotors	FEDD Distribution Subject Category 02

19. Security Classif. (of this report)	20. Security Classif. (of this page)	21. No. of Pages	22. Price*
Unclassified	Unclassified	92	$6.00